UNIVERSITÀ DEGLI STUDI DI PALERMO

Dottorato in Ingegneria dell'Innovazione Tecnologica
Dipartimento dell'Innovazione Industriale e Digitale
ING-IND/13 Meccanica Applicata alle Macchine

Split-Way CVTs: Parametric Analysis and Design

IL DOTTORE
Ing. Dario Rotella

IL COORDINATORE
Ch.mo Prof. Antonio Chella

IL TUTOR
Ch.mo Prof. Emiliano Pipitone

CO TUTOR
Ch.mo Prof. Marco Cammalleri

CICLO XXXI
ANNO CONSEGUIMENTO TITOLO 2019

Preface

In the last few years, transmission technology has evolved rapidly in order to pursue drivability and efficiency. Nowadays, as internal combustion engines approach their optimal performances, hybrid propulsion systems introduce new challenges and opportunities for the designers. Unfortunately, the mutual interference between power sources and gearbox requires abandoning the traditional heuristic approach, optimizing the system as a whole. As a result, new mathematical models become necessary to predict the behavior of the involved devices.

The aim of this work is to provide a simple analysis and design tool for Power-Split Continuously Variable Transmissions, which represent the most promising solution for modern hybrid electric vehicles. Nonetheless, the method presented in this manuscript is intended to offer the maximum generality, thus being able to address potentially any kind of variator drive and planetary gearbox.

In particular, significant efforts have been spent to conceive a modular and intelligible procedure. This is a key feature in order to exploit the full potentiality of Power-Split CVTs, as it allows the transmission engineer to rapidly assess the fitness of such drivelines in comparison with other solutions and to have a deep understanding of the effects of his design choices, thus pursuing the optimization of the selected concept with the necessary confidence.

Furthermore, the parametric approach is the ideal basis for the development of new control strategies, as it does not require a deep insight of the driveline, thus offering a neutral environment to the engineers with a different field of expertise.

CONTENTS

INTRODUCTION

In recent years, reducing fuel consumptions and pollution has become a significant concern. In this scenario, Power-Split CVTs represent the most flexible and promising solution for modern automotive transmissions.

Indeed, even though discrete gearboxes try to reproduce, albeit approximately, the ideal traction characteristic of a vehicle, the latter remains a prerogative of those transmissions able to achieve a continuous variation of the speed ratio, i.e. CVTs. Among the many advantages that distinguish a CVT, there is the ability to operate the primary power unit independently from the load, thus obtaining a perfectly elastic traction characteristic and optimal operative conditions in terms of fuel consumptions and pollutants. In some applications, typically vehicles with modest installed powers (scooters, golf carts), their use is a consolidated practice, as it is source of simplification both in terms of construction and use. Similar reasons, in addition to more stringent ones (very low and/or intermittent movement speeds etc.), encourage a wide use of hydrostatic CVTs in agricultural and construction working machines. Nonetheless, in the automotive field, the use of mechanical CVTs is still a prerogative of the Japanese market and, to a lesser extent, of the North American one.

On the other hand, the disadvantages that still characterize variator drives remain significant when compared with gear reducers, especially in terms of modest efficiency, low transmissible powers, limited speed ratio spreads and significant costs. In addition, the use of CVTs does not always guarantee the possibility to avoid the clutch or the torque converter [1-13].

The Power-Split technology is intended to overcome the limits of simple CVT transmissions. The basic idea is to divide the power flow, transmitting only a portion of it through the variator drive, thus sizing the latter accordingly. In particular, by combining the variator drive with a mechanical planetary gearbox, it will be possible to generate infinite transmission ratios, while maintaining an overall efficiency closer to that of traditional gearboxes.

The first prototypes of PS - CVTs date back to the end of the nineteenth century. The most effective ones still use a gear system including at least one planetary gear train (notoriously characterized by high efficiencies), which operates in parallel with a variator drive. In comparison with the variator drive alone, such solution permits to alter the fraction of power transmitted by the latter, and, depending on the design specifications, to reduce its power class (also enhancing efficiency), or, alternatively, to increase the overall transmission ratio spread. On the other hand, the possible onset of power recirculation phenomena, if not properly mitigated, can seriously compromise its efficiency.

Compound PS-CVTs, i.e. mechanical drivelines including at least two active planetary gear sets, can improve the performances of simple PS-CVTs. Indeed, these solutions permit to modulate the power fraction sent to the variator drive, thus better complying with the constructive and functional constraints. In other words, this solutions maintain the advantages of a simple Split-Way CVT (wider operating range, downsizing of the variator drive, better efficiency), and benefit from further degrees of design freedom, to be used to enhance certain aspects, such as the yield at a given regime, the power class of the CVT etc.

The next step, aimed at expanding the working range without compromising performances, consists in the realization of the so-called multimode split-way transmissions, i.e. transmissions that can perform two or more contiguous speed ranges, which commute to each other by brakes or clutches. In fact, their operation is split into several distinct phases, during which only specific components are active; this will limit the extension of the operative range of each stage, with the direct consequence of moderating the power fraction sent to the variator drive. In particular, it will be possible to design the transmission so that the transition between two contiguous modes occurs under synchronous conditions, i.e. in absence of slips and tears, thus making the presence of the torque converter superfluous. Usually, the division of the operative range into several adjacent phases is achieved by mean of techniques similar to those already used in modern discrete automatic transmissions, but with the further advantage of being able to avoid any speed jumps upstream, which would be harmful both in terms of pollution and of driving comfort. Nonetheless, the greater encumbrances, weights and costs, and a particularly insidious design starting from the preliminary phases, has hindered a wide diffusion of multimode PS-CVTs until the present days.

Nonetheless, their use in hybrid electric cars can enhance both vehicle dynamics and energy recovery systems, and it offers cost reductions due to the downsizing of the batteries and propulsion systems. Indeed, current electric vehicles suffer objective technical limits due to their weights, costs, performances, autonomy, and they determine additional (and often overlooked) environmental issues, such as the pollution caused by rare earths, and the need for an adequate electricity distribution network, which requires improving its production, transport and storage efficiency and capability. Moreover, to date, the purchase of a purely electric solution requires sustaining a high initial investment, which takes advantage of a particularly favorable tax regime in the long term, but that risks becoming unsustainable if these vehicles eventually take over. If we add that several power consumptions are present in the vehicle regardless of the propulsion system, and that some can take advantage of the presence of a thermic engine (for instance heating), to choose a hybrid solution seems more reasonable [7-13].

As a result, these drawbacks have led many car manufacturers to move towards the development of hybrid solutions in order to meet anyway the growing environmental sensitivity shown by governments and public opinion.

In particular, the main downsides that characterize the simplest hybrid configurations (dimensioning, and therefore cost, of the electrical component for the hybrid series, univocal link between speed of the engine and speed of the vehicle for the parallel hybrid), can be indeed attenuated or eliminated thanks to the use of PS-CVTs. Among the best-known examples, there are certainly several Toyota models (Prius, Highlander, Camry), Nissan and Ford. The mass production of multimodal compound transmissions is more recent and is the result of a joint venture between GM, BMW, Daimler and Chrysler LLC (2005). This project aimed at the realization of multimodal hybrid transmissions for cars with all-wheels or rear traction, including the BMW X6 ActiveHybrid, the Mercedes 450 ML Hybrid and the second generation of the Chevrolet Volt. Previously, numerous prototypes have been proposed, among which the bi-modal Renault (2003) [23].

The main aim of the present discussion is to identify a parametric analytical method, which allows addressing the problem of the analysis and design of PS-CVTs regardless of the knowledge of the construction parameters specific to each scheme.

The first part of this thesis is focused on the description and analysis of PS-CVTs. This task is easy, as several authors have proposed their own methods for the study of similar transmissions, so that there are numerous examples of such analyses in literature [21, 22, 30 32 46 50 69 71 75 84 87 et al.]; nevertheless, none seems to provide a reasonably simple general model, especially for multi-mode PS-CVTs.

Accordingly, the main purpose of section 1 is to provide a unified model for the analysis of such transmissions, by describing its functioning by mean of a set of functional parameters.

In particular, the original concept of characteristic function is introduced in section 2. The characteristic functions are determined by the functional parameters, and can be used for both analysis and design purposes.

In section 3, the most common driveline structures are analyzed. In particular, a simple general additive method, intended to generate whichever planetary transmission starting from the simplest shunt designs, is described. In respect with other method, which tend to be more explorative, this method shows the fundamental advantage to do not generate redundant or meaningless structures.

In section 4, a method to calculate the functional parameters from known designs is proposed. A general approach is described so that any driveline could be addressed. Such method permits to analyze an existing PS-CVT or to explore comparable designs, but it can be also used to verify a newly conceived design. Indeed, it may be problematic to achieve exactly the desired design by means of real devices, because gear ratios are discrete. Therefore, it represents a quick analysis method to assess the impact of approximated constructive parameters on the transmission functioning. Some explicit results (relative to the most common solutions) have been listed as well.

Section 5 is focused on the power flow analysis of ideal PS-CVTs. This topic has been extensively addressed in literature, especially thanks to Macmillan [74-75], M.J. French [52], Sanger [22] and Polder [46, 76]. Numerous papers are indeed insightful and describe some of the key features of specific case studies; nevertheless, most of them lack generality. On the other hand, the theory presented in this manuscript starts from [24, 77-80] and [18], and the use of functional parameters and characteristic functions eases the power flow analysis, making such task truly general and straightforward.

Section 6 deals with the mechanical losses within the planetary transmission. Indeed, assessing mechanical losses allow the engineer to discriminate among functionally equivalent solutions and to tune their control properly, so that true optimal condition could be achieved. Various methods adopt convoluted or encyclopedic formularies, requiring a laborious task in order to identify losses, especially when analyzing complex multimode PS-CVTs. Vice versa, the proposed method requires performing simple tests and is truly intelligible, as it relies on the physical meaning of the parameters, avoiding mathematical formalism.

In section 7 we address the power flow analysis in presence of mechanical losses. A rigorous study of the mechanical losses is firstly proposed, however, it requires identifying the conditions responsible for the torque discontinuities characterizing the functioning of PS-CVTs. To address this issue, we propose also an approximated method, which offers verisimilar results readily.

In section 8 an implicit method for the analysis of PS-CVT is proposed. It has been conceived specifically for numerical implementation, as it is both concise and general, it being able to address easily the analysis of any driveline (mechanical power losses included), but it has the main drawback of being iterative.

In section 9 the dynamic effects on the driveline are addressed. In particular, a simple formulation able to translate any inertial effects in terms of fictitious input and output torques is proposed. This allows to maintain the same formulation described in the previous section, thus adopting an automated approach for the calculation of the control torque even when both inertial effects and mechanical losses are taken into account.

In section 10 two real transmission are analyzed with the methods described above.

Section 11 gives a brief insight about the general requirements constituting the disturbance for a driveline (section 11.1) and the most common control strategies (section 11.2).

In section 12 the design procedure is described, explaining the role of the characteristic functions. In particular, the results are generalized for any order of driveline in section 12.3

Section 13 describes some strategies able to achieve multimode transmissions. General methods are described in section 13.1 and 13.2, while more detailed results about the most common solutions are examined in section 13.3.

In section 14 some functional guidelines (14.1) and constructive guidelines (14.2) are provided for the planetary driveline.

Section 15 offers some models for the main power sources of the PS-CVT, i.e. the engine, the electric motors and the energy storage systems.

Section 16 describes some design applications.

1. Parametrization of PS-CVTs

A Power-Split Continuously Variable Transmission (PS-CVT) (see Fig. 1) comprises a Continuously Variable Unit (CVU), i.e. a variator drive of any kind, and a Power-Split Unit (PSU), i.e. a planetary driveline made of a combination of three-port mechanisms (TPMs). The generic TPM consists of a planetary gear train (PG) and three ordinary gear sets (OGs) (see Fig. 2).

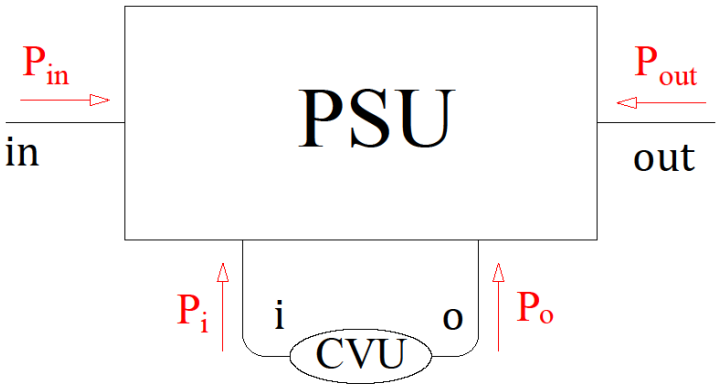

Fig. 1 Generic PS-CVT.

Fig. 1 shows the generic functional scheme of a PS-CVT. The shafts i, o, in and out represent the main ports of the PSU. The ports in and out are the input and output shafts of the driveline, while the ports i and o are the conventional input and output shafts of the CVU. Since the CVU can be subject to power flow reversals, in most cases such labels can be assigned arbitrarily. The red arrows represent power flows. In particular, the main power flows P_i, P_o, P_{in} and P_{out} are considered positive if entering the PSU (as in Fig. 1). On the other hand, defining the sign of speeds and torques is not necessary in this phase.

As it will be clear in the next sections, the kinematics, torques and power flows of the main ports are ruled by few functional parameters, regardless the actual constructive layout of the PSU. This property will be exploited throughout the manuscript for both analysis and design purposes.

1.1. Kinematics

Within the PSU, each angular speed is a linear function of two others. In particular, in order to describe the mutual relationships between overall transmission ratio τ (eq. (1)) and CVU transmission ratios τ_i and τ_o (eq. (2) and eq. (3)), we need at least four parameters.

$$\tau = \frac{\omega_{out}}{\omega_{in}} \tag{1}$$

$$\tau_i = \frac{\omega_i}{\omega_{in}} \tag{2}$$

$$\tau_o = \frac{\omega_o}{\omega_{in}} \tag{3}$$

The mechanical points $\tau_{\#i}$ and $\tau_{\#o}$ (eq. (4) and (5)) represent the overall transmission ratios for which the shaft of either the conventional input i or the conventional output o of the CVU is motionless:

$$\tau_{\#i} = \left.\frac{\omega_{out}}{\omega_{in}}\right|_{\omega_i=0} \tag{4}$$

$$\tau_{\#o} = \left.\frac{\omega_{out}}{\omega_{in}}\right|_{\omega_o=0} \tag{5}$$

Accordingly, the related CVU speed ratios $\tau_{o_{\#i}}$ and $\tau_{i_{\#o}}$ are defined as:

$$\tau_{i_{\#o}} = \left.\frac{\omega_i}{\omega_{in}}\right|_{\omega_o=0} \tag{6}$$

$$\tau_{o_{\#i}} = \left.\frac{\omega_o}{\omega_{in}}\right|_{\omega_i=0} \tag{7}$$

As stated before, the ratios τ_i and τ_o are linear functions of τ. Therefore, after some math, they can be written as:

$$\tau_i = \tau_{i_{\#o}} \cdot \frac{\tau - \tau_{\#i}}{\tau_{\#o} - \tau_{\#i}} \tag{8}$$

$$\tau_o = \tau_{o_{\#i}} \cdot \frac{\tau - \tau_{\#o}}{\tau_{\#i} - \tau_{\#o}} \tag{9}$$

Their ratio is:

$$\tau_v = \frac{\omega_o}{\omega_i} = \tau_{v_\#} \cdot \frac{\tau - \tau_{\#o}}{\tau - \tau_{\#i}} \tag{10}$$

In which:

$$\tau_{v_\#} = -\frac{\tau_{o_{\#i}}}{\tau_{i_{\#o}}} \tag{11}$$

The ratio $\tau_{v_\#}$ is the asymptotic CVU transmission ratio, as it is the value of τ_v for $\tau \to \pm\infty$, but also its opposite for $\tau = \frac{\tau_{\#i}+\tau_{\#o}}{2}$.

The inverse functions are respectively:

$$\tau = \tau_i \frac{\tau_{\#o} - \tau_{\#i}}{\tau_{i_{\#o}}} + \tau_{\#i} \tag{12}$$

$$\tau = \tau_o \frac{\tau_{\#i} - \tau_{\#o}}{\tau_{o_{\#i}}} + \tau_{\#o} \tag{13}$$

$$\tau = \frac{\tau_{\#o} - \left(\tau_v / \tau_{v_\#}\right) \tau_{\#i}}{1 - \left(\tau_v / \tau_{v_\#}\right)} \tag{14}$$

Accordingly, the functional parameters of the PS-CVT are the overall speed ratios $\tau_{\#i}$ and $\tau_{\#o}$, calculated when one shaft of the CVU is motionless, and the related CVU speed ratios $\tau_{o_{\#i}}$ and $\tau_{i_{\#o}}$.

Eq. (10), (11) and (14) are intended for mechanical CVUs, as in these circumstances the CVU speed ratio τ_v is the most significant control parameter.

1.2. Ideal torques

In absence of mechanical losses in the PSU, for a given overall torque ratio Θ (eq. (15)), the normalized torques θ_i and θ_o (eq. (16)-(17)) applied to the PSU from the shafts of the CVU are functions of the aforementioned kinematics parameters $\tau_{i_{\#o}}$, $\tau_{\#o}$, $\tau_{\#i}$ and $\tau_{o_{\#i}}$ (eq. (18) - (19)):

$$\Theta = \frac{T_{out}}{T_{in}} \tag{15}$$

$$\theta_i = \frac{T_i}{T_{in}} \tag{16}$$

$$\theta_o = \frac{T_o}{T_{in}} \tag{17}$$

$$\theta_i = -\frac{1 + \Theta\, \tau_{\#o}}{\tau_{i_{\#o}}} \tag{18}$$

$$\theta_o = -\frac{1 + \Theta\, \tau_{\#i}}{\tau_{o_{\#i}}} \tag{19}$$

The inverse relationships are the following:

$$\Theta = -\frac{1}{\tau_{i_{\#o}}\, \theta_i + \tau_{\#o}} \tag{20}$$

$$\Theta = -\frac{1}{\tau_{o_{\#i}}\, \theta_o + \tau_{\#i}} \tag{21}$$

It is self-evident that $\tau_{i_{\#o}}$ and $\tau_{o_{\#i}}$ modulate the CVU's torques whichever it is the overall torque ratio Θ. In particular, the modules of $\tau_{i_{\#o}}$ and $\tau_{o_{\#i}}$ are subject to an upper constraint, as they determine the speed reached by the shafts of the CVU (eq. (8) and (9)), which is subject to a limit due to obvious constructive reasons.

1.3. Ideal main power flows

In absence of mechanical losses and for given overall speed and torque ratio τ and Θ, the relative powers p_i and p_o (eq. (22)-(23)) flowing through the shafts of the CVU are functions of the mechanical points $\tau_{\#i}$ and $\tau_{\#o}$ only (eq. (26)-(27)), which means that the latter are primary design parameters. In particular, p_i will be null when $\Theta = -1/\tau_{\#o}$ or $\tau = \tau_{\#i}$, while p_o will be null when $\Theta = -1/\tau_{\#i}$ or $\tau = \tau_{\#o}$:

$$p_i = \frac{P_i}{P_{in}} \tag{22}$$

$$p_o = \frac{P_o}{P_{in}} \tag{23}$$

$$\eta_v = -\frac{P_o}{P_i} \tag{24}$$

$$\eta = -\frac{P_{out}}{P_{in}} \tag{25}$$

Eq. (26) and (27) can be obtained from the relationships of section 1.1 and 1.2:

$$p_i = -\frac{(\tau - \tau_{\#i})\,(1 + \Theta\,\tau_{\#o})}{\tau_{\#o} - \tau_{\#i}} \tag{26}$$

$$p_o = \frac{(\tau - \tau_{\#o})\,(1 + \Theta\,\tau_{\#i})}{\tau_{\#o} - \tau_{\#i}} \tag{27}$$

$$\eta_v = \frac{\tau - \tau_{\#o}}{\tau - \tau_{\#i}} \frac{1 + \Theta\,\tau_{\#i}}{1 + \Theta\,\tau_{\#o}} \tag{28}$$

$$\eta = -\tau\,\Theta \tag{29}$$

In the previous relationships, η_v is the CVU's apparent efficiency, calculated as the negative ratio between the power flowing through the conventional output shaft "o" and the power

flowing through the conventional input shaft "i" of the PSU. Similarly, η is the overall apparent efficiency.

We use the adjective "apparent" because we expect a CVU with the ability to store and release energy, which means that the observed power ratios are not entirely due to power losses. Accordingly, such parameters will be comprised between zero and one only if the CVU is a passive device, such as a V-belt variator, but in general both η_v and η will be able to assume values outside the aforementioned interval.

The inverse relationships of eq. (26) and (27) are the following:

$$\eta = \frac{\tau}{\tau_{\#o}}\left(1 + p_i \frac{\tau_{\#o} - \tau_{\#i}}{\tau - \tau_{\#i}}\right) \tag{30}$$

$$\eta = \frac{\tau}{\tau_{\#i}}\left(1 - p_o \frac{\tau_{\#o} - \tau_{\#i}}{\tau - \tau_{\#o}}\right) \tag{31}$$

And it is easy to verify that they satisfy the general power balance:

$$\eta = 1 + p_i + p_o \tag{32}$$

As stated before, all the previous relationship are independent from the actual constructive layout.

1.3.1. Normalized powers

For given overall torque ratio Θ, the powers p_i and p_o are related to their values calculated for a generic base speed ratio τ_b. In particular, the normalized CVU power flow is a function of the reciprocal distance of the overall speed ratios from the associated mechanical point:

$$p_i' = \frac{p_i}{p_{i_b}} = \frac{\tau - \tau_{\#i}}{\tau_b - \tau_{\#i}} \tag{33}$$

$$p'_o = \frac{p_o}{p_{o_b}} = \frac{\tau - \tau_{\#o}}{\tau_b - \tau_{\#o}} \tag{34}$$

This is the result of an unaltered torque distribution, so that the power change is due to speed variations only.

In particular, when $\eta = 1$, it can be observed that $p_i = -p_o$ and the power p_i is related to its value calculated for τ_b in accordance to the following expression:

$$p'_i = \frac{p_i}{p_{i_b}} = \frac{\tau'_o \, \tau'_i}{\tau'} \tag{35}$$

In which τ', τ'_i or τ'_o are speed ratios normalized in respect of their base values:

$$\tau' = \frac{\tau}{\tau_i} \tag{36}$$

$$\tau'_i = \frac{\tau_i}{\tau_{i_b}} \tag{37}$$

$$\tau'_o = \frac{\tau_o}{\tau_{o_b}} \tag{38}$$

Accordingly, it is evident that the sign of τ', τ'_i or τ'_o determines the sign of p_i, and therefore speed reversal on the main ports imply the use of CVUs that support the reversal of the power flow as well.

2. Three Port Mechanisms

The TPM is the fundamental core structure of the PSU. The generic TPM (Fig. 2) consists of one planetary gear train with constructive parameter ψ and three ordinary gear sets with constructive parameters k_j (not always present). The red arrows represent power flows, which are assumed positive if entering the TPM.

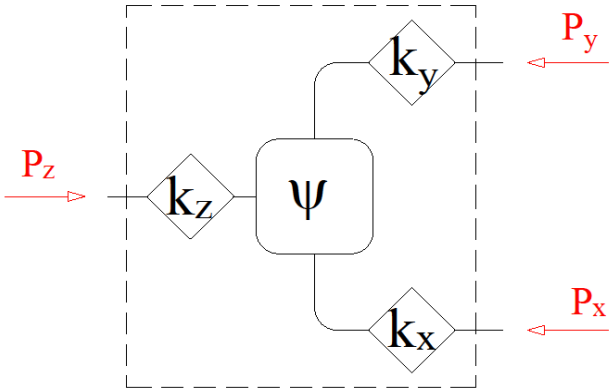

Fig. 2 Generic TPM

As it will be clear in the next section 3, any PSU is a particular combination of TPMs. In particular, the number of TPMs in a PSU equates its number of nodal ratios, i.e. overall transmission ratios when a branch of the PSU is motionless (see section 3.3.). The mechanical points $\tau_{\#i}$ and $\tau_{\#o}$ represent a particular sub-group of nodal ratios. The discriminant factor is that the mechanical points refer to the external ports of the PSU, while the nodal ratios can refer also to neutral nodes, i.e. internal branches of the PSU not linked to any external port.

Each TPM is characterized by a particular set of functions, which determine the relationships between the power flowing through the shafts of the TPM itself and the link between synchronous ratio and constructive parameter of the PG. These relationships are crucial for the model described in this manuscript, and hereinafter we refer to them as the *characteristic functions* of the TPM.

2.1. Characteristic functions of the TPM

The nodal ratios govern the generic characteristic functions $\phi^z_{x/y}$, defined as follows:

$$\phi^z_{x/y} = \frac{\tau_y}{\tau_x} \cdot \frac{\tau_x}{\tau_y}\bigg|_{\tau_z=0} = \frac{\tau - \tau_{\#y}}{\tau - \tau_{\#x}} \cdot \frac{\tau_{\#z} - \tau_{\#x}}{\tau_{\#z} - \tau_{\#y}} \tag{39}$$

The function $\phi^z_{x/y}$ represents the speed ratio between two shafts y and x of a TPM (see Fig. 2), normalized in respect to itself when the third shaft z is motionless. As it can be easily verified, eq. (39) can be deduced from the kinematic relationships provided in section 1.1. For known nodal ratios and considering that $\tau_{\#out} = 0$ and $\tau_{\#in} = \infty$ by definition, it is possible to obtain a set of characteristic functions by mean of simple index substitutions. For instance, with reference to the mechanical points only, it is possible to define four functional groups for the TPMs depending on the involved shafts (Table 1), each one related to one (arbitrarily selected) basic characteristic function.

Table 1 Functional groups, involved main shafts and basic characteristic functions

Group	Shafts	Basic characteristic function
$\boldsymbol{C_{in}}$	i, o, in	$\phi^{in}_{o/i} = \dfrac{1 - \tau_{\#i}/\tau}{1 - \tau_{\#o}/\tau}$
$\boldsymbol{C_{out}}$	i, o, out	$\phi^{out}_{o/i} = \dfrac{1 - (\tau_{\#i}/\tau)^{-1}}{1 - (\tau_{\#o}/\tau)^{-1}}$
$\boldsymbol{D_i}$	in, out, i	$\phi^{i}_{out/in} = \tau_{\#i}/\tau$
$\boldsymbol{D_o}$	in, out, o	$\phi^{o}_{out/in} = \tau_{\#o}/\tau$

There are five additional characteristic functions belonging to each group, which might be calculated by switching the shafts' indexes in eq. (39). However, as it can be easily verified, the characteristic functions are mutually dependent, so they can be derived from the basic function thanks to the simple relationships listed in the last row of Table 2.

Obviously, this approach can be easily applied to the description of transmissions that involve any number of PGs (although the number of groups increases factorially with the TPMs), such as complex multimode PS-CVTs or discrete automatic transmissions. Obviously, all the nodal ratios (including those related to the neutral nodes) must be known, or otherwise calculated as in section 4.

Table 2 Table for the calculation of the characteristic functions from basic ones.

Group	**Characteristic functions**					
$\boldsymbol{D_i}$	$\phi^{i}_{out/in}$	$\phi^{i}_{in/out}$	$\phi^{in}_{out/i}$	$\phi^{in}_{i/out}$	$\phi^{out}_{in/i}$	$\phi^{out}_{i/in}$
$\boldsymbol{D_o}$	$\phi^{o}_{out/in}$	$\phi^{o}_{in/out}$	$\phi^{in}_{out/o}$	$\phi^{in}_{o/out}$	$\phi^{out}_{in/o}$	$\phi^{out}_{o/in}$
$\boldsymbol{C}_{in}$	$\phi^{in}_{o/i}$	$\phi^{in}_{i/o}$	$\phi^{i}_{o/in}$	$\phi^{i}_{in/o}$	$\phi^{o}_{i/in}$	$\phi^{o}_{in/i}$
$\boldsymbol{C}_{out}$	$\phi^{out}_{o/i}$	$\phi^{out}_{i/o}$	$\phi^{i}_{o/out}$	$\phi^{i}_{out/o}$	$\phi^{o}_{i/out}$	$\phi^{o}_{out/i}$
	$\boldsymbol{\varphi}$	$\frac{1}{\boldsymbol{\varphi}}$	$1-\boldsymbol{\varphi}$	$\frac{1}{1-\boldsymbol{\varphi}}$	$1-\frac{1}{\boldsymbol{\varphi}}$	$\frac{-\boldsymbol{\varphi}}{1-\boldsymbol{\varphi}}$

2.1.1. Properties of the characteristic functions

Primarily, the characteristic functions represent the ideal ratios between the powers transmitted by two shafts of a TPM

$$\phi_{x/y}^{z} = -\frac{P_y}{P_x} \tag{40}$$

The reason is that when the shaft z is motionless, the power balance between the shafts y and x requires their torque ratio to be:

$$\frac{T_y}{T_x} = -\frac{\tau_x}{\tau_y}\bigg|_{\tau_z=0} \tag{41}$$

Secondly, they are independent from the OGs, and thus equal for the PG and TPM. The simple physical explanation is that they represent an ideal power ratio, and the ideal power flows on the shafts of the TPM are not altered by the OGs.

Eventually, as it will be explained in detail in section 12.1, the characteristic functions represent also the link between the synchronous conditions of the PGs and their respective Willis' ratios.

$$\psi = \phi_{R/S}^{C}(\tau_*) \tag{42}$$

Therefore, they will be used for design purposes too.

3. Power Split Units

The PSU (Fig. 1) is a planetary driveline comprising several TPMs (Fig. 2). The physical presence of brakes and clutches is required in order to perform mode switches, yet their mathematical modeling is not strictly necessary.

In particular, it exists a functional difference between PSUs using just one TPM, and PSUs using two or more TPMs. Indeed, the mechanical points $\tau_{\#i}$ and $\tau_{\#o}$ are both free design parameters only in the latter case, as the number of TPMs determine the total number of nodal ratios.

The use of more than two TPMs permits to cover a wider speed ratio range, but does not bring direct advantages in terms of modulation of the power flowing through the CVU in each mode. On the other hand, the complexity of the PSU is detrimental under several aspects, including costs, weights, encumbrances, mechanicals losses and design issues.

For the reason stated above, in most PSUs the number of active TPMs will range between one and three. The following sections describe the most common architectures and generalize their fundamental characteristics.

3.1. Shunt PSUs - One TPM

The simplest PSU is the so-called variable shunt, as its core structure is one TPM (Fig. 2). In general, the shunt PS-CVT represents a suboptimal solution if used alone, but it is not necessarily always detrimental, as it can help limiting the power sent to the variator drive under specific circumstances, such as the stall condition.

The group of the TPM of a shunt PS-CVT falls within the cases listed in Table 1. Indeed, the three indexes of the TPM must be chosen between i, o, in and out, so the total number of characteristic functions for shunt PS-CVTs is 24 (see Table 2).

Shunts PS-CVTs can be Input Split (Output Coupled) or Output Split (Input Coupled) transmissions (Fig. 3). In Fig. 3 the square (with sharp edges) represents the TPM and the rhombus an additional OG.

If the free shaft of the CVU (not connected to the PG) is linked to:

- the output shaft (possibly by mean of an ordinary gear set), the PS-CVT is an Input Split
- the input shaft, the PS-CVT is an Output Split.

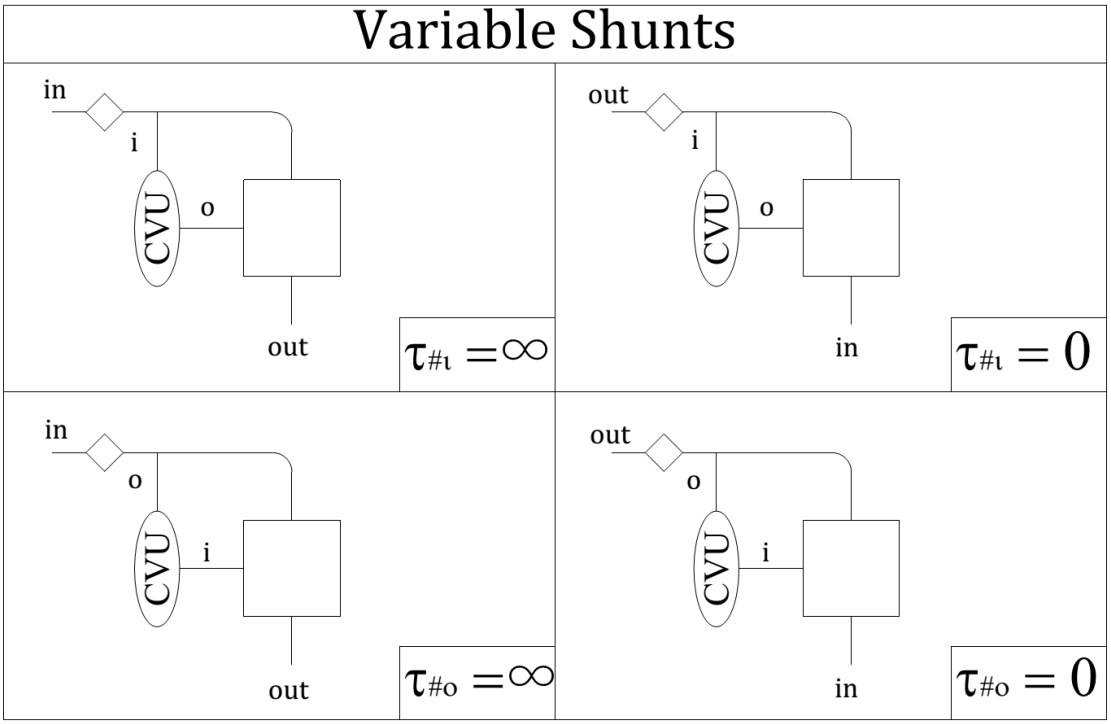

Fig. 3 Shunt PS-CVTs: Output Splits (left), Input Splits (right)

As stated above, the immediate consequence in terms of functional parameters is that the related mechanical point is not free, but coincides with either zero or infinite, i.e. $\tau_{\#out}$ and $\tau_{\#in}$ (see Table 3).

Table 3 Functional parameters for shunt PS-CVTs

Type	$\tau_{\#i}$	$\tau_{\#o}$	$\tau_{o_{\#i}}$	$\tau_{i_{\#o}}$
INPUT SPLIT	0	$\tau_{\#o}$	$\tau_o(0)$	$\tau_{\#o}/k_{out}$
	$\tau_{\#i}$	0	$\tau_{\#i}/k_{out}$	$\tau_i(0)$
OUTPUT SPLIT	∞	$\tau_{\#o}$	$\tau_o(\infty)$	$1/k_{in}$
	$\tau_{\#i}$	∞	$1/k_{in}$	$\tau_i(\infty)$

3.2. Compound PSUs - two TPMs

If the compound PSU is made of two TPMs connected to each other, it offers two nodes (IJs) and two free shafts as external ports. It is possible to observe that the core structure of the PSU remains identical (Fig. 4), but the functional solutions are distinct because the CVU connects either nodes, free shafts or both (Fig. 5).

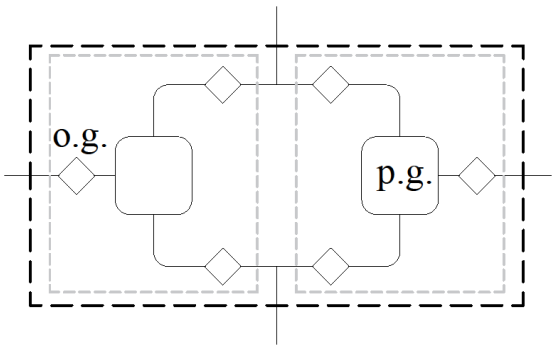

Fig. 4 Core structure of PSU consisting of two TPMs

In Fig. 4 and Fig. 5, rhombs represent ordinary gears, while squares (with rounded edges) represent planetary gear trains. In Fig. 5 is easy to identify three basic layouts, two of which are symmetric. Since the asymmetric layout is present in four distinct versions depending on the relative position of the main shafts, there are six functional schemes in total.

The relationships already listed in Table 1 are sufficient to describe compound PS-CVTs also in this case. There are four groups ($C_{in}, C_{out}, D_i, D_o$), each one represented by a particular combination of capital letter and subscript. The subscript of groups with the same capital letter refers to the shaft possessed in exclusive, while capital letter themselves permit to identify easily the fundamental compound layouts of Fig. 5. Indeed, two TPMs belonging to a D group combine in a "Direct bridge" symmetric layout, in which the CVU connects the two TPMs, while two TPMs belonging to a C group combine in a "Cross bridge" symmetric layout, as the CVU connects the two nodes. Eventually, TPMs belonging to either groups combine in an Asymmetric Bridge layout.

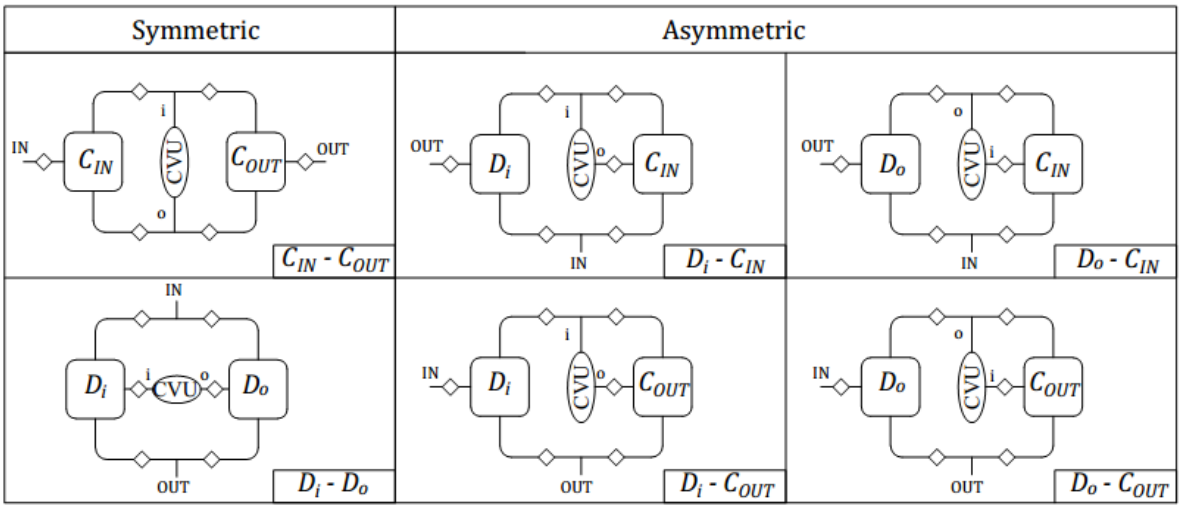

Fig. 5 Functional schemes for compound PS-CVTs.

Besides the similarities with shunt PS-CVTs, as stated before compound PS-CVTs offer more control over the relationships listed in section 1, thus being a more flexible design option.

In theory, whichever couple of mechanical points can be obtained by mean of any of the aforementioned layouts. However, constructive boundaries often limit the choice to fewer possibilities.

3.3. Compound PSUs - 3+ TPMs

In order to achieve a complex multimode transmission, or when feasible solution with two or less planetary gear trains do not exist, it is certainly possible to use any (reasonable) number of additional TPMs. The two mechanical points related to the CVU still govern the behavior of the variator drive, but additional nodal ratios (in the same number of the additional TPMs) must be defined to describe the driveline.

Obviously, since the number of characteristic functions increases very rapidly with the number of nodal ratios, it is not practical to list them all, so in this section we will describe the case of a compound PSU with three TPMs, using it as a general example.

A node (or isokinetic joint) is the union of two or more shafts belonging to different TPMs, while a free shaft is a branch of a TPM not linked to the other TPMs of the PSU. In terms of characteristic functions, there is not real difference between a node linked to the variator drive and the generic neutral node n, which is not. Accordingly, in the case of a compound PSU with three TPMs, the additional characteristic functions will be analogous to that listed in Table 2, mostly by mean of the substitution of either the index i or o with n, for a total of 36 new characteristic functions. In particular, some of the new characteristic functions (shafts i, o, n) assume instead the same form of the generic expression (39), as no further simplification is possible.

In order to generate the new core structures, it is sufficient to consider that the new TPM must not alter the already existing kinematic relationships, which means that removing it must lead to the same core structure (Fig. 4) already observed in section 3.2. Accordingly, starting from the aforementioned core structure, the new TPM can be linked to two IJs, two free shafts or one of each, thus obtaining three new core structures, apparently similar to the functional layouts previously observed in Fig. 5, but with five available external ports (Fig. 6).

It is then possible to obtain the new functional schemes by linking the external ports to the four main ports i, o, in, out. The choice is mostly free, but it is necessary to guarantee that all the PGs are loaded with torque, which means abiding to the following rules:

- The neutral node n must be a isokinetic joint
- All the remaining free shafts must connect a main port (i, o, in or out)

The same logic can be applied to PSU with four TPMs: starting from the core structures represented in Fig. 6, an additional TPM is connected, with the same rules applying to the free shafts and neutral nodes. Obviously, the number of core structures and related layouts raises rapidly, so it will not be furtherly addressed in this section.

Eventually, it is worth noting that each OG, even when it is not actually present in the PSU, can be used to model a brake connecting the shaft of one PG to the frame. This solution is commonly used to perform a mode switch (see section 13.3), and can be simulated by imposing a fictitious infinite value to the related fixed gear ratio.

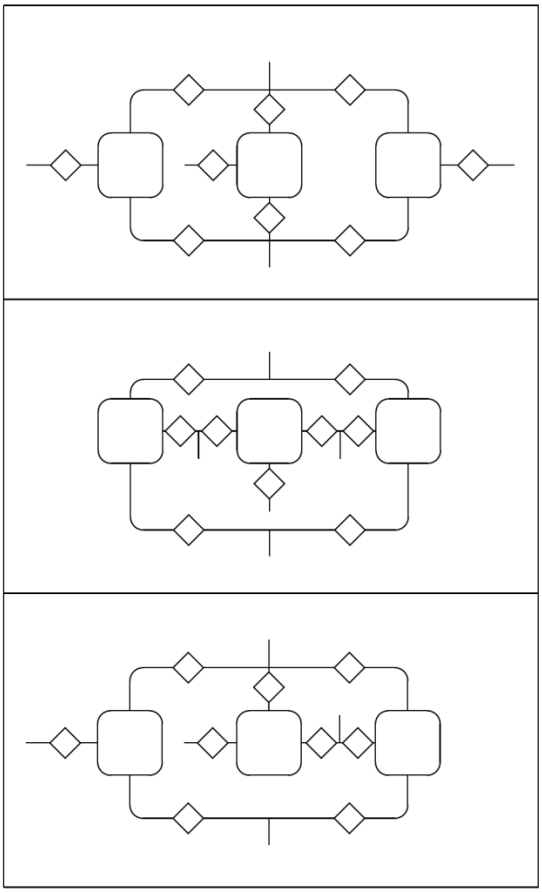

Fig. 6 Core structures for PSU with three TPMs

The functional schemes are too numerous (144) to be represented in this manuscript, so we will limit the example to only one functional scheme (Fig. 7) of PSU with 3 TPMs, which coincides with the layout of the Cadillac CT6 transmission.

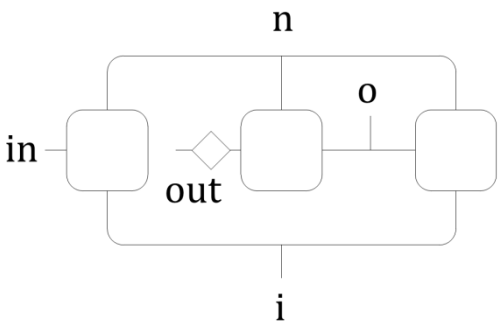

Fig. 7 Example of PSU with 3 TPMs

4. Kinematic Analysis of PSUs

The analysis of existing PS-CVTs by mean of the relationships of section 1 is particularly straightforward if the manufacturer discloses the functional parameters. This is frequently true, as many PS-CVTs include parallel hybrid modes concurrent with the mechanical points. However, when the transmission is known in terms of mutual connections and teeth ratios, it is indeed necessary to calculate or measure the aforementioned functional parameters.

This procedure may not seem convenient at first, as the engineer could rely on a traditional approach instead, solving two systems of equations for both speed and torques. However, since PS-CVTs are subject to speed and torque inversions, such approach is particularly prone to error, as the closed-loop structure of the driveline makes difficult to verify that the direction and/or value of a power flow is verisimilar. Besides, the result is a set of analytical relationships specific for each constructive solution, which makes explorative analyses bulky and tiresome, especially when several functioning modes are involved.

On the other hand, using the mechanical points:

- makes superfluous developing any further analytical model
- brings to easily comparable results
- permits to spot inconsistences even when analyzing complex or unusual designs

Moreover, since the mechanical points occur when a branch of the driveline is motionless:

- their calculation is an intuitive analytical task
- their measurement is a trivial experimental task

Eventually, as it will be clear in section 12, calculating the mechanical points is necessary in order to assess the impact of a small variation of the constructive parameters on the functional parameters when designing a new PS-CVT. This is due to the discrete nature of teeth ratios, which makes almost impossible to satisfy exactly the optimal design requirements.

4.1. Calculation approach

The known data are:

- Arrangement of the devices within the PSU and their mutual connections
- Constructive ratios of the involved gear sets (teeth ratios of OGs and PGs etc.)

The primary objective is to assess the following functional parameters:

- The mechanical points $\tau_{\#i}$ and $\tau_{\#o}$
- The related CVU speed ratios $\tau_{o_{\#i}}$ and $\tau_{i_{\#o}}$

For this purpose, we suggest the following analysis approach:

1. Labelling each branch of the PSU
2. Assigning to the shafts of each TPM their labels
3. Detailing the TPM's generic kinematic equation (eq. (43))
4. To impose $\tau_i = 0$, indexing the other unknown speed ratios accordingly ($\tau_j = \tau_{j_{\#i}}$)
5. To solve the system, thus finding the concurrent speed ratios $\tau_{\#i}$ and $\tau_{o_{\#i}}$
6. To impose $\tau_o = 0$, indexing the other unknown speed ratios accordingly ($\tau_j = \tau_{j_{\#o}}$)
7. To solve the new system, thus finding the concurrent speed ratios $\tau_{\#o}$ and $\tau_{i_{\#o}}$

Obviously, the same approach applies to the nodal ratios related to the neutral nodes. If n labels the generic neutral node, then for each neutral node it is necessary:

8. To impose $\tau_n = 0$, indexing the other unknown speed ratios accordingly ($\tau_j = \tau_{j_{\#n}}$)
9. To solve the new system, thus finding the concurrent speed ratio $\tau_{\#n}$

Labeling the PSU is trivial. The index in represents the input shaft of the transmission, which is linked to the prime mover, while the index out represents the output shaft, which is linked to the loads. The other branches of the transmission can be labeled arbitrarily, but considering that i and o refer only to the CVU.

The generic kinematic equation is obtained considering that in a TPM the speed of each port is a linear function of two others. Therefore, for each TPM we can write:

$$\tau_y = \psi_{Y/X}^{Z} \cdot \frac{k_y}{k_x} \cdot \tau_x + \psi_{Y/Z}^{X} \cdot \frac{k_y}{k_z} \cdot \tau_z \tag{43}$$

In eq. (43), k_j is the fixed ratio between ω_j (external to the TPM, see Fig. 2) and the matching speed of the planetary gear train ω_J (see Fig. 5), while $\psi_{Y/X}^{Z}$ is the ratio between the Y-speed over the X-speed when Z is motionless.

Each TPM is linked to three different branches of the PSU, so the generic indexes x, y, z must be adapted accordingly. As soon as eq. (43) has been detailed for the TPM, $\psi_{Y/X}^{Z}$ becomes a simple and univocal function of the constructive ratio $\psi = \psi_{R/S}^{C}$ of the PG (see Table 4).

Table 4 Relationships between fixed-shaft ratios of a PG and it constructive parameter.

$\psi_{R/S}^{C}$	$\psi_{S/R}^{C}$	$\psi_{S/C}^{R}$	$\psi_{C/S}^{R}$	$\psi_{C/R}^{S}$	$\psi_{R/C}^{S}$
ψ	$\frac{1}{\psi}$	$1-\frac{1}{\psi}$	$\frac{-\psi}{1-\psi}$	$\frac{1}{1-\psi}$	$1-\psi$

In general, in order to obtain the variables $\tau_{\#i}$, $\tau_{o_{\#i}}$, $\tau_{\#o}$ and $\tau_{i_{\#o}}$, it is necessary to calculate a number of variables that is twice the number of nodal ratios (including those related to the neutral nodes). In particular, we can summarize the obtained systems of equations as follows:

$$[Y_{\#i}]\begin{pmatrix} \boldsymbol{\tau_{\#i}} \\ \boldsymbol{\tau_{o\#i}} \\ \vdots \\ \boldsymbol{\tau_{n\#i}} \end{pmatrix} = \{b\} \qquad [Y_{\#o}]\begin{pmatrix} \boldsymbol{\tau_{\#o}} \\ \boldsymbol{\tau_{i\#o}} \\ \vdots \\ \boldsymbol{\tau_{n\#o}} \end{pmatrix} = \{b\} \tag{44}$$

4.2. Example

For instance, compound PSUs with up to two TPMs (section 3.2) show just four groups, so their generic kinematic equations (43) become:

$$\boldsymbol{C_{in}} \qquad 1 = \psi^{o}_{in/i} \cdot \frac{k_{in}}{k_i} \cdot \tau_i + \psi^{i}_{in/o} \cdot \frac{k_{in}}{k_o} \cdot \tau_o \tag{45}$$

$$\boldsymbol{C_{out}} \qquad \tau = \psi^{o}_{out/i} \cdot \frac{k_{out}}{k_i} \cdot \tau_i + \psi^{i}_{out/o} \cdot \frac{k_{out}}{k_o} \cdot \tau_o \tag{46}$$

$$\boldsymbol{D_i} \qquad \tau = \psi^{i}_{out/in} \cdot \frac{k_{out}}{k_{in}} \cdot 1 + \psi^{in}_{out/i} \cdot \frac{k_{out}}{k_i} \cdot \tau_i \tag{47}$$

$$\boldsymbol{D_o} \qquad \tau = \psi^{o}_{out/in} \cdot \frac{k_{out}}{k_{in}} \cdot 1 + \psi^{in}_{out/o} \cdot \frac{k_{out}}{k_o} \cdot \tau_o \tag{48}$$

If we rewrite the previous equations for the conditions in which either i or o is stopped, we obtain two linear equations for each group. If we summarize such relationships as in eq. (44), the coefficients of $[\boldsymbol{Y_{\#i}}]$, $[\boldsymbol{Y_{\#o}}]$ and $\{\boldsymbol{b}\}$ are listed in Table 5.

Table 5 Coefficients for the calculation of the mechanical points from the constructive data.

Group	$[\boldsymbol{Y}_{\#\boldsymbol{i}}]$	$[\boldsymbol{Y}_{\#\boldsymbol{o}}]$	$\{\boldsymbol{b}\}$
$\boldsymbol{C_{in}}$	$\begin{pmatrix} 0 & \psi^{i}_{in/o}\cdot\frac{k_{in}}{k_o} \\ 1 & -\psi^{i}_{out/o}\cdot\frac{k_{out}}{k_o} \\ 1 & 0 \\ 1 & -\psi^{in}_{out/o}\cdot\frac{k_{out}}{k_o} \end{pmatrix}$	$\begin{pmatrix} 0 & \psi^{o}_{in/i}\cdot\frac{k_{in}}{k_i} \\ 1 & -\psi^{o}_{out/i}\cdot\frac{k_{out}}{k_i} \\ 1 & -\psi^{in}_{out/i}\cdot\frac{k_{out}}{k_i} \\ 1 & 0 \end{pmatrix}$	$\begin{pmatrix} 1 \\ 0 \\ \psi^{i}_{out/in}\cdot\frac{k_{out}}{k_{in}} \\ \psi^{o}_{out/in}\cdot\frac{k_{out}}{k_{in}} \end{pmatrix}$
$\boldsymbol{C_{out}}$			
$\boldsymbol{D_i}$			
$\boldsymbol{D_o}$			

In order to solve eq. (44) for a specific layout, it is necessary to extract the related rows from Table 5, thus obtaining invertible square matrices.

The explicit solutions for compound designs with up to two TPMs (section 3.2) have been listed in Table 6 and in Table 7. What is more, it is possible to adapt such relationships to address shunt PS-CVTs as well, simply by introducing fictitious constructive parameters that convert the second PG into an OG (see [17]).

Table 6 Explicit solutions for the calculation of $\tau_{\#i}$ and $\tau_{o\#i}$

Scheme	$\boldsymbol{\tau_{\#i}}$	$\boldsymbol{\tau_{o\#i}}$
$\boldsymbol{C_{in}-C_{out}}$	$\frac{\boldsymbol{\tau_{o\#i}}}{\psi^{i}_{o/out}} \cdot \frac{k_{out}}{k_o}\Big\vert_{C_{out}}$	$\psi^{i}_{o/in}\frac{k_o}{k_{in}}\Big\vert_{C_{in}}$
$\boldsymbol{D_i-D_o}$	$\psi^{i}_{out/in}\frac{k_{out}}{k_{in}}\Big\vert_{D_i}$	$\frac{k_o}{\psi^{in}_{out/o}}\Big\vert_{D_o} \cdot \left(\frac{\boldsymbol{\tau_{\#i}}}{k_{out}} - \frac{\psi^{o}_{out/in}}{k_{in}}\right)\Big\vert_{D_o}$
$\boldsymbol{D_i-C_{in}}$	$\psi^{i}_{out/in}\frac{k_{out}}{k_{in}}\Big\vert_{D_i}$	$\psi^{i}_{o/in}\frac{k_o}{k_{in}}\Big\vert_{C_{in}}$
$\boldsymbol{D_i-C_{out}}$	$\psi^{i}_{out/in}\frac{k_{out}}{k_{in}}\Big\vert_{D_i}$	$\boldsymbol{\tau_{\#i}} \cdot \psi^{i}_{o/out}\frac{k_o}{k_{out}}\Big\vert_{C_{out}}$
$\boldsymbol{D_o-C_{in}}$	$\boldsymbol{\tau_{\#o}} + \boldsymbol{\tau_{o\#i}} \cdot \psi^{in}_{out/o}\frac{k_{out}}{k_o}\Big\vert_{D_o}$	$\psi^{i}_{o/in}\frac{k_o}{k_{in}}\Big\vert_{C_{in}}$
$\boldsymbol{D_o-C_{out}}$	$\frac{\boldsymbol{\tau_{\#o}}}{1-\frac{k_{out}\,\psi^{in}_{out/o}}{k_o}\Big\vert_{D_o} \cdot \frac{k_o\,\psi^{i}_{o/out}}{k_{out}}\Big\vert_{C_{out}}}$	$\boldsymbol{\tau_{\#i}} \cdot \frac{k_o\,\psi^{i}_{o/out}}{k_{out}}\Big\vert_{C_{out}}$

Table 7 Explicit solutions for the calculation of $\tau_{\#o}$ and $\tau_{i_{\#o}}$

Scheme	$\boldsymbol{\tau_{\#o}}$	$\boldsymbol{\tau_{i_{\#o}}}$
$\boldsymbol{C_{in} - C_{out}}$	$\frac{\tau_{i_{\#o}}}{\psi^{o}_{i/out}} \cdot \frac{k_{out}}{k_i}\Big\vert_{C_{out}}$	$\psi^{o}_{i/in} \frac{k_i}{k_{in}}\Big\vert_{C_{in}}$
$\boldsymbol{D_i - D_o}$	$\psi^{o}_{out/in} \frac{k_{out}}{k_{in}}\Big\vert_{D_o}$	$\frac{k_i}{\psi^{in}_{out/i}}\Big\vert_{D_i} \cdot \left(\frac{\tau_{\#o}}{k_{out}} - \frac{\psi^{i}_{out/in}}{k_{in}}\right)\Big\vert_{D_i}$
$\boldsymbol{D_i - C_{in}}$	$\tau_{\#i} + \tau_{i_{\#o}} \cdot \psi^{in}_{out/i} \frac{k_{out}}{k_i}\Big\vert_{D_i}$	$\psi^{o}_{i/in} \frac{k_i}{k_{in}}\Big\vert_{C_{in}}$
$\boldsymbol{D_i - C_{out}}$	$\frac{\tau_{\#i}}{1 - \frac{k_{out}\,\psi^{in}_{out/i}}{k_i}\Big\vert_{D_i} \cdot \frac{k_i\,\psi^{o}_{i/out}}{k_{out}}\Big\vert_{C_{out}}}$	$-\tau_{\#o} \cdot \psi^{o}_{i/out} \frac{k_i}{k_{out}}\Big\vert_{C_{out}}$
$\boldsymbol{D_o - C_{in}}$	$\psi^{o}_{out/in} \frac{k_{out}}{k_{IN}}\Big\vert_{D_o}$	$\psi^{o}_{i/in} \frac{k_i}{k_{in}}\Big\vert_{C_{in}}$
$\boldsymbol{D_o - C_{out}}$	$\psi^{o}_{out/in} \frac{k_{out}}{k_{IN}}\Big\vert_{D_o}$	$\tau_{\#o} \cdot \psi^{o}_{i/out} \frac{k_i}{k_{out}}\Big\vert_{C_{out}}$

5. Ideal power-flow analysis of PSUs

In a PS-CVT, several power flows change sign with τ and Θ in a hardly predictable way. Indeed, conditions such as power recirculation, acceleration assistance and regenerative braking considerably alter the power flow distribution.

This might lead to errors, and thus inaccurate results. Accordingly, their preliminary calculation is essential in order to obtain physically reliable models.

In particular, if we assume that the losses in the PSU are negligible, it is possible to perform the preliminary calculation of the internal power flows using the method described in detail in section 1.3.

5.1. Ratios between powers transmitted by the shafts internal to the PSU

In section 2 we have described a set of characteristic functions ruled by the nodal ratios. In particular, in section 2.1.1. we have stated that they represent the ideal ratios between the powers transmitted by two shafts of a TPM (see Fig. 2).

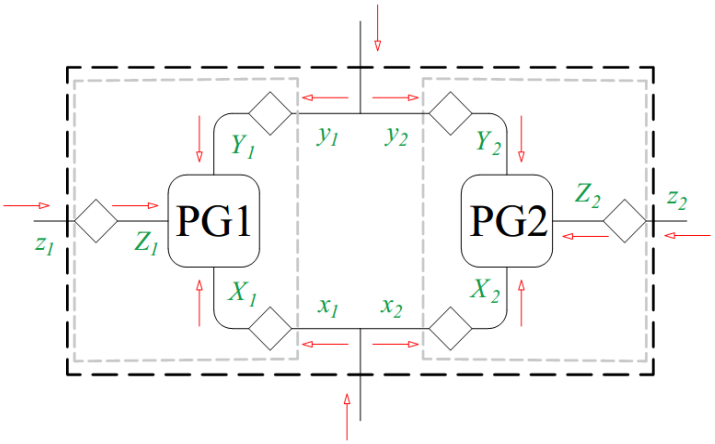

Fig. 8 PSU with two TPMs

Fig. 8 is an example of PSU with two TPMs. The main ports are linked directly to the TPMs (left and right) or to the isokinetic joints (up and down). Squares and rhombi represent

planetary and ordinary gear sets. The capital letters refer to the shafts of the PGs, the lowercases to the external shafts of the TPMs. The red arrows represent the power flows. Such powers are assumed to be positive if entering their reference subsystem, which is either the PSU, the TPM or the PG (Fig. 8).

For each TPM, it is possible to write two linearly independent relationships by mean of the general expression (39) and (40) provided in section 2 :

$$\phi_{x/y}^{z}\, P_x + P_y = 0 \tag{49}$$

$$\phi_{x/z}^{y}\, P_x + P_z = 0 \tag{50}$$

5.2. Isokinetic joints (nodes)

A PSU include two or more isokinetic joints (IJ), i.e. shafts of different TPMs that spin together. For these joints is always valid the principle of conservation of power:

$$P_n|_1 + P_n|_2 + \ldots = 0 \tag{51}$$

In which $P_n|_j$ is the power flowing through the shaft of the j-th TPM linked to n-th isokinetic joint.

5.3. Calculation

For given input and output power, two eq. (49)-(50) for each TPM and one eq. (51) for each IJ permit to assess the ideal internal power flow distribution, as described in [20].

This approach can be applied to the analysis of any PS-CVT, provided that its nodal ratios are known, or have been calculated as in section 4. Yet, if the PSU includes up to two active TPMs, it is not necessary to solve a system of equations, as, for given input and output power, we can calculate the powers incoming from the CVU regardless the layout of the PSU.

Indeed, in section 1 it has been shown that the mechanical points $\tau_{\#i}$ and $\tau_{\#o}$ (see section 1.1) permit calculating the relative power flows and torques on the main shafts of any ideal PSU by mean of the equations in section 1.2 and 1.3. However, in this case one of the power flowing in the TPM is known, so it is always possible to calculate the other two by mean of eq. (39) and (40).

6. Mechanical losses in the PSU

Each gear set within the PSU is accountable for a certain amount of mechanical losses.

As stated before, the core structure of the PSU is the TPM, which consists of one PG and up to three OGs (Fig. 2).

In order to predict the power losses of the generic TPM as a whole, the behavior of its constituent devices must be analyzed separately.

6.1. Losses in the planetary gear trains

In literature, the calculation of the mechanical efficiency of a PG is often achieved assuming the real power flow distribution as the sum of two virtual powers, which refer to fixed-shaft conditions [44, 45]. However, it has been shown in [125] that under specific circumstances the validity of the previous relationships ceases to subsist. For this reason, their correct application requires to distinguish between several conditions accordingly to the mutual relations between the angular velocities of the PG. Nonetheless, in this section we propose a simpler approach, which permits to address the problem by mean of a synthetic test, performed directly on the sign of the calculated mechanical loss. Since the test itself relies on the physical consistence of the obtained results, our model behaves properly in any condition, including the synchronism of the PG.

We will refer to the generic shafts of the PGs with the capital labels X, Y, Z, as in Fig. 8. In ideal conditions, for a PG the following power balance is valid:

$$P_X + P_Y + P_Z = 0 \tag{52}$$

However, in real conditions, it is:

$$\bar{P}_X + \bar{P}_Y + \bar{P}_Z + \bar{P}_L = 0 \tag{53}$$

Since the powers are positive if entering their reference subsystem, it must be $\bar{P}_L \leq 0$. Accordingly, if $\eta_{Y/X}^Z$ is the fixed-Z apparent efficiency, defined as follows:

$$\eta_{Y/X}^Z = -\frac{\bar{P}_Y}{\bar{P}_X}\bigg|_{\tau_Z=0} = \frac{\bar{T}_Y}{\bar{T}_X}\cdot\frac{T_X}{T_Y} = \left(\frac{\bar{P}_Y}{\bar{P}_X}\right)\Big/\left(\frac{P_Y}{P_X}\right) \tag{54}$$

then the real torque ratios applied to the PG are respectively:

$$\frac{\bar{T}_Y}{\bar{T}_X} = -\frac{\eta_{Y/X}^Z}{\psi_{Y/X}^Z} \tag{55}$$

$$\frac{\bar{T}_Z}{\bar{T}_X} = \frac{\eta_{Y/X}^Z - \psi_{Y/X}^Z}{\psi_{Y/X}^Z} \tag{56}$$

in which $\psi_{Y/X}^Z$ is:

$$\psi_{Y/X}^Z = \frac{\omega_Y - \omega_Z}{\omega_X - \omega_Z} \tag{57}$$

Substituting the previous eq. (54)-(57) in (53), we obtain:

$$\bar{P}_L|_{PG} = -\left(1 - \eta_{Y/X}^Z\right)(\omega_X - \omega_Z)\,\bar{T}_X \tag{58}$$

Since $\bar{P}_L \leq 0$, then the previous relationship (58) implies that $\eta_{Y/X}^Z$ switches its value. In particular, this condition occurs when:

- The planetary gear train reaches its synchronism.
- The torque transmitted by the shafts of the PG changes sign.

It is convenient to rewrite the latter relationship (58) in terms of characteristic functions (eq. 39), as they are independent from the OGs, and thus equal for the PG and TPM (see section 2.1.1.):

$$\bar{P}_L|_{PG} = -\left(1 - \eta_{Y/X}^Z\right)\left(\frac{\phi_{x/y}^z - \psi_{x/y}^z}{1 - \psi_{x/y}^z}\right)\bar{P}_X \tag{59}$$

In which $\psi^z_{x/y} = \phi^z_{x/y}\big|_{\tau_*}$, and τ_* is the overall speed ratio concurrent with the synchronism of the PG.

Therefore, we can formulate the following test:

$$\begin{matrix} \eta^Z_{Y/X} < 1 \\ \text{if} \\ \eta^Z_{Y/X} > 1 \end{matrix} \qquad \begin{matrix} \left(\frac{\phi^z_{x/y} - \psi^z_{x/y}}{1 - \psi^z_{x/y}}\right) \bar{P}_X > 0 \\ \\ \left(\frac{\phi^z_{x/y} - \psi^z_{x/y}}{1 - \psi^z_{x/y}}\right) \bar{P}_X < 0 \end{matrix} \tag{60}$$

Typically, for a PG it is known the fixed-carrier (aka basic) efficiency, i.e. $\eta_0 = \eta^C_{R/S}$, where R, C and S represent the ring, carrier and sun gear of the PG. Considering that the torques applied to a PG are speed independent, the fixed-ring and fixed-sun efficiencies can be calculated by mean of the relationships of Table 8, in which $\psi = \psi^C_{R/S}$ is the Willis' ratio as usual.

Table 8 Relationships between fixed-shaft apparent efficiencies of a PG.

$\boldsymbol{\eta^C_{R/S}}$	$\boldsymbol{\eta^C_{S/R}}$	$\boldsymbol{\eta^R_{S/C}}$	$\boldsymbol{\eta^R_{C/S}}$	$\boldsymbol{\eta^S_{C/R}}$	$\boldsymbol{\eta^S_{R/C}}$
η_0	$\frac{1}{\eta_0}$	$\frac{1-\psi}{\eta_0-\psi}$	$\frac{\eta_0-\psi}{1-\psi}$	$\frac{\eta_0-\psi}{\eta_0(1-\psi)}$	$\frac{\eta_0(1-\psi)}{\eta_0-\psi}$

Assessing $\eta^Z_{Y/X}$ and $\eta^Y_{Z/X}$ between the shafts of a PG requires:

- replacing *X,Y,Z* with *R,C,S* of the PG in the proper order
- performing the test (60) on one parameter $\eta^Z_{Y/X}$
- using the related relationship listed in Table 8 to establish if $\eta^Z_{Y/X}$ takes the correct value for $\eta_0 < 1$ or for its reciprocal
- calculating $\eta^Y_{Z/X}$ by mean of Table 8

The test (60) should be performed using the real power $\bar{P}_X$ flowing through the shaft X of the PG. Yet, such power is altered not only by the mechanical loss in the ordinary gear set in the same branch of the TPM, but also by all the other mechanical losses within the PSU.

Accordingly, if the real power flow $\bar{P}_X$ is not known, the test must be performed using its ideal value, which can lead to errors, especially in proximity of reversals of the real power flow $\bar{P}_X$ itself. The error in terms of $\bar{P}_L|_{PG}$ (eq. 59) in this case is generally tolerable, as the module of $\bar{P}_X$ in proximity of power flow reversals is intrinsically small. Nonetheless, in this case an iterative calculation might be adopted in order to obtain completely reliable results.

6.2. Losses in the ordinary gears

For an OG (or any kinematically equivalent device), we can write:

$$\eta_{X/x} = \frac{\bar{P}_X}{\bar{P}_x} \tag{61}$$

in which $\bar{P}_x$ is the power flowing in the *x*-th shaft, which is external to the TPM, and $\bar{P}_X$ is the power flowing in the *X*-th shaft, which belongs to the PG. Their ratio $\eta_{X/x}$ is the apparent efficiency of the ordinary gearing k_x linking the shafts *x* to the shaft *X* (see Fig. 8). Accordingly, the absolute losses in the OG is simply:

$$\bar{P}_L|_{OG} = -\left(1 - \eta_{X/x}\right)\bar{P}_x \tag{62}$$

Such losses are negative, so when $\bar{P}_x$ changes sign, so does $\left(1 - \eta_{X/x}\right)$. The related test can be summarized as follows:

$$\begin{matrix} \eta_{X/x} < 1 & & \bar{P}_x > 0 \\ & \text{if} & \\ \eta_{X/x} > 1 & & \bar{P}_x < 0 \end{matrix} \tag{63}$$

If the OG is obtained using a PG, then it is possible calculating the parameter $\eta_{X/x} = \eta^z_{X/x}$ by mean of the relationships listed Table 8, assuming that the blocked shaft is Z. In this case it is sufficient to replace the labels x, X, Z with R, C, S (representing ring, carrier and sun gear of the PG) in the observed order.

7. Real power flow distribution

The mechanical losses alter the torque distribution in the PSU; therefore, a reliable model for their prediction is necessary in order to permit an effective control of the PS-CVT.

7.1. Exact method

It is possible to follow a procedure analogous to that described in section 5 in order to assess the real power flow distribution. The efficiency parameters must be calculated for each OG and PG as in section 6.1 and 6.2, and then it is possible to correct the power ratios between the shafts of each TPM. Indeed, if we combine eq. (39), (54) and (61), the real power ratio is:

$$\frac{\bar{P}_y}{\bar{P}_x} = \eta^z_{y/x} \frac{P_y}{P_x} = -\left(\eta^z_{Y/X} \cdot \frac{\eta_{X/x}}{\eta_{Y/y}}\right) \phi^z_{x/y} \tag{64}$$

Which is similar to eq. (40).

Similarly, each IJ still provides the power balance:

$$\bar{P}_n|_1 + \bar{P}_n|_2 + \ldots = 0 \tag{65}$$

Two eq. (64) for each TPM and one eq. (65) for each IJ, for given input and output power, permit to calculate the internal power flow distribution, including the real powers flowing through the shafts of the CVU.

Eventually, in order to assess the mechanical losses is enough to sum the powers flowing through the main shafts:

$$\bar{P}_L = -(\bar{P}_i + \bar{P}_o + \bar{P}_{in} + \bar{P}_{out}) \tag{66}$$

7.2. Approximated method

The method described in section 7.1 leads to exact results. Nevertheless, since $\bar{P}_L \leq 0$, $\eta^z_{y/x}$ often switches accordingly to the sign of speeds and applied torques (see eq. (60) and (63)). In other terms, the real power ratio (64) will be discontinuously proportional to the ideal one, and it will be necessary segmenting each functioning mode in order to predict the efficiency parameter of each TPM, which can show numerous discontinuities.

This leads to several variants of the analytical description of the model, making the analysis and design problem quite obscure. Furthermore, performing the tests (60) and (63) by mean of the ideal power flow distribution requires some iterations in order to get exact results. For these reasons, the exact analytic process can be time-consuming and tedious, especially when multiple functioning modes are involved.

Therefore, hereinafter we describe an approximate "blind" model; it is derived from the exact one, but it permits to ignore the discontinuities.

In particular, a proper functioning of this model requires low mechanical losses in the PGs, and thus limited deviations of the parameters $\eta^Z_{Y/X}$ from one. This is very likely for a PS-CVT designed for hybrid electric vehicles, as the efficiency of the mechanical path is supposed to be high. Nevertheless, some PGs can show very low values of $\eta^Z_{Y/X}$, even with a very high basic efficiency η_0. For instance, if we consider tolerable a deviation of $|1 - \eta^Z_{Y/X}| < 0.1$ (see next eq. (67)), then, for $\eta_0 \approx 0.95$, from Table 8 we get that all the existing transmissions including PGs with a constructive ratio $0.5 < \psi < 1.5$ cannot be addressed with the approximated model.

In particular, if $\eta_0 \to 1$, when it switches to its reciprocal in eq. (62), also the related value of $\eta^Z_{Y/X}$, calculated from Table 8, becomes about the reciprocal of the previous one. In addition, if we linearize the latter by mean of the Taylor formula, we obtain:

$$\frac{1}{\eta^Z_{Y/X}} \approx 2 - \eta^Z_{Y/X} \tag{67}$$

Therefore, when η_0 switches, $\eta_{Y/X}^Z \approx 2 - \eta_{Y/X}^Z$, and the module of the power loss equation (62) remains basically the same.

In addition, in this case, it is licit to use directly the ideal power flow distribution, i.e. to assume that $\bar{P}_x \approx P_x$. Indeed, the mechanical losses are a small fraction of the power flows, and their effects on them are small. As a result, we can write simply:

$$\bar{P}_L|_{PG} \approx -\left|\left(1 - \eta_{Y/X}^Z\right)\left(\frac{\phi_{x/y}^z - \psi_{x/y}^z}{1 - \psi_{x/y}^z}\right) P_x\right| \tag{68}$$

The absolute operator is conceivable because power loss must be negative in any case.

In conclusion, if the basic efficiency η_0 of PG is high, and ψ is far from one, eq. (68) permits to assess the PG's power loss by mean of the ideal power flow distribution and ignoring the switches of the basic efficiency η_0, and thus of the related parameter $\eta_{Y/X}^Z$.

Similarly, if an OG is present in TPM, under the same simplification hypothesis of the PGs, its losses can be approximated to:

$$\bar{P}_L|_{OG} \approx -\left|\left(1 - \eta_{X/x}\right) P_x\right| \tag{69}$$

Such losses, summed to those of the planetary gear trains, qualifies the mechanical efficiency of the transmission.

7.3. Link between power losses and CVU power flows

It is important to assess with sufficient precision the real power flowing through each shaft of the CVU. Indeed, for given input and output power, the PSU's mechanical losses will be compensated by the CVU, whose power flows will be slightly different from the ideal ones.

The overall mechanical losses, normalized in respect of P_{in}, can be written as follows:

$$\bar{p}_L = \sum \bar{p}_{loss}|_{PG} + \sum \bar{p}_{loss}|_{OG} \tag{70}$$

Furthermore, the following relationships exists:

$$\bar{p}_i + \bar{p}_o = \bar{\theta}_i\,\tau_i + \bar{\theta}_o\tau_o = -(1 - \eta + \bar{p}_L) \tag{71}$$

The real torque ratios $\bar{\theta}_i$ and $\bar{\theta}_o$ applied to the shafts of the CVU are discontinuous, but they continue to be linear functions of $\Theta = -\eta/\tau$, just like θ_i and θ_o (see section 1.2). Accordingly, in order to assess their new value, we can write a system of two equations, i.e. eq. (71) and its directional derivative for which Θ is constant (and so $\bar{\theta}_i$ and $\bar{\theta}_o$ remain constant as well), which is in the direction of the vector $\begin{bmatrix}\tau\\ \eta\end{bmatrix} = \sqrt{\tau^2+\eta^2}\begin{bmatrix}\hat{\tau}\\ \hat{\eta}\end{bmatrix}$:

$$\begin{bmatrix} \tau_i & \tau_o \\ \dfrac{d\tau_i}{d\tau}\,\hat{\tau} & \dfrac{d\tau_o}{d\tau}\,\hat{\tau} \end{bmatrix}\begin{pmatrix}\bar{\theta}_i\\ \\ \bar{\theta}_o\end{pmatrix} = \begin{pmatrix} \eta - 1 - \bar{p}_L \\ \\ \hat{\eta} \; - \nabla\bar{p}_L \cdot \begin{bmatrix}\hat{\tau}\\ \hat{\eta}\end{bmatrix}\end{pmatrix} \tag{72}$$

After extensive math, we get:

$$\bar{p}_i = \bar{\theta}_i\,\tau_i = \; p_i - \bar{p}_L\frac{\tau_i}{\tau_{i_{\#o}}} - \nabla\bar{p}_L \cdot \begin{bmatrix}\tau\\ \eta\end{bmatrix} p_i|_{\eta=1} \tag{73}$$

$$\bar{p}_o = \; \bar{\theta}_o\tau_o = p_o - \bar{p}_L\frac{\tau_o}{\tau_{o_{\#i}}} - \nabla\bar{p}_L \cdot \begin{bmatrix}\tau\\ \eta\end{bmatrix} p_o|_{\eta=1} \tag{74}$$

in which $\nabla\bar{p}_L$ is the gradient of $\bar{p}_L$, defined as $\nabla\bar{p}_L = \begin{bmatrix}\frac{d\bar{p}_L}{d\tau} & \frac{d\bar{p}_L}{d\eta}\end{bmatrix}$, $p_o|_{\eta=1} = -p_i|_{\eta=1}$ and $\frac{\tau_i}{\tau_{i_{\#o}}} = \frac{\tau - \tau_{\#i}}{\tau_{\#o} - \tau_{\#i}} = 1 - \frac{\tau_o}{\tau_{o_{\#i}}}$ (see section 1.1).

For given $\bar{p}_L$ and $\nabla\bar{p}_L$, eq.(73) and (74) are scheme independent and have been obtained with no simplifying assumptions (i.e. are exact), so only the calculation of $\bar{p}_L$ is a possible source of errors.

Moreover, if we keep the relationship between η and $\bar{p}_L$ as implicit, calculating the latter as a function of Θ and τ instead, then $\frac{d\bar{p}_L}{d\eta} = 0$, the previous equations can be simplified even more:

$$\bar{p}_i = p_i - \bar{p}_L \frac{\tau_i}{\tau_{i_{\#o}}} - \frac{d\bar{p}_L}{d\tau} p_i|_{\eta=1} \quad (75)$$

$$\bar{p}_o = p_o - \bar{p}_L \frac{\tau_o}{\tau_{o_{\#i}}} - \frac{d\bar{p}_L}{d\tau} p_o|_{\eta=1} \quad (76)$$

In order to calculate the losses within the CVU is necessary to assess the absolute powers transmitted by the CVU's shafts to the PSU by mean of the previous relationships, taking into account also absolute speeds and applied torques. Then, with the aid of an efficiency map or of an analytical model of the CVU, it is possible to calculate with precision the power lost within the variator drive, thus calculating the overall power loss of the PS-CVT in its entirety.

8. Implicit Automatic approach

In the previous section (see also [19]), we have provided a simplified analytical approach to the problem, which permits to quantify the different sources of loss and offers design criteria to the engineer. Thanks to its modularity and to the intelligibility of its intermediate results, such method is particularly suitable during the preliminary design of the PSU, as it allows the engineer to compare constructive alternatives.

However, when the transmission is defined, it is possible to forego such advantages in favor of a faster and simpler numeric implementation. The key assumption is that, in presence of mechanical losses, the torque distribution of any planetary transmission is still related to the kinematic of an ideal PSU, but with its constructive parameters slightly altered by the related loss factors. A similar concept has been proposed in [46,76] with the reticulator and responsivity theorems, and lately it has been elaborated furtherly in [60,61, 68], but, to our knowledge, there is not a truly general, systematic and ready-to-use method available in literature so far.

In this chapter, we describe the relationships between speeds and torques applied to the main shafts of an ideal PSU, and how they change when mechanical losses are taken into account. Eventually, a general expression for the calculation of the global power losses themselves is achieved.

8.1. Theory

In absence of mechanical losses, the relationships between speeds and torques of the main shaft of the PSU are:

$$\begin{Bmatrix} \omega_o \\ \\ \omega_i \end{Bmatrix} = [\Omega] \begin{Bmatrix} \omega_{out} \\ \\ \omega_{in} \end{Bmatrix} \tag{77}$$

$$\begin{Bmatrix} T_o \\ T_i \end{Bmatrix} = [T] \begin{Bmatrix} T_{out} \\ T_{in} \end{Bmatrix} \tag{78}$$

In which the matrices [Ω] and [T] can be expressed in their general forms as:

$$[\Omega] = \frac{1}{\tau_{\#o} - \tau_{\#i}} \begin{bmatrix} -\tau_{o_{\#i}} & \tau_{\#o}\,\tau_{o_{\#i}} \\ \tau_{i_{\#o}} & -\tau_{\#i}\,\tau_{i_{\#o}} \end{bmatrix} \tag{79}$$

$$[\mathrm{T}] = -[\Omega^{-1}]' \tag{80}$$

The elements of [Ω] and [T] are the functional parameters of the PS-CVT, which can be calculated from the constructive parameters of the PSU. In other words, it is:

$$\Omega = \Omega(k_1, k_2, \dots k_N) \tag{81}$$

$$\mathrm{T} = \mathrm{T}(k_1, k_2, \dots k_N) \tag{82}$$

The relationships between functional and constructive parameters depend on the layout of the transmission and have been listed in section 4.2 for compound PS-CVTs with up to two PGs and six OGs. On the other hand, the functional parameters $\tau_{\#o}$, $\tau_{\#i}$, $\tau_{i_{\#o}}$ and $\tau_{o_{\#i}}$, which are the mechanical points and the related speed ratios of the electric machines, represent the true key design parameters, as they govern either the kinematic and the ideal power flow distribution, whichever it is the layout of the transmission.

If now we take into account the mechanical losses within the PSU, the torque matrix [T] must change into $[\widetilde{\mathrm{T}}]$, as each torque ratio between shafts belonging to the same device is modified by the related loss factor. Nonetheless, each loss factor $\eta_j^{\pm 1}$ affects exclusively the related constructive parameter k_j, so that the system of equations that lead to the new matrix $[\widetilde{\mathrm{T}}]$ remains formally identical to the former, but with slightly different fictitious kinematic

parameters $\tilde{k}_j = \eta_j^{\pm 1}\, k_j$. Accordingly, the relationship (80) between speed and torque matrix continues to subsist, but now it is:

$$\begin{Bmatrix} \bar{T}_o \\ \bar{T}_i \end{Bmatrix} = \left[\widetilde{\mathrm{T}}\right] \begin{Bmatrix} \bar{T}_{out} \\ \bar{T}_{in} \end{Bmatrix} \tag{83}$$

Similarly, it is:

$$\left[\widetilde{\mathrm{T}}\right] = -\left[\widetilde{\Omega}^{-1}\right]' \tag{84}$$

In which $\widetilde{\Omega}$ is the altered kinematic matrix:

$$\widetilde{\Omega} = \Omega\left(k_1\eta_1^{\pm 1}, k_2\eta_2^{\pm 1}, \dots k_N\eta_N^{\pm 1}\right) \tag{85}$$

As a result, we have to calculate a new set of fictitious functional parameters $\tilde{\tau}_{o_{\#i}}$, $\tilde{\tau}_{i_{\#o}}$, $\tilde{\tau}_{\#i}$ and $\tilde{\tau}_{\#o}$ using the altered constructive parameters $\tilde{k}_j = k_j\eta_j^{\pm 1}$. In particular, in section 4 we provide a general automated method to perform such task. Nonetheless, this method applies to any kinematic description of the PS-CVT, which means that the use of our functional parameters is not mandatory.

Now, in order to obtain the general expression of the overall mechanical loss, it is sufficient to perform some simple matrix operations. In particular, we know that the neat power exchanged by the main shafts will be equal to the mechanical losses within the PSU:

$$\bar{P}_L = -(\bar{P}_i + \bar{P}_o) - (\bar{P}_{in} + \bar{P}_{out}) \tag{86}$$

The element $\bar{P}_i + \bar{P}_o$ can be easily assessed in its parts thanks to eq. (77) and (83)-(84):

$$\bar{P}_i + \bar{P}_o = \begin{Bmatrix} \omega_o \\ \omega_i \end{Bmatrix}' \begin{Bmatrix} \bar{T}_o \\ \bar{T}_i \end{Bmatrix} = -\begin{Bmatrix} \omega_{out} \\ \omega_{in} \end{Bmatrix}' [\Omega]' \left[\widetilde{\Omega}^{-1}\right]' \begin{Bmatrix} \bar{T}_{out} \\ \bar{T}_{in} \end{Bmatrix} \tag{87}$$

While the element $\bar{P}_{in} + \bar{P}_{out}$ is simply:

$$\bar{P}_{in} + \bar{P}_{out} = \begin{Bmatrix} \omega_{out} \\ \omega_{in} \end{Bmatrix}' [I] \begin{Bmatrix} \bar{T}_{out} \\ \bar{T}_{in} \end{Bmatrix} \tag{88}$$

In which $[I]$ is the identity matrix. Accordingly, the absolute power loss is equal to:

$$\bar{P}_L = \begin{Bmatrix} \omega_{out} \\ \omega_{in} \end{Bmatrix}' \left([\Omega]' \left[\widetilde{\Omega}^{-1}\right]' - [I] \right) \begin{Bmatrix} \bar{T}_{out} \\ \bar{T}_{in} \end{Bmatrix} \tag{89}$$

Such quantity must be always negative, as we consider positive the powers entering the PSU. In addition, it can be normalized in respect of the power supplied by the engine, thus being expressed in terms of overall speed and torque ratios τ and Θ:

$$\bar{p}_L = \frac{\bar{P}_L}{\bar{P}_{in}} = \begin{Bmatrix} \tau \\ 1 \end{Bmatrix}' \left([\Omega]' \left[\widetilde{\Omega}^{-1}\right]' - [I] \right) \begin{Bmatrix} \Theta \\ 1 \end{Bmatrix} \tag{90}$$

Which can be used to build a general efficiency map (an additional map may be calculated in order to address the cranking of the engine, as in this case $\bar{p}_L$ becomes positive).

8.2. Calculation of $[\widetilde{\Omega}]$

The main drawback of eq. (89) is that we don't know yet which coefficient c_j must be assigned to the loss factor η_j^{cj} of the *j*th constructive parameter k_j (see eq.(85)), and thus we cannot calculate $\widetilde{\Omega}$. However, we can be certain that each loss factor will cause an increase of the mechanical losses. As a result, we can proceed iteratively, by assigning a guess value (± 1) to the coefficient c_j (previously null) for $j = 1{:}N$, thus calculating the updated value of the altered kinematic matrix $\tilde{\Omega}_j$:

$$\tilde{\Omega}_j = \Omega\left(k_1\, \eta_1^{c1}, k_2\, \eta_2^{c2}, \dots\, k_j\, \eta_j^{cj}, k_{j+1}\, \eta_{j+1}^{0}, \dots k_N\, \eta_N^{0}\right) \tag{91}$$

If the related value of overall power loss (always negative):

$$\bar{P}_{L_j} = \begin{Bmatrix} \omega_{out} \\ \omega_{in} \end{Bmatrix}' \left([\Omega]' \left[\widetilde{\Omega}_j^{-1} \right]' - [I] \right) \begin{Bmatrix} \bar{T}_{out} \\ \bar{T}_{in} \end{Bmatrix} \tag{92}$$

is greater than the previous one $\left(\bar{P}_{L_j} > \bar{P}_{L_{j-1}} \right)$, we change the sign of c_j and proceed guessing the next c_{j+1} until $\tilde{\Omega} = \tilde{\Omega}_N$ is definite.

8.3. Calculation of the transition zones for $[\widetilde{\Omega}]$

While $[\Omega]$ is constant within a mode whichever are the working conditions, $[\widetilde{\Omega}]$ can be constant only within limited zones, provided that the loss factors are constant as well. In particular, $\bar{p}_L$ doesn't show discontinuities in its value, but it does in its gradient. As a result, we can assert that the *j*th loss factor responsible for the gradient's discontinuity doesn't cause losses concurrently, which implies that it exists a relationship between τ and Θ that foils the contribution of η_j to $[\widetilde{\Omega}]$. Accordingly, if $\widetilde{\Omega}_j$ is the speed matrix calculated when only $c_j = 0$:

$$\widetilde{\Omega}_j = \Omega\left(k_1 \eta_1^{c1}, \dots k_j \eta_j^0, \dots, k_N \eta_N^{cN}\right) \tag{93}$$

The difference of eq. (90) calculated for both $\widetilde{\Omega}_j$ and $\widetilde{\Omega}$ is null for points belonging to the transition zones:

$$0 = \begin{Bmatrix} \tau \\ 1 \end{Bmatrix}' [\Lambda_j] \begin{Bmatrix} \Theta \\ 1 \end{Bmatrix} \tag{94}$$

With:

$$[\Lambda_j] = [\Omega]' \left(\left[\widetilde{\Omega}^{-1} \right]' - \left[\widetilde{\Omega}_j^{-1} \right]' \right) \tag{95}$$

In particular, the relationship between Θ and τ (and vice versa) introduced by eq. (94) is respectively:

$$\Theta_j = -\frac{\lambda_{j(2,2)} + \tau\,\lambda_{j(1,2)}}{\lambda_{j(2,1)} + \tau\,\lambda_{j(1,1)}} \tag{96}$$

$$\tau_j = -\frac{\lambda_{j(2,2)} + \Theta\,\lambda_{j(2,1)}}{\lambda_{j(1,2)} + \Theta\,\lambda_{j(1,1)}} \tag{97}$$

In which $\lambda_{j(\mathrm{m,n})}$ is the element of $[\Lambda_j]$ in the row *m* and column *n*. Two points are within the same zone if their coordinates satisfy all the boundaries calculated for $j = 1{:}\,N$ by mean of eq. (96) accordingly to the same criteria. In particular, it can happen that $\Theta_j \to \pm\infty$ when the actual boundary is entirely due to kinematics (for instance, because one PG is synchronous). In this case, it is appropriate to introduce a numeric threshold and assign to the boundary a positive arbitrarily high value, as the code may suffer numeric instability or produce an error (in theory, it is performing a division by zero). On the other hand, $\Theta \to \pm\infty$ doesn't imply any factual boundary, so it is safe to assign to it a value that produces always the same outcome when compared to the torque ratio of any working point. Obviously eq. (96) produce N boundaries for both τ and Θ, so the actual boundaries are the ones closer to the analyzed working point. In particular, the zones appear to be rectangular (see Fig. 23), so it is enough to calculate the boundaries for just one point within each zone.

Calculating the transition lines is interesting because the computational effort is analogous to that necessary to calculate $\tilde{\Omega}_j$ in a (couple) of nearby points, as it is necessary to calculate and invert $\widetilde{\Omega}_j$ and $[\Lambda_j]$ for $j = 1{:}\,N$. Vice versa, "blindly" applying eq.(91) and (92) to a tight grid of points would bring to potentially hundreds of unnecessary calculation within the same zone. In addition, it permits to identify which coefficient(s) will switch when crossing a boundary, which means that the iterative approach described by eq.(91) and (92) can be largely avoided when the working point transits to a different zone contiguous to the first one.

8.4. Internal power flows

The internal power flows might be calculated using the same methodology described in section 7.1, considering that the efficiency parameters have already been established.

However, it is possible to extend the same concept described above to any branch of the PSU. In particular, the real torque applied to the generic shaft x of a TPM is equal to the ideal torque calculated for constructive parameters altered by their efficiencies:

$$\bar{\theta}_x\big|_{TPM} = \theta_x(k_1\eta_1^{c1}, k_2\eta_2^{c2}, \dots k_N\eta_N^{cN})|_{TPM} \tag{98}$$

We did not provide relationships for the calculation of internal torques of the PSU; however, the latter are indeed ratios between powers and speeds. Accordingly, the relative power flowing through the same shaft is:

$$\bar{p}_x|_{TPM} = \tau_x \cdot \left.\frac{p_x(k_1\eta_1^{c1}, k_2\eta_2^{c2}, \dots k_N\eta_N^{cN})}{\tau_x(k_1\eta_1^{c1}, k_2\eta_2^{c2}, \dots k_N\eta_N^{cN})}\right|_{TPM} \tag{99}$$

The advantage is that we can continue to refer to the ideal functioning of the PSU, using the kinematic and power relationships of section 1.1 and 5 to calculate the real power flow distribution, just changing the actual functional parameters $\tau_{o\#i}$, $\tau_{i\#o}$, $\tau_{\#i}$ and $\tau_{\#o}$ with their fictitious counterparts $\tilde{\tau}_{o\#i}$, $\tilde{\tau}_{i\#o}$, $\tilde{\tau}_{\#i}$ and $\tilde{\tau}_{\#o}$.

Obviously, the exact assessment of the internal power flow has a secondary importance here, since the impact of the mechanical losses on the preliminary ideal power flow distribution is most likely insignificant in terms of dimensioning of the gear sets.

Eventually, it is worth noting that eq. (99) can refer to either the shaft of the PG or the linked shaft of the TPM. The obvious consequence is that $p_x(k_1\eta_1^{c1}, k_2\eta_2^{c2}, \dots k_N\eta_N^{cN})$ remains unaltered, while the ratio between τ_x and $\tau_x(k_1\eta_1^{c1}, k_2\eta_2^{c2}, \dots k_N\eta_N^{cN})$ coincides with the efficiency parameter of the fixed ratio (possibly) present in the shaft x.

9. Inertial effects

The previous calculations do not account for the inertial effects associated to the involved devices. The relationship between accelerations of the main ports are simply:

$$\begin{Bmatrix} \dot{\omega}_o \\ \dot{\omega}_i \end{Bmatrix} = [\Omega] \begin{Bmatrix} \dot{\omega}_{out} \\ \dot{\omega}_{in} \end{Bmatrix} \tag{100}$$

Usually $\dot{\omega}_{out}$ is known, therefore when τ is the control parameter, then

$$\dot{\omega}_{in} = \frac{1}{\tau}\left(\frac{\dot{\tau}}{\tau}\omega_{out} - \dot{\omega}_{out}\right) \tag{101}$$

Vice versa, eq. (102) in intended to address the case for which either ω_i or ω_o is the control parameter, so that $\dot{\omega}_{in}$ can be calculated later by mean of the inverse of eq. (100).

$$\dot{\omega}_o = -\frac{\tau_{\#o}\,\tau_{o_{\#i}}}{\tau_{\#i}\,\tau_{i_{\#o}}}\,\dot{\omega}_i + \frac{\tau_{i_{\#o}} - \tau_{o_{\#i}}}{\tau_{\#o} - \tau_{\#i}}\dot{\omega}_{out} \tag{102}$$

9.1. Lumped inertial effects

It is obvious that the inertia of the PSU itself is negligible when compared to the inertia of the vehicle, the engine and the motors. Accordingly, the previous relationships (section 1-8) are still roughly valid for the neat power flows, i.e. the powers actually flowing through the main shafts of the PSU.

In particular, each mover is compensating its own inertial effects, which means that an additional torque term must be calculated in order to establish the actual working conditions of the engine and the motors.

If I_j is the generic inertia of each main port, then the associated inertial torques are:

$$\begin{Bmatrix} \Delta T_{out} \\ \Delta T_{in} \\ \Delta T_o \\ \Delta T_i \end{Bmatrix} = -\begin{pmatrix} I_{out} & 0 & 0 & 0 \\ 0 & I_{in} & 0 & 0 \\ 0 & 0 & I_o & 0 \\ 0 & 0 & 0 & I_i \end{pmatrix} \begin{Bmatrix} \dot{\omega}_{out} \\ \dot{\omega}_{in} \\ \dot{\omega}_o \\ \dot{\omega}_i \end{Bmatrix} \tag{103}$$

Now, if we observe the simple PSUs, it is possible to notice that most branches of the transmission are linked to one port by mean of fixed gear ratios $k_j\big|_{TPM}$, which means that their equivalent inertia can be easily calculated in order to be added to the inertia of the aforementioned port, thus obtaining a more accurate model of the driveline.

$$I_j^{eq} = I_j + \sum \frac{I_j}{k_j^2}\bigg|_{TPM} \tag{104}$$

Unfortunately, the previous method does not apply to PSUs including neutral nodes.

9.2. Generalization

If we consider that there is not real mathematic difference between neutral nodes and CVU ports, then, for the principle of superposition of effects, we can affirm that the effect of the inertial torque of the neutral node ΔT_n has the following impact on driveline:

$$\frac{\Delta T_n}{\Delta T_{in}} = -\frac{1 + \Theta\,\tau_{\#o}}{\tau_{n_{\#o}}} \tag{105}$$

$$\frac{\Delta T_o}{\Delta T_{in}} = 0 = -\frac{1 + \Theta\,\tau_{\#n}}{\tau_{o_{\#i}}} \tag{106}$$

Which implies that the disturbance on the input and output shaft is respectively:

$$\Delta T_{in} = -\Delta T_n \frac{\tau_{n_{\#o}}}{1 - \frac{\tau_{\#o}}{\tau_{\#n}}} \tag{107}$$

$$\Delta T_{out} = \Delta T_n \frac{\tau_{n_{\#o}}}{\tau_{\#n} - \tau_{\#o}} \tag{108}$$

In which $\Delta T_n = -I_n \dot{\omega}_n$. However, more generally, it is:

$$\Delta T_{in} = \sum_j \Delta T_j \frac{\tau_{j_{\#l}}}{1 - \frac{\tau_{\#l}}{\tau_{\#j}}} \tag{109}$$

$$\Delta T_{out} = \sum_j \Delta T_j \frac{\tau_{j_{\#l}}}{\tau_{\#j} - \tau_{\#l}} \tag{110}$$

In which $l \neq j$. However, if we are reasoning in terms of fixed input and output torque, the inertial effects due to the neutral nodes must be balanced by the CVU, i.e. $\Delta T_{in} = \Delta T_{out} = 0$, and so we obtain the following system of equations:

$$\Delta T_o \frac{\tau_{o_{\#i}}}{1 - \frac{\tau_{\#i}}{\tau_{\#o}}} + \Delta T_i \frac{\tau_{i_{\#o}}}{1 - \frac{\tau_{\#o}}{\tau_{\#i}}} = -\sum_{j \in N} \Delta T_j \frac{\tau_{j_{\#l}}}{1 - \frac{\tau_{\#l}}{\tau_{\#j}}} \tag{111}$$

$$\Delta T_o \frac{\tau_{o_{\#i}}}{\tau_{\#o} - \tau_{\#i}} + \Delta T_i \frac{\tau_{i_{\#o}}}{\tau_{\#i} - \tau_{\#o}} = -\sum_{j \in N} \Delta T_j \frac{\tau_{j_{\#l}}}{\tau_{\#j} - \tau_{\#l}} \tag{112}$$

In which N includes all the neutral nodes. In particular, the previous system is formally analogous to the general torque relationship (78), just considering two equivalent output and input torques

$$\hat{T}_{in} = \sum_j \Delta T_j \frac{\tau_{j_{\#l}}}{1 - \frac{\tau_{\#l}}{\tau_{\#j}}} \tag{113}$$

$$\hat{T}_{out} = \sum_j \Delta T_j \frac{\tau_{j_{\#l}}}{\tau_{\#j} - \tau_{\#l}} \tag{114}$$

Which means that the inertial effects of the neutral node on the CVU can be calculated as:

$$\begin{Bmatrix} \Delta T_o \\ \Delta T_i \end{Bmatrix} = [\Omega^{-1}]' \begin{Bmatrix} \hat{T}_{out} \\ \hat{T}_{in} \end{Bmatrix} \tag{115}$$

However, eq. (114)-(115) de facto are not restricted to the neutral nodes, but they can be for the ports as well (including input and output shaft themselves), which means that the same algorithm can be applied to the whole driveline.

Another interesting result is that since the index l is not influent, then the following relationship must be true:

$$\tau_{\#n} = \frac{\tau_{n_{\#i}} \tau_{\#o} - \tau_{n_{\#o}} \tau_{\#i}}{\tau_{n_{\#i}} - \tau_{n_{\#o}}} \tag{116}$$

This relationship can be useful in the calculation of the functional parameters of such drivelines.

9.3. Inertial effects in presence of mechanical losses

Obviously, the same logic described in section 8 still applies here. However, it is evident that the matrix $\widetilde{\Omega}$ is the result of the total power flow distribution, and not just of the power flows due to the inertial effects. The real torques at the CVU are:

$$\begin{Bmatrix} \bar{T}_o \\ \bar{T}_i \end{Bmatrix} = \left[\widetilde{\Omega}^{-1}\right]' \begin{Bmatrix} \bar{T}_{out} + \hat{T}_{out} \\ \bar{T}_{in} + \hat{T}_{in} \end{Bmatrix} \tag{117}$$

While the neat kinetic power must be equal to the variation in the CVU:

$$P_I = \begin{Bmatrix} \omega_{out} \\ \omega_{in} \end{Bmatrix}' [\Omega]'[\Omega^{-1}]' \begin{Bmatrix} \hat{T}_{out} \\ \hat{T}_{in} \end{Bmatrix} = \begin{Bmatrix} \omega_{out} \\ \omega_{in} \end{Bmatrix}' [I] \begin{Bmatrix} \hat{T}_{out} \\ \hat{T}_{in} \end{Bmatrix} \tag{118}$$

Which means that the power loss is equal to:

$$\bar{P}_{L_j} = \begin{Bmatrix} \omega_{out} \\ \omega_{in} \end{Bmatrix}' \left([\Omega]'\left[\widetilde{\Omega}_j^{-1}\right]' - [I] \right) \begin{Bmatrix} \bar{T}_{out} + \hat{T}_{out} \\ \bar{T}_{in} + \hat{T}_{in} \end{Bmatrix} \tag{119}$$

The problem is that both $\hat{T}_{out}$ and $\hat{T}_{in}$ depend on the altered functional parameters.

$$\hat{T}_{in} = \sum_j \Delta T_j \frac{\tilde{\tau}_{j\,\#l}}{1 - \frac{\tilde{\tau}_{\#l}}{\tilde{\tau}_{\#j}}} \tag{120}$$

$$\hat{T}_{out} = \sum_j \Delta T_j \frac{\tilde{\tau}_{j\,\#l}}{\tilde{\tau}_{\#j} - \tilde{\tau}_{\#l}} \tag{121}$$

which means that further iterations are necessary.

In this case, it is opportune to use the eq. (113) and (114) as first guess values, thus calculating a first attempt of $[\widetilde{\Omega}]$ by mean of the iterative approach summarized by eq. (116) and described in detail in section 8.2. Then the process is repeated using eq. (120)-(121) instead, until $[\widetilde{\Omega}]$ stops changing.

10. PS-CVT analysis: Applications

10.1. Chevrolet Volt

In this section, we apply the method described in section 4.2, 7.2 and 7.3 to the Voltec PS-CVT (Fig. 9).

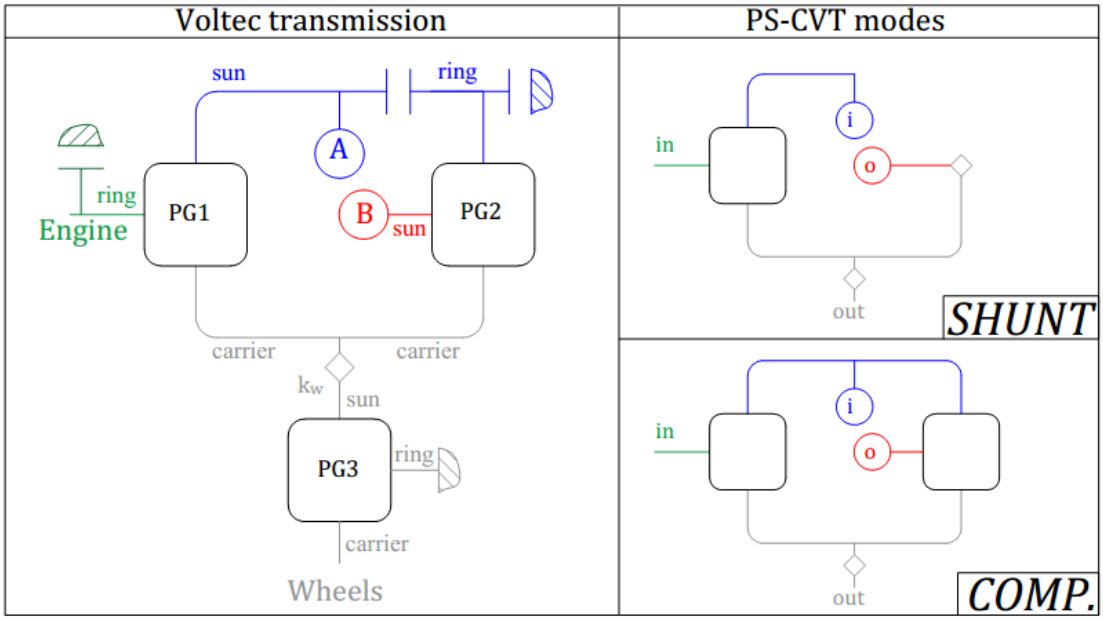

Fig. 9 GM Voltec: constructive and functional schematics.

10.1.1. Functional parameters

The Voltec has two PS-CVT modes, and the switch occurs when motor A (the shaft "i") is motionless. The Voltec offers also a parallel mode and a FEV mode, which can be considered sub-cases of the PS-CVT functioning. The mechanical points, calculated by mean of the relationships listed in 4.2 for a $D_i - C_{out}$ PSU, are listed in Table 9 (see also Fig. 10):

Table 9 Functional parameters of the Voltec transmission.

Mode	$\tau_{\#i}$	$\tau_{o\#i}$	$\tau_{\#o}$	$\tau_{i\#o}$
Shunt	0.247	2.00	0	-1.87
Compound	0.247	2.00	0.510	2.00

In the compound mode, the synchronous condition is common to both the planetary gear trains and occurs for $\tau_* = k_{out} = 0.379$, which is exactly between the mechanical points. This is because there are no internal ordinary gear sets. On the other hand, PG1 maintains the same synchronous ratio after switching to the shunt mode, while PG2 cannot be synchronous anymore, as it has become an OG.

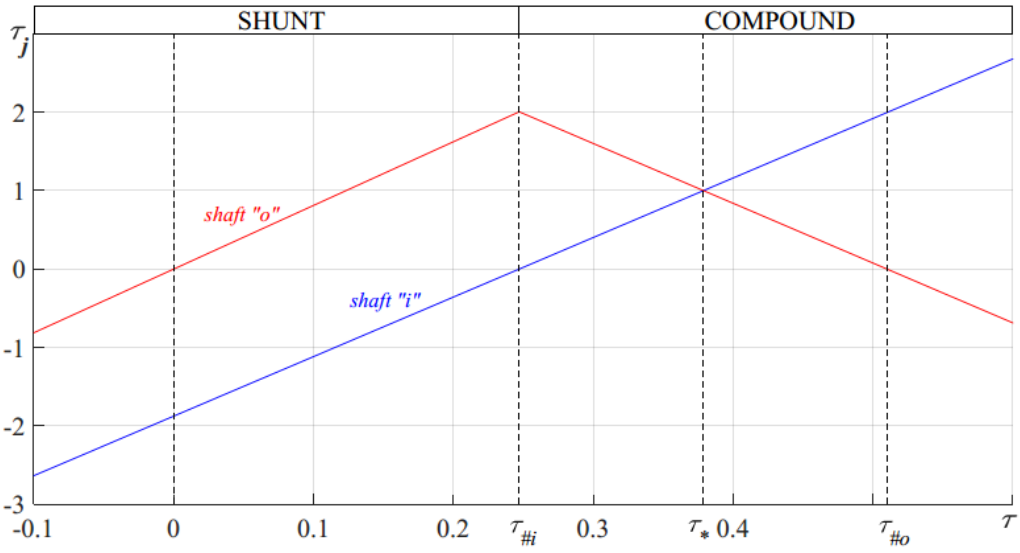

Fig. 10 Kinematic relationships between the main shafts of the Voltec.

10.1.2. Apparent efficiencies

As regards the apparent efficiencies, we assume a basic efficiency $\eta_0 = 0.96$ for all the PGs. For both PG1 and PG2, we have simply $\eta_{I/IN}^{OUT} = \eta_{I/O}^{OUT} = 0.96$, as the output shaft is linked the carrier. The overall final drive ratio $k_{out} = \frac{1}{2.64} = 0.379$ consists of a chain drive linked to the sun of a PG, with the carrier linked to the final differential and the ring linked to the frame. The constructive ratio of PG3 is $\psi_3 = -0.461$ under the hypotheses that the wrapping pair ratio is $k_w = 1.2$. Its apparent efficiency (Table 8) is equal to

$$\eta_{S/C}^{R} = \frac{1-\psi_3}{\frac{1}{\eta_o}-\psi_3} = 0.972$$

Accordingly, if the chain efficiency is $\eta_w = 0.98$, it is $\eta_{OUT/out} = 0.953$.

10.1.3. Power Losses

The approximated power losses are (see section 7.2):

$$\bar{p}_{loss}|_{PG1} = -\left|\left(1-\eta_{I/IN}^{OUT}\right)\left(\frac{\phi_{in/i}^{out}-\psi_{in/i}^{out}}{1-\psi_{in/i}^{out}}\right)p_{in}\right|$$

$$\bar{p}_{loss}|_{PG2} = -\left|\left(1-\eta_{I/O}^{OUT}\right)\left(\frac{\phi_{o/i}^{out}-\psi_{o/i}^{out}}{1-\psi_{o/i}^{out}}\right)p_{o}\right|$$

$$\bar{p}_{loss}|_{OG} = -\left|\left(1-\eta_{OUT/out}\right)p_{out}\right|$$

The characteristic functions and the related constructive parameters are calculated by mean of eq. (39). In particular, it is:

$$\phi_{in/i}^{out} = \frac{\tau-\tau_{\#i}}{\tau_{\#i}}$$

$$\psi_{in/i}^{out} = \psi_1$$

$$\phi_{o/i}^{out} = \frac{\tau-\tau_{\#i}}{\tau-\tau_{\#o}}\cdot\frac{\tau_{\#o}}{\tau_{\#i}}$$

$$\psi_{o/i}^{out} = \frac{1}{\psi_2}$$

The previous relationships are valid for both the shunt and the compound mode. The Willis' ratios are constructive teeth ratios and do not change, while $\tau_{\#o}$ does change (see Table 9), modifying p_o and $\phi_{o/i}^{out}$ accordingly to section 1.3 and eq. (39).

10.1.4. Results – total mechanical loss

Fig. 11 represents the contour map of the mechanical loss as a fraction of the dimensionless output power η and overall speed ratio τ.

The power losses is minimum in correspondence of the synchronous condition ($\tau = 0.379$) and for $\eta = 0$, while they become significant during assisted acceleration ($\eta > 1$) and regenerative braking ($\eta < 0$), as these conditions imply more power circulating within the PSU. The shunt mode generally shows worse mechanical losses, and this is likely due to the fact that PG1 is far from its synchronous condition, and PG2 cannot reach it at all.

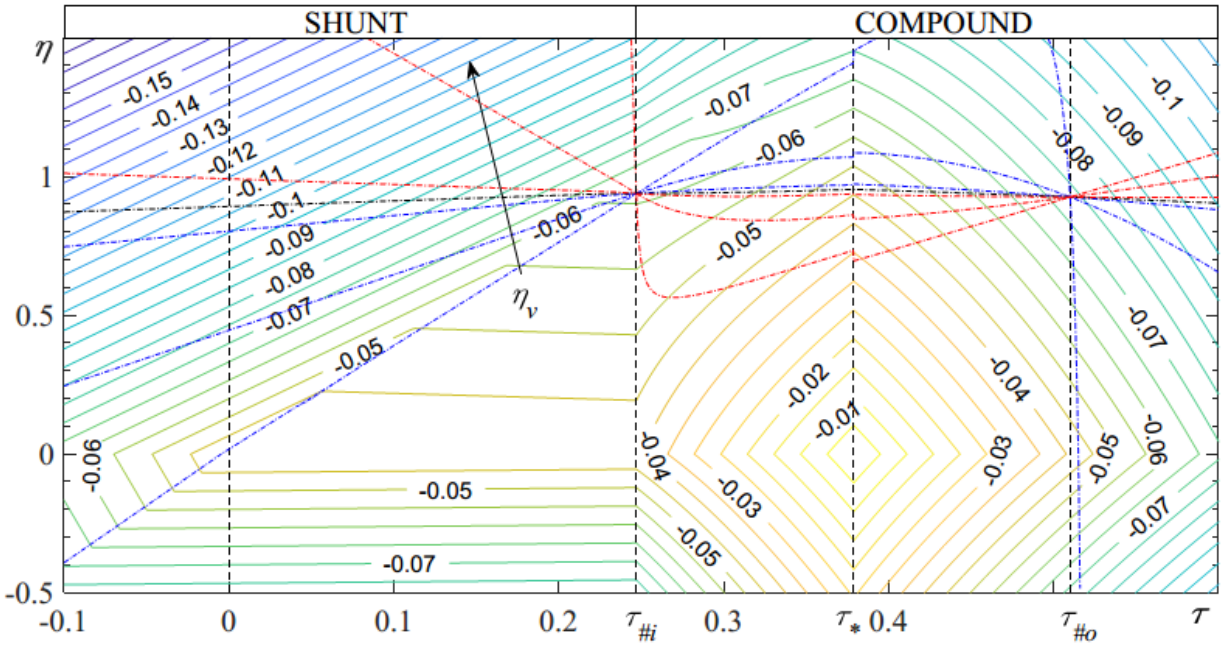

Fig. 11 Mechanical losses $\overline{p}_L$ for the Voltec PS-CVT

The dash-dot lines represent points of functioning for which η_v is constant. In figure the curves relatives to $\eta_v = 0.02, \eta_v = 0.5, \eta_v = 0.9$ have been represented in blue, while those relative to their reciprocal values have been represented in red. The black line refers to $\eta_v = 1.0$. In conditions of battery charge sustaining, it is licit to expect $\eta_v \approx 0.9$, or its reciprocal, because of the electrical losses in the motors and related power electronics; such condition

is represented by the dash-dot line right below the black ($\eta_v = 1.0$), which is approximately constant in most of the operative range.

In correspondence of the stall speed ($\tau = 0$) the overall apparent efficiency η must be null as well. Such condition is indeed intercepted by the dash-dot curve for $\eta_v \to 0$, because, for $\tau = 0$ in the shunt mode, the shaft "o" must be still as well.

In correspondence of the mechanical points, all dash-dot lines intercept in a point, which is representative of the fixed-ratio efficiency of the transmission; indeed, in this condition, finite values of η_v imply that an electric motor is kept still and the other runs unloaded. Vice versa, if the latter is supplying power, η_v is not finite, and for this speed ratio the value of $\bar{p}_L$ can change accordingly to η. In particular, this condition occurs during the parallel mode.

10.1.5. Real CVU power flows

Since we know the mechanical loss map, we can calculate the real powers flowing through the electric path, by mean of eq. (73) and (74). Fig. 12 and Fig. 13 represent the maps of the relative power flows through the electric machines A and B (respectively main shafts "i" and "o"). Despite the gradient of the mechanical loss $\bar{p}_L$ shows numerous discontinuities, the value of the function itself remains continuous and it causes a small jump for both $\bar{p}_i$ and $\bar{p}_o$ only in correspondence of the synchronous condition.

In particular, the normalized power flowing through the shaft "i" is (Fig. 12):

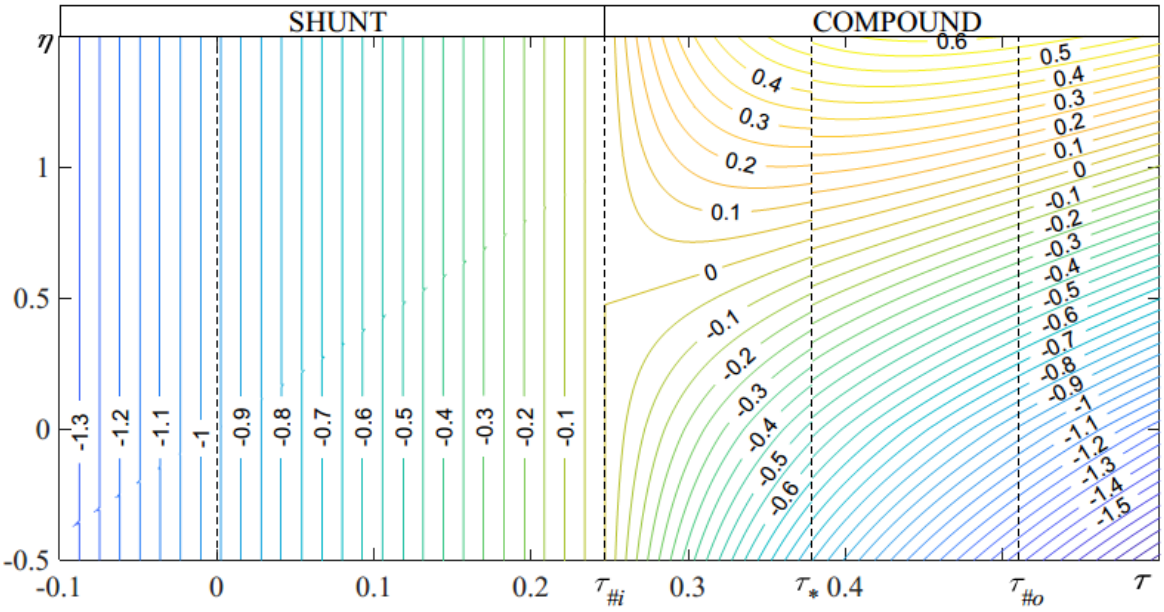

Fig. 12 Power transmitted by the shaft "i".

Conversely, the normalized power flowing through the shaft "*o*" is (Fig. 13):

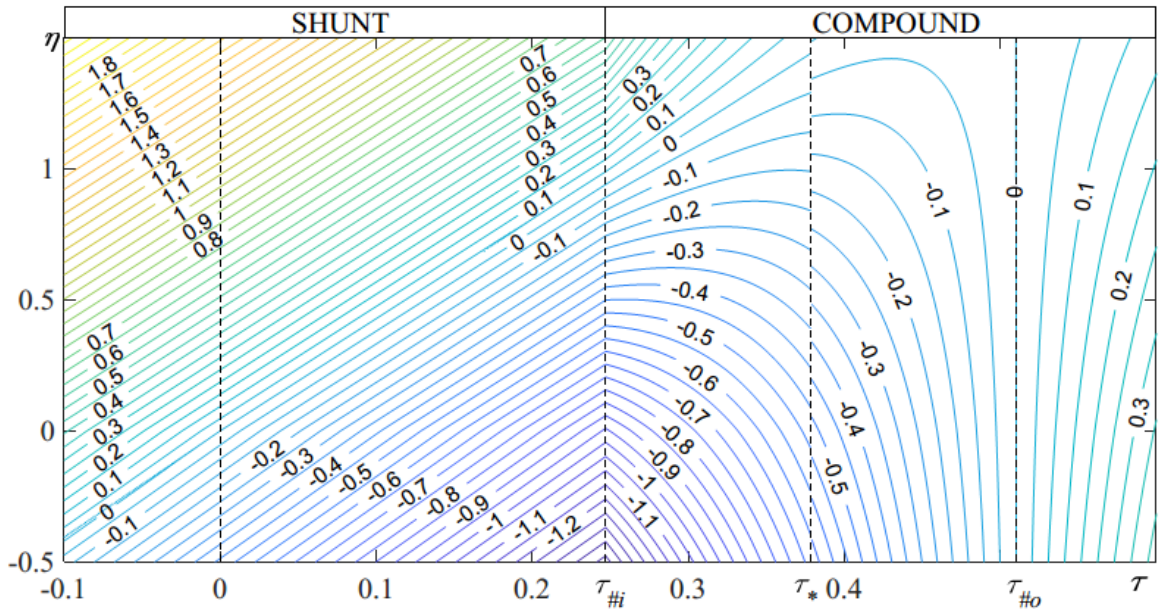

Fig. 13 Power transmitted by the shaft "o" (as a fraction of the input power).

10.1.6. Transition zones

Fig. 14 highlights where the gradient of mechanical loss $\bar{p}_L$ (Fig. 11) shows discontinuities. Despite the transmission is reasonably simple (just two power-split PGs and no ordinary gears internal to the PSU), it shows, within the studied interval, nine transition zones.

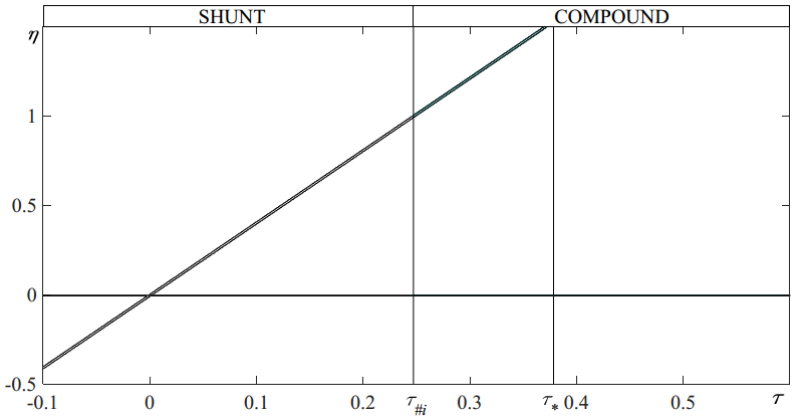

Fig. 14 Transition zones of the constructive efficiency parameters.

10.1.7. Errors

We have simulated the transmission in Simulink Simscape for different values of overall apparent efficiency η (for η = 1.5, 1, 0.5, 0, -0.5) in order to verify the accuracy of the proposed model.

Fig. 15 to Fig. 19 show the comparison between simulated points (markers) and calculated points (solid lines), for both the overall mechanical loss (left) and for the power flowing through the electric motors (right). As usual, the blue lines refers to the main shaft "i" (motor A) and the red ones refers to the main shaft "o" (motor B).

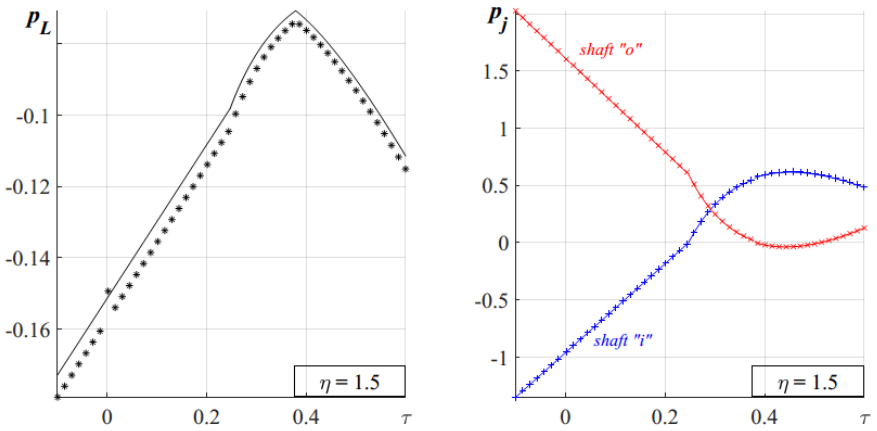

Fig. 15 Mechanical losses (left) and CVU's power flows for $\eta = 1.5$

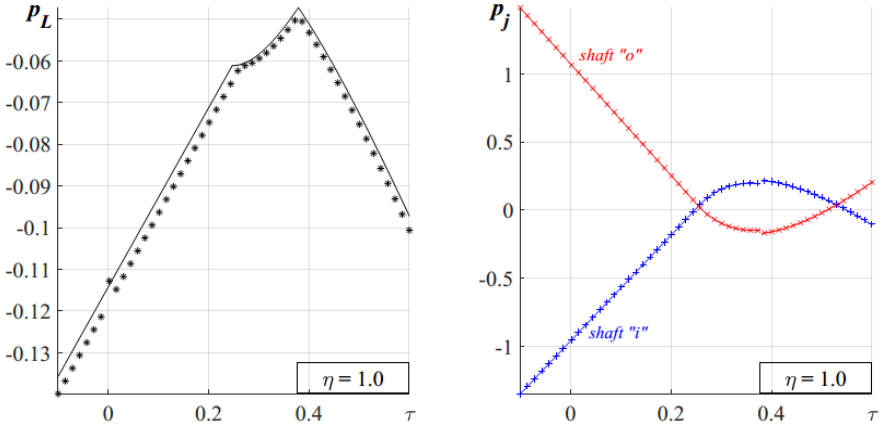

Fig. 16 Mechanical losses (left) and CVU's power flows for $\eta = 1.0$

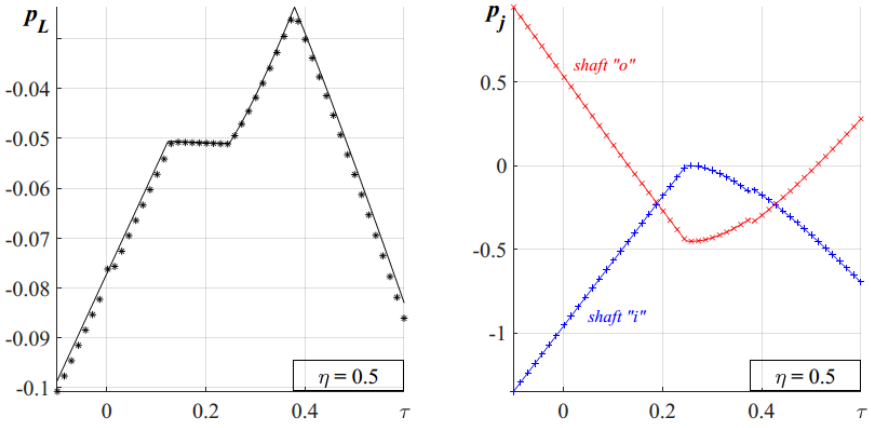

Fig. 17 Mechanical losses (left) and CVU's power flows for $\eta = 0.5$

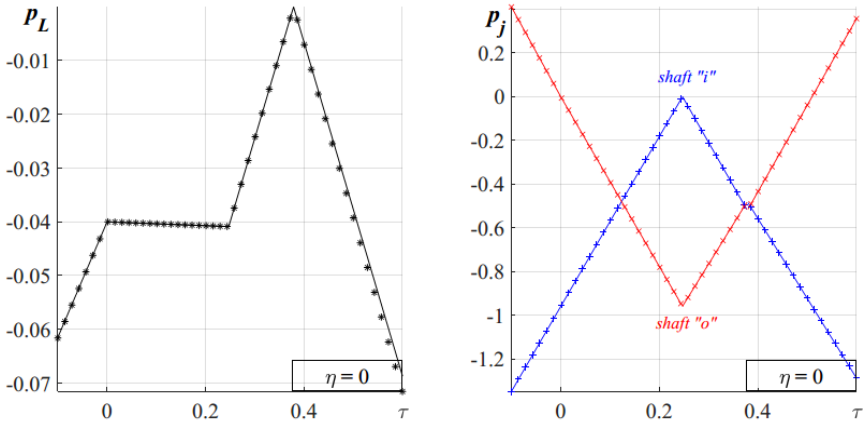

Fig. 18 Mechanical losses (left) and CVU's power flows for $\eta = 0$

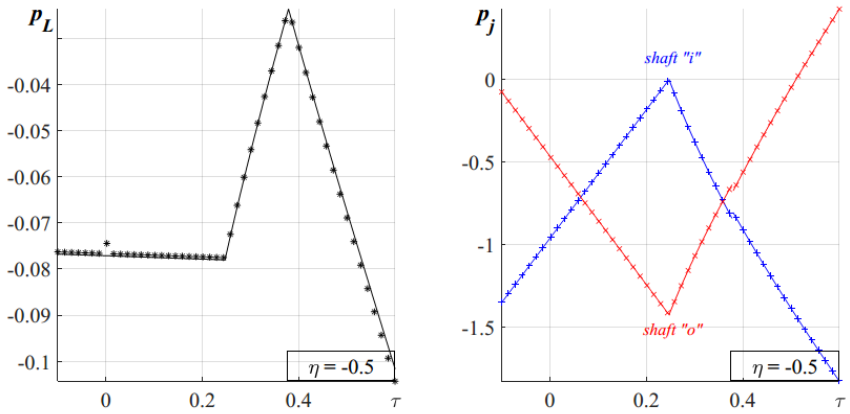

Fig. 19 Mechanical losses (left) and CVU's power flows for $\eta = -0.5$

As it can be observed for Fig. 15 to Fig. 19, the error in the assessment of the power loss is within the fraction of centesimal, while the error for both $\bar{p}_i$ and $\bar{p}_o$ is hardly noticeable.

10.2. Cadillac CT6

The Cadillac CT6 transmission (Fig. 20) represents a complex multi-mode PS-CVT. It includes two reversible electric machines, three PGs and five clutches. PG3 is a double pinion PG. In this section, we will perform its analysis using the results of section 8.

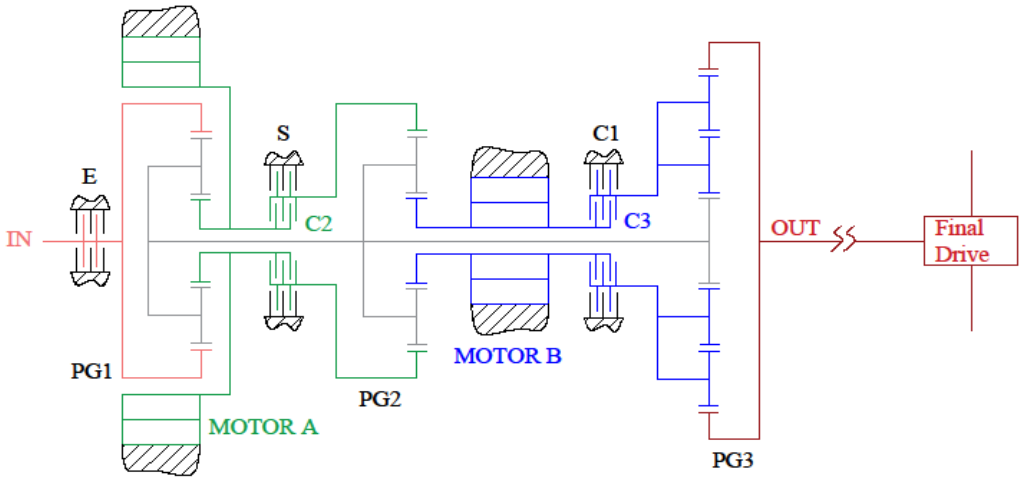

Fig. 20 Cadillac CT6 transmission

10.2.1. Functional parameters and functioning modes.

The CT6 is potentially able to perform two input-split and two compound power-split modes (EVT), as well as three parallel (FG) and four full electric (EV) functioning modes (Fig. 22). For simplicity, we round the mechanical points given in [113] to the closest two digit value, assuming that they are exact (Table 10).

Table 10 Mechanical points for the CT6

MODE	EVT1	EVT2	EVT2	EVT2
$\boldsymbol{\tau_{\#i}}$	0	0.6	0.6	0
$\boldsymbol{\tau_{\#o}}$	0.3	0.3	1.4	1.4

The kinematics of the main shafts of the CT6 is represented in Fig. 21.

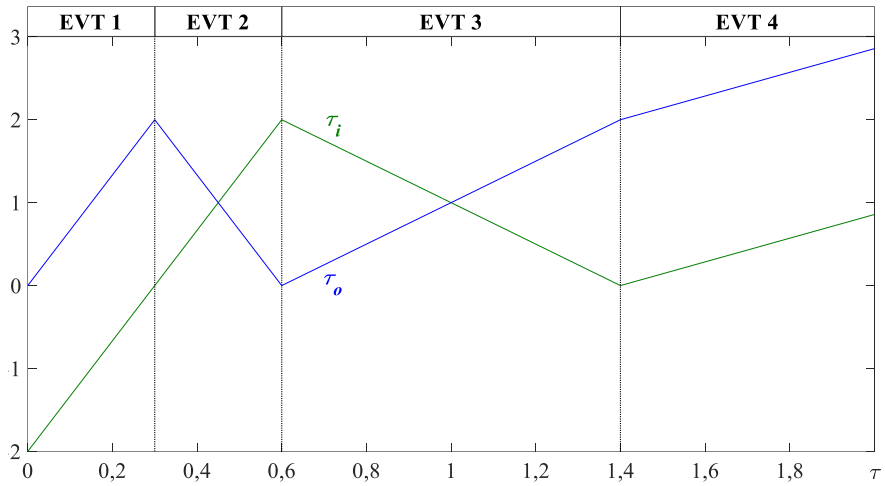

Fig. 21 CT6: kinematics of the two electric machines

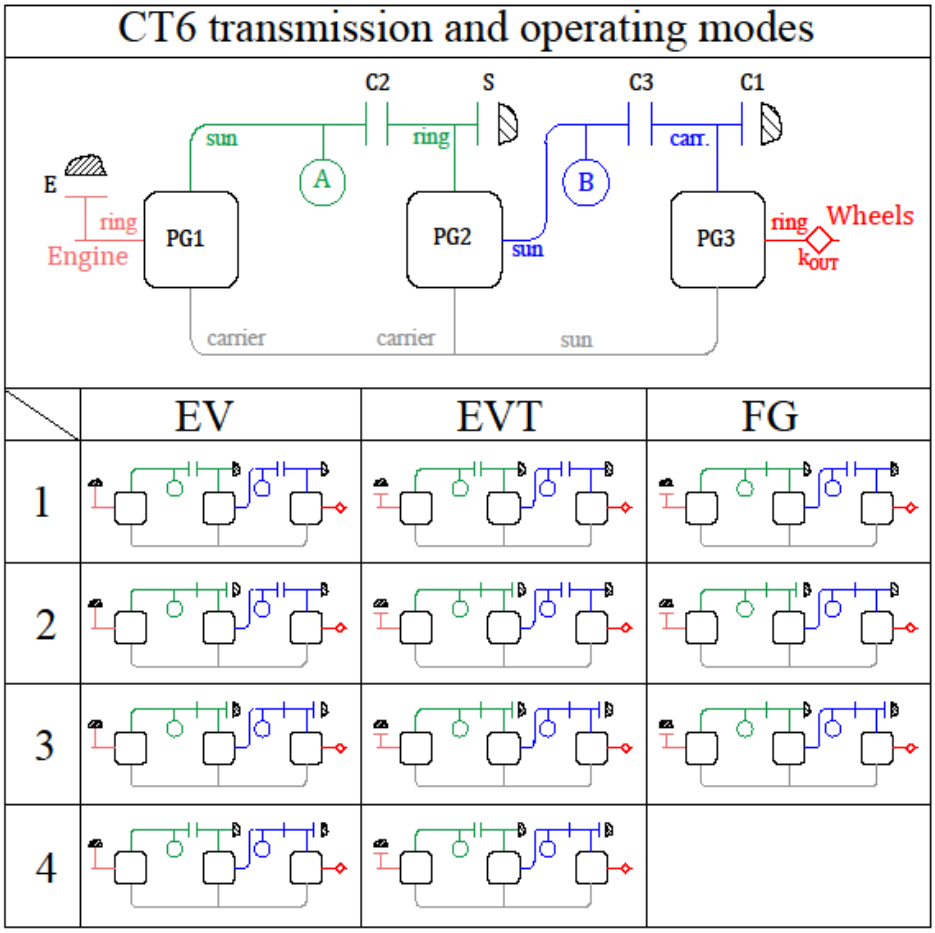

Fig. 22 CT6 functional scheme and working modes

10.2.2. Constructive parameters

The exact constructive parameters of the CT6 transmission could be obtained by the fixed ratios provided in [113], which are the reciprocal of the mechanical points. However, their precision in not enough to permit a reliable assessment of the constructive ratios of the first two PGs, since a small uncertainty brings significantly different results.

On the basis of the values in Table 10, the constructive ratio of PG3 is equal to the overall transmission ratio when PG1 and PG2 are synchronous in the EVT2 mode, i.e. $\psi_3 = 0.45$. The constructive ratio of PG1 and PG2 can be found considering that their carriers are motionless when $\tau_i = -2$ (EVT1), which happens again if the mode EVT3 is ideally extended to $\tau = 2.2$ (see Fig. 21). Concurrently, it will be also $\tau_o = 4$, and so $\psi_1 = 1/\tau_i = -0.5$ and $\psi_2 = \tau_i/\tau_o = -0.5$.

In practice, it is not necessary to address all the modes separately, as two disconnected shafts, one of which is blocked, can be modeled by the same two shafts linked by an infinite fixed gear ratio. Indeed, even though the two shaft appear falsely connected, the kinematic equivalence of the system will guarantee correct results even in terms of power flows [17].

Table 11 Constructive Willis' ratios and equivalent fictitious ordinary gears.

	$PG1$	$PG2$	k_{R2}	$PG3$	k_{C3}	k_{R3}
teeth ratio	-0.5	-0.5	$1\ or\ \infty$	0.45	$1\ or\ \infty$	1
efficiency	0.97	0.97	1	0.96	1	0.98

10.2.3. Apparent efficiencies

As regards the efficiencies, we can assume a constant fixed-carrier efficiency of 0.97 for PG1 and PG2, and a fixed-carrier efficiency of 0.96 for PG3, as it is a double-pinion planetary gear. The gear ratio of the final drive is not specified, but we can take into account the related losses anyway. Indeed, if the mechanical loss in a series of ordinary gears depends only on their overall efficiency, it is safe to lump all the losses into one meshing pair, assuming the other ideal. Accordingly, we can assume the (unknown) final drive to be ideal,

introducing a fictitious ordinary gear k_{R3} between the ring of PG3 and the actual final drive, with a unitary constructive ratio and an efficiency equal to 0.98. In this way, we do not need to know the final drive ratio a priori, and we preserve the ability to calculate later the tractive force, which depends also on the effective wheel radius, by considering ideal the final drive itself.

10.2.4. Transition zones

From the analysis of the transition zones, it follows that 18 distinct zones are present for τ ranging from 0 to 2 and Θ ranging from -5 to 5. Kinematic boundaries are predictable (mode switch or synchronism of one or more PGs), while torque-related boundaries can be trickier. In particular, the boundaries for $\Theta \approx 3.2$ (see Fig. 23) indicate that the torque applied to PG2 is null.

While the kinematic matrix is constant within each mode (see Table 12), each zone shows a specific altered kinematic matrix (see Fig. 23).

Table 12 Kinematic matrices of CT6 transmission

	EVT1	EVT2	EVT2	EVT2
[Ω]	$\begin{pmatrix} 20/3 & 0 \\ 20/3 & -2 \end{pmatrix}$	$\begin{pmatrix} -20/3 & 4 \\ 20/3 & -2 \end{pmatrix}$	$\begin{pmatrix} 5/2 & -3/2 \\ -5/2 & 7/2 \end{pmatrix}$	$\begin{pmatrix} 10/7 & 0 \\ 10/7 & -2 \end{pmatrix}$

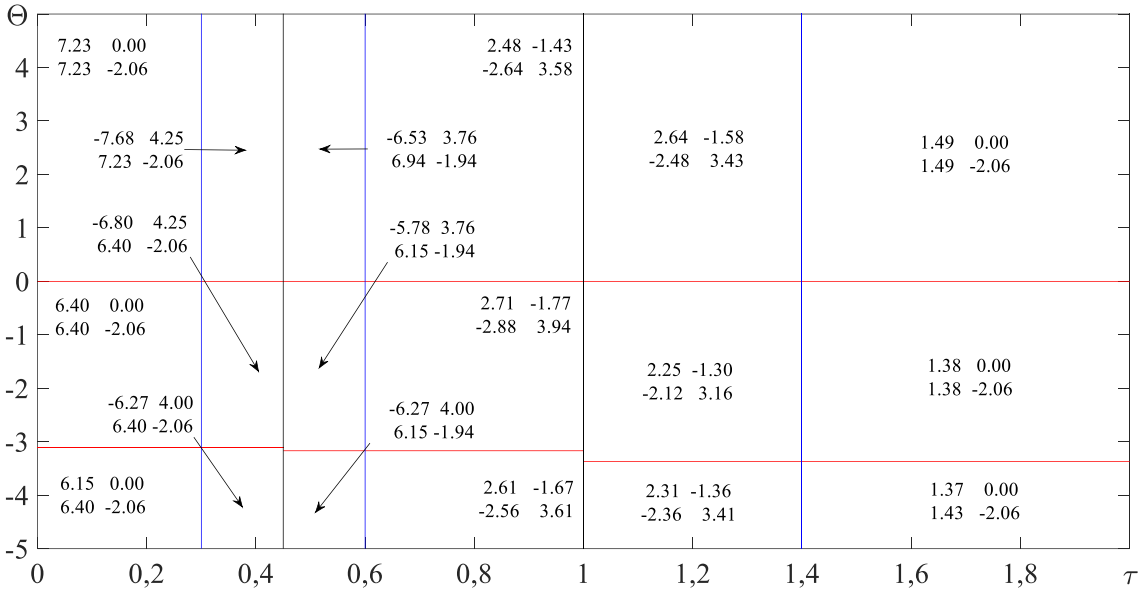

Fig. 23 Altered kinematic matrices $[\tilde{\Omega}]$. Transition lines: synchronism (black), mode switch (blue), torque switch (red)

10.2.5. Mechanical loss

In Fig. 24 we have plotted the overall mechanical loss into the PSU, normalized in respect of the input power, as a function of the overall speed ratio τ and torque ratio Θ. The spacing between contour lines is equal to 1%. The gradient shows several discontinuities, notably in correspondence of the mode switches and synchronous conditions. The transmission is more efficient when the torque ratio is small and negative, i.e. when the wheels are in traction and the assistance of the electric motors is limited. The power losses show an asymptotic behavior in correspondence of the stall speed, which means that in such circumstances they tend to remain a constant fraction of the power delivered by the engine, whichever it is its speed and torque. Obviously, both the synchronous points represent local maxima for the efficiency, but EVT2 can be expected to be sensibly worse than EVT3, the main reason being the losses of PG3 (which is not synchronous) and the generally higher torque ratios characterizing low speed ratios.

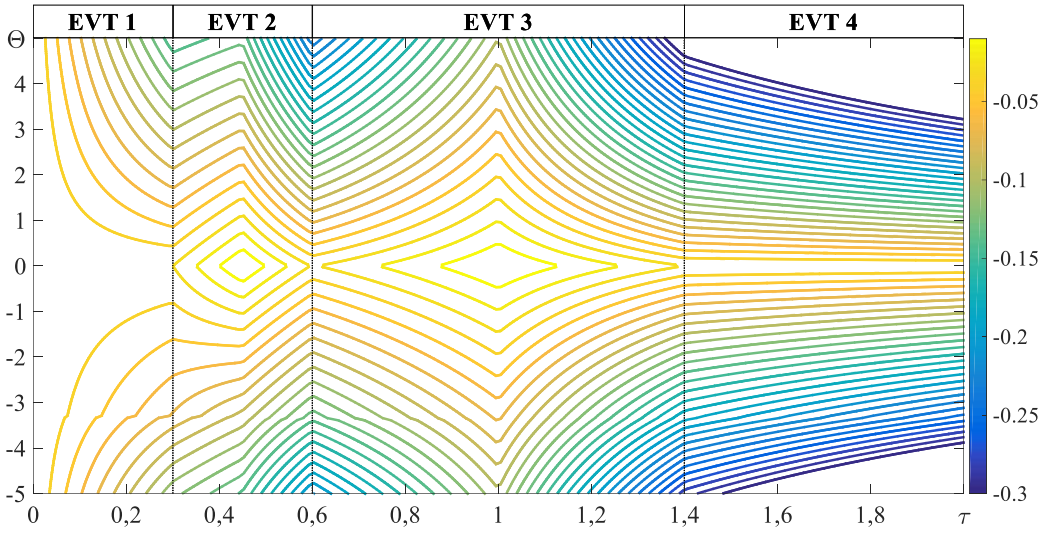

Fig. 24 Mechanical losses of CT6's PS-CVT as a fraction of the input power.

10.2.6. Real CVU power flows

In Fig. 25 we have plotted the mechanical power to be delivered by MG_o (motor B), as a fraction of the input power, positive if entering the electric machine. The contour spacing is equal to the 10%. The power shows discontinuities due to torque jumps. The jump is due to the loading (or unloading) of a brake clutch during a mode switch, or to a discontinuity in the coefficient of one or more loss factors (notably in correspondence of the synchronisms). The multiplying factor can take very high values, thus precluding the possibility to obtain relevant values of Θ outside EVT1.

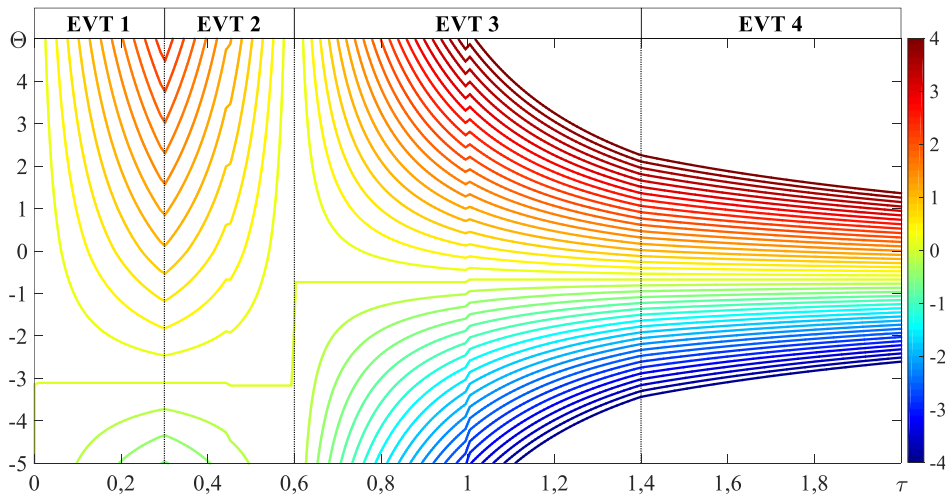

Fig. 25 Mechanical power supplied by/to MG_o (MOTOR B) as a fraction of the input power.

Similarly, in Fig. 26 we have plotted the mechanical power to be delivered by MG_i (motor A), as a fraction of the input power, positive if entering the electric machine. The contour spacing is equal to the 20%. Both the machines require low relative power only in correspondence of a tight band of torque ratios close to the hyperbole $\Theta = -1/\tau$. Accordingly, the assistance of the electric machines induces both high mechanical and electrical losses.

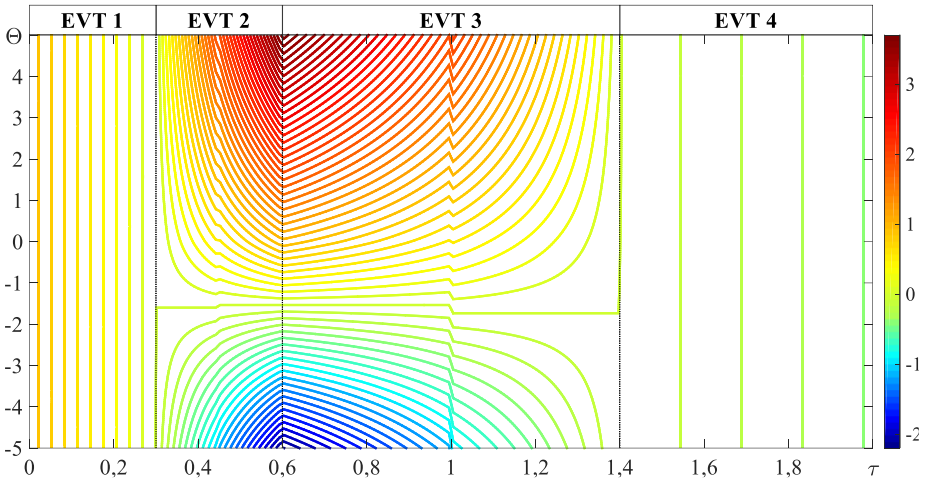

Fig. 26 Mechanical power supplied by/to MG_i (MOTOR A) as a fraction of the input power.

11. General requirements and control

11.1. Vehicle's requirements

Vehicles' traction requirements, in terms of power, acceleration, comfort, consumptions and emissions, are mostly independent from the adopted driveline, as briefly described in the following sections.

11.1.1. Traction demand

Vehicles face several sources of resistance to their motion, many of which are dissipative. In terms of traction, the nature of the forces hindering the movement makes no difference, yet it is necessary to distinguish among them in order to develop physically consistent models.

Table 13 Main sources of motion resistance force

Aerodynamic	***Rolling***	***Slope***	***Inertial***
$0.5\ c_x\ \rho\ A\ V_r^2$	$f_R\ m\ g\ \cos(\alpha)$	$m\ g\ \sin(\alpha)$	$m_{eq}\ \dot{V}$

In general, such forces depend on the vehicle's interactions with a dynamically mutable environment, thus being the result of complex phenomena [1,2,6]. Nonetheless, this work is not intended to be a meticulous assessment of such phenomena, so the resistance forces will be modeled by mean of simple equations (see Table 13), neglecting the influence of any secondary effects on c_x and f_R, which will be assumed constants.

11.1.2. Drivability requirements

The vehicle is supposed to fulfill basic performance requirements. The power necessary to reach the top speed is due to aerodynamic resistances to the greatest extent. Vice versa, since uphill driving is supposed to be performed at relatively low speeds, other sources of resistance beyond gravity can be neglected. Acceleration is a dynamic problem involving mutable coexisting sources of motion resistance, yet a rough esteem can be carried out considering that about half of the input power increases the kinetic energy of the vehicle. A corrective factor f_0 may be introduced in order to model different engine characteristics (see Table 14), but the uncertainty remains high.

Table 14 Power requirements

Top Speed	***Uphill driving***	***Accelerating***
$0.5\ c_x\ \rho\ A\ V_{max}^3$	$m\ g \sin(\alpha)\ V_\alpha$	$f_0\ m_{eq}\ V_0^2/t_0$

11.1.3. Fuel consumptions

The energy demand of a vehicle can be assessed according to specific test cycles. A test cycle requires following a certain speed profile under strictly controlled environmental conditions; the initial thermal regime of the engine is regulated as well, as it influences the release of pollutants. In general, it is possible to witness the following:

- The power necessary to complete a cycle is well below the drivability requirements.
- A significant part of the tractive force is not immediately dissipated, as it is naturally stored by the vehicle as potential and kinetic energy.
- Lightweight vehicles perform significantly better.
- The measured average consumptions are not accurate in terms of real operating conditions, although they are useful for comparison purposes.
- Local differences exist between calculated and measured fuel consumptions, but average results are accurate.

11.2. Control

A PS-CVT is a complex mechanism, and both its design and control involve a large set of parameters constrained by drivability requirements and constructive limits.

The traditional approach to the control of PS-CVT is largely heuristic, which means that a set of intuitive rules, tuned by experience, is applied to the energy management. The key point are that the SOC must stay within determined limits and that the engine must be operated only in its high efficiency region, which means that the control will prioritize full electric functioning whenever the engine cannot operate at full load. A certain set of exceptions to this rule will apply in transitory conditions, such as warm-ups.

In general, the speed and torque request imply the functioning mode in accordance with various state parameters, such as the battery temperature or SOC. If properly implemented, this approach can lead to good performances, but generally requires a significant tuning effort, especially when the transmission model is particularly sophisticated.

Unfortunately, the results of heuristic models are necessarily sub-optimal, so a proper control optimization is required to exploit the driveline. Usually, the control strategy is tailored to addresses a definite driveline, yet a rigorous optimization would require to design both the driveline and its control strategy simultaneously.

In particular, we have shown that the domain of the design variables can be sensibly reduced thanks to the functional parametrization of the PS-CVT. Accordingly, a comprehensive preliminary optimization appears viable.

11.2.1. Optimization Theory

Generally speaking, an optimization problem must be expressed in terms of a scalar objective function. If such function is globally convex, then the local minimum is determined by its gradient and by its Hessian matrix, which must be positive definite. A typical cost function is the overall fuel consumption, which can be combined with other parameters, such as pollutants and driving smoothness, by means of user-defined penalty factors.

In an unconstrained optimization problem, the input variables change following the direction of the gradient, until the variation of the objective function falls within an arbitrary threshold. Higher order methods involve the approximation of the objective function by mean of a Taylor expansion, thus solving the optimization problem in closed form.

If the problem is constrained, then the optimal condition is located in the point of tangency between the constraint itself and the iso-level curve of the objective function, which means that their gradients are aligned. If the constraint is an inequality, then it is necessary to verify the local direction of the gradient, as the former may not be active, which means that the optimum is not located on the boundary, but it is within the free domain. Often is suitable to introduce some limit as a soft-constraint, i.e. the deviation from the expected value penalizes the cost function in an arbitrarily definite way.

The instantaneous evolution of a dynamic system depends on its current state, on the disturbance factors and on the input parameters. However, when the same system is performing a specific task, alternative control strategies can determine considerably different outcomes in terms of the chosen objective function. In general, such function summarizes one or more performance parameters of the system, such as global emissions and fuel consumptions.

If the disturbance function is known a priori, e.g. when it is the result a specific driving cycle, then a determinist approach to the control problem is possible. Unfortunately, most circumstances require an on-line controller, as the disturbance function is indeed unpredictable. Such controllers are supposed to perform worse than a deterministic controller does on a specific cycle, but better on average. For these reasons, the deterministic controller remains the ideal benchmark for on-line controllers, but it is also useful to compare the quality of different designs.

11.2.2. Deterministic controllers: Dynamic Programming

Dynamic programming is a successful deterministic control strategy, which permits to address complex constrained problems with a relatively low computational effort, although it requires knowing the evolution of the disturbance factors a priori

In general, we can affirm that the disturbances, the dynamic states and the control inputs of a dynamic system are continuous functions of the time. However, if we discretize such parameters both in time and in value, we obtain a finite domain of possible discrete statuses, each one represented by a specific set of numbers. At every time step, a different set of optimal control parameters can be associated to each status belonging to the aforementioned domain. These parameters make the system evolve accordingly to an optimal control trajectory, i.e. the cumulative cost required to go from the current system status to the final one is minimum. In other terms, for a given final status, the minimum cumulative cost (and the related control trajectory) is univocally associated with the current system status.

Accordingly, for every time step it is possible to build maps of cumulative costs and optimal controls parameters associated with every status, moving retroactively from the final time step. The whole method can be summarized as follows:

- Discretization of time, state and control variables.
- Final time step: definition of the system statuses and of the associated cumulative costs. In general, if a specific final status is set, arbitrarily high cumulative costs will be associated to all the other statuses.
- Previous time step: calculation of the current cumulative costs for every system status, summing costs-to-go and future (but previously calculated) cumulative costs. This passage include an optimization sub-problem, as the optimal control parameters are unknown a priori. Indeed, each status has optimal control parameters for the current time step, which univocally determine both the costs-to-go and the new system status in the following time step, whose cumulative costs are already known in the domain of discrete statuses. Accordingly, the future cumulative cost must be interpolated using the current prediction while varying the control parameters, until the minimum current cumulative cost is established for this time step. The cost-to-go function is likely to include penalty factors effective when the status prediction violates the constraints of the problem.
- Repeat the previous point until the initial time step is reached.
- Verify the control strategy in forward time direction.

The same approach is valid even if the disturbance is not deterministic, but follows a known probability distribution. In this case, the cumulated cost coincides with the expected value.

The main drawback of dynamic programming is that the computational effort scales exponentially with both the number of state variables and control inputs, so complex problems are generally addressed with approximated methods. Obviously, also the discretization of each variable implies a compromise between computational times and accuracy. In particular, it is worth noting that a fine grid permits faster interpolation methods for the future cumulative cost.

11.2.3. Causal controllers

Real time controllers are supposed to address unpredictable drive cycles.

The predictive control system usually uses deterministic methods to address a significantly shorter time span. The short-term evolution of the system is guessed on the basis of onboard and GPS data (speed, torque, traffic conditions etc.), thus obtaining a verisimilar disturbance function.

Feedback controllers extrapolate a set of statistical rules by analyzing deterministic optimal solutions. However, in order to obtain satisfactory results over random drive cycles, it is necessary to use stochastic dynamic programming, as the rules obtained by a specific drive cycle will perform poorly on a broader range of application.

ECMS (Equivalent Consumption Minimization Strategy) controllers perform an estimation of the equivalence factor, which converts battery power into an equivalent fuel power. In this case, the optimal value of the equivalence factor is calculated for different pattern of driving conditions, and then the controller associates the instantaneous state parameters with one of these patterns. The equivalence factor can be further adapted to the current driving conditions to better pursue charge sustainability, for instance by correcting it based on the SOC deviation from a target value. Eventually, in case of limited battery capacity, it is important to include some predictive features to the controller, so that the regenerative breaking could be fully exploited. This may be achieved by providing at any moment enough battery capacity to fully recuperate the kinetic energy of the vehicle, but can be furtherly enhanced by considering route and traffic predictions.

12. PSU design

Good PS-CVTs:

1. Minimize the power transmitted by the CVU (small working range near mechanical points)
2. Minimize the torque transmitted by the CVU (its shafts should rotate as fast as possible)
3. Have a wide working range (several modes)
4. Are as simple as possible (costs, dimensions)
5. Have low mechanical losses (planetary gears work near their synchronism)

The mechanical points $\tau_{\#i}$ and $\tau_{\#o}$ govern the CVU power flows; the related CVU speed ratios $\tau_{o_{\#i}}$ and $\tau_{i_{\#o}}$ govern the applied torques. The layout influence the internal power flow distribution and the ability to achieve multimode transmissions. Obviously, each additional TPM is a source of costs and potential power losses, so it is more convenient to assess the simpler solutions before increasing the complexity of the PSU. Eventually, we suppose that the PGs reach their synchronism for a speed ratio τ_* within the working range.

12.1. Link between constructive ratio and synchronism

A simple planetary gear train is conventionally defined by its *constructive parameter*, also known as the Willis' ratio or the characteristic ratio, i.e. the ratio between the speed of the ring over the speed of the sun when the carrier is motionless:

$$\psi_{R/S}^{C} = \frac{\omega_R - \omega_C}{\omega_S - \omega_C} = \left.\frac{\omega_R}{\omega_S}\right|_{\omega_C=0} \tag{122}$$

As stated before, the arrangement of the shafts of the planetary gear trains and their synchronous points are not definite at this stage. Accordingly, we can use X,Y,Z to represent all the different possible arrangements.

$$\psi_{Y/X}^{Z} = \frac{\omega_Y - \omega_Z}{\omega_X - \omega_Z} = \left.\frac{\omega_Y}{\omega_X}\right|_{\omega_Z=0} \tag{123}$$

However, a TPM can include up to three fixed ratio joints. If k_j is the fixed ratio between the *j-th* speed, which is external to the TPM, and the matching internal shaft's speed, then imposing the synchronous conditions to the planetary gearing leads to the following relationships:

$$\frac{\omega_x|_{\tau_*}}{k_x} = \frac{\omega_y|_{\tau_*}}{k_y} = \frac{\omega_z|_{\tau_*}}{k_z} \tag{124}$$

valid for any position of carrier, sun and ring gear. Yet, since we are working with the normalized exit speeds of the tree port differential, then we can write it as:

$$\psi_{Y/X}^{Z} = \left.\left(\frac{\omega_y}{k_y}\cdot\frac{k_x}{\omega_x}\right)\right|_{\frac{\omega_z}{k_z}=0} = \left.\frac{k_x}{k_y}\cdot\frac{\omega_y}{\omega_x}\right|_{\omega_z=0} = \left.\frac{\omega_x}{\omega_y}\right|_{\tau_*}\cdot\left.\frac{\omega_y}{\omega_x}\right|_{\omega_z=0} \tag{125}$$

As a result, such formulation is identical to the generic expression of the characteristic function (39) when the latter is calculated for the synchronous condition of the PG:

$$\psi_{Y/X}^{Z} = \phi_{y/x}^{z}(\tau_*) = \left.\frac{\tau_y}{\tau_x}\right|_{\tau_*}\cdot\left.\frac{\tau_x}{\tau_y}\right|_{\tau_z=0} \tag{126}$$

Since the characteristic functions depend only on the mechanical points, which are also the only parameters modulating the power flows within the CVU, it is possible to perform a preliminary optimization of such functional parameters, and then proceed with the choice of a synchronous ratio, which will lead to a particular layout.

12.2. Link between fixed ratios and synchronism

Imposing a synchronous condition to the planetary gear train of a TPM implies the following two (mutually independent) constraints for the speed ratios of its ordinary gear trains (or any equivalent fixed-ratio joint):

$$\frac{k_x}{k_y} = \frac{\tau_x}{\tau_y}\bigg|_{\tau_*} = \frac{\tau_{x_{\#y}}}{\tau_{y_{\#x}}} \cdot \frac{\tau_* - \tau_{\#x}}{\tau_* - \tau_{\#y}} \tag{127}$$

$$\frac{k_x}{k_z} = \frac{\tau_x}{\tau_z}\bigg|_{\tau_*} = \frac{\tau_{x_{\#z}}}{\tau_{z_{\#x}}} \cdot \frac{\tau_* - \tau_{\#x}}{\tau_* - \tau_{\#z}} \tag{128}$$

In which x, y, z represent the main shafts and/or neutral nodes linked to the TPM. For a desired kinematic distribution (i.e. mechanical points and related speed ratios), these constraints are univocally determined by the synchronous ratio τ_*.

Freely tuning the kinematic of a compound transmission implies two different design constraints, and thus at least two ordinary joints, for each TPM. This result can be obtained by:

- eliminating one ordinary joint in each TPM;
- eliminating only one ordinary joint and imposing the same value to a pair of *homologous joints* (i.e. linked the same IJ, but belonging to different branches of the transmission), so that they can be merged in just one.

In general, to eliminate one or more ordinary gears is possible if the remaining fixed ratios are feasible.

On the other hand, if no ordinary gear is used, all the planetary gear trains share necessarily the same synchronous point τ_*, thus constraining the nodal ratios $\tau_{o\#i}$ and $\tau_{i\#o}$ concurrent with the mechanical points, which have a strong impact on the module of the torque applied to the CVU for a given power flow distribution (See section 1.2) .

12.3. Generic design procedure

Whatever it is the layout of the PSU, each TPM is linked to three main shafts; therefore, we can identify distinct possible typologies of TPMs depending on the involved main shafts.

For each group we get six *characteristic functions* by permuting the three shaft indexes in eq. (39). Formerly, each value of a *characteristic function* is a possible Willis' ratio providing synchronism. Since the kinematic parameters are known, all the characteristic functions are defined, and each group can suggest six Willis' ratios (but only three actually different, due to a changed position of the planet-carrier) for a given synchronous working point τ_*.

Therefore, in order to explore the feasible layouts, and then select the most appropriate one, it is convenient to perform the following steps:

- to calculate the optimal mechanical points;
- to build a *design-chart* by plotting all the characteristic functions in the working range of τ;
- to discard those curves that do not possess values within the desired range of Willis' ratios;
- to select points from characteristic curves belonging to different groups (i.e. the Willis' ratios and the related synchronous working points).

Definitively, to choose the Willis' ratio from a specific curve determines the position of the carrier, sun and ring of each planetary gear train, while the groups to which these functions belong determine the final layout.

12.3.1. Design procedure for shunt PSUs

The presented model, developed for a generic compound transmission, results valid even though only one planetary gear train is employed, i.e. for the so-called variable shunt transmissions. In these cases, two out of the four main shafts have proportional speeds, and therefore one mechanical point assume a limit value (zero or infinite).

Accordingly, if during the optimization process such limit conditions happen to be (almost) fulfilled, then the compound layout might be avoided at all.

In these cases, the characteristic functions of different groups appear overlapped in the design chart, and it is sufficient to:

- choose one Willis' ratio (or the related synchronous working point);
- constraint the ordinary gears of the remaining TPM by two of the expressions (127)-(128);
- introduce an additional ordinary joint between the two connected main shafts in order to satisfy the relationship between their respective initial speed ratios (see Fig. 3).

12.3.2. Design procedure for compound PSUs with two TPMs

Using more than two TPMs has not kinematics effects, then it is convenient to think to the PSU as a device consisting in a couple of TPMs sharing two distinct ports (Fig. 4) before extending the method to more complex PSUs.

In this case, in order to explore the feasible layouts (see section 3.2) and then select the most appropriate one, it is convenient to perform the following steps:

- To select from two characteristic curves, belonging to different groups, two points (i.e. the Willis' ratios and the related synchronous working points).
- To constraint the ordinary gears of the remaining three-port differential by two of the expressions of (127)-(128);
- To identify the layout by mean of the groups' name.

Definitively, to choose the Willis' ratio from a specific curve determines the position of the carrier, sun and ring of each planetary gear train, while the groups to which these functions belong determine the final layout.

Table 15 Design constraints for the ordinary gears of PSU with up to two TPMs.

Groups	Constraint	Expression
$\boldsymbol{C_{in}, D_i}$	$\frac{k_i}{k_{in}}$	$-\tau_{i_{\#o}} \cdot \frac{\tau_* - \tau_{\#i}}{\tau_{\#o} - \tau_{\#i}}$
$\boldsymbol{C_{in}, D_o}$	$\frac{k_o}{k_{in}}$	$\tau_{o_{\#i}} \cdot \frac{\tau_* - \tau_{\#o}}{\tau_{\#o} - \tau_{\#i}}$
$\boldsymbol{C_{out}, D_i}$	$\frac{k_i}{k_{out}}$	$-\frac{\tau_{i_{\#o}}}{\tau_*} \cdot \frac{\tau_* - \tau_{\#i}}{\tau_{\#o} - \tau_{\#i}}$
$\boldsymbol{C_{out}, D_o}$	$\frac{k_o}{k_{out}}$	$\frac{\tau_{o_{\#i}}}{\tau_*} \cdot \frac{\tau_* - \tau_{\#o}}{\tau_{\#o} - \tau_{\#i}}$

In particular, two three-ports differentials both belonging to a *D* group will combine in a "Direct bridge" symmetric layout, in which the CVU directly connects the two free shafts of the three-port differentials, while two three-ports differentials both belonging to a *C* group will combine in a "Cross bridge" symmetric layout (the CVU connects nodes). Conversely, one *C* and one *D* group always combine in an Asymmetric Bridge layout (see section 3.2). It is easy to identify the scheme as the indexes belonging to both groups represent the shafts linked to the isokinetic joints.

12.3.3. Design procedure for compound PSUs with three or more TPMs

The design process is formally analogous to the previous ones, but it is subject to a certain procedure related to the choice of the characteristic functions. Indeed, in a PSU with 3 TPMs there are five mains shafts (4 ports and one neutral node), so their indexes must appear nine times in total. Each port index must appear at least one time, while the neutral node index must appear at least two times (vice versa the linked PG would be unloaded). Up to two

indexes can appear 3 times, as it is the maximum number of shafts connected together, which is coincident with the number of TPMs. Accordingly:

- Provided that the neutral node appears at least once, the first two characteristic curves, belonging to different groups, can be selected freely.
- If one port index is not present in the previous groups and/or the neutral nodal appears just once, the third characteristic function, chosen among the remaining groups, must complete the series.

The constraints for the ordinary gears continue to rely on the general expressions of (127)-(128). The identification of the layout is less straightforward, as it necessary to identify the two groups able to generate a nested kernel structure identical to that of a compound PSU with 2 TPMs. Such groups must contain 2 couples of homonymous indexes. Once the kernel is known, it is easy to identify the actual core structure by linking the third TPM. It can be observed that the 3 possible core structures resemble the three functional layout of the original 2-TPMs compound PSU, but each one is able to express a different number of completely new functional layouts.

It is self-evident that the same procedure can be applied to PSUs with more than three TPMs, just considering that each additional TPM introduces a new neutral node (the aforementioned rules still apply to nodes and ports). The final layout can be obtained by building the lower core structures, considering that each new TPM must share two ports with the previous kernel. Nonetheless, we will limit our dissertations to cases described above, as two or three TPMs are sufficient for most applications.

13. Multimode PSUs

The speeds of the shafts of the CVU, for given speed of the engine, are linear functions of the overall speed ratio; therefore, the CVU limits the working range of the PS-CVT because of its speed and torque constructive boundaries.

In order to extend such working range, it is possible to modify the mutual connections between the frame, the PSU and/or its four main shafts. There are several ways to achieve such results, and hereinafter we address the two most common methods.

13.1. Crypto-shunts

In general, it is possible to connect two main shafts by mean of a fixed-ratio gear set, without modifying the internal connections within the PSU.

Interestingly, since the kinematic relationships between the main shafts do not change, this kind of mode switch does not depend on the layout of the planetary transmission itself. In other terms, the choice of the mutual connections and the constructive ratios of the involved mechanical devices can be delayed, and the design of the CVU can be performed preliminarily, despite comprising the switch control strategy.

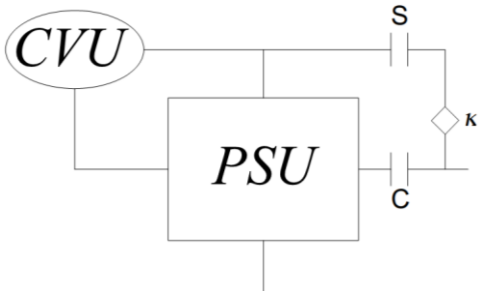

Fig. 27 General scheme for a dual mode PS-CVT. Two out of the four main shafts are always connected to the CVU

In order to create an additional PS-CVT mode, we have to disengage the clutch C and link a main shaft of the PS-CVT ("in" or "out") with a shaft of the CVU ("i" or "o") by mean of the clutch S, for a total of four possible solutions (linking "in" with "out" or "i" with "o" would produce just fixed-ratio transmissions). Obviously, the CVU is subject to power flow reversals, so its shafts "i" and "o" can be assigned arbitrarily, for example assuming $\tau_{\#i} < \tau_{\#o}$. When we disengage the clutch C linked to the main shaft of the PS-CVT, we modify the internal torque distribution, but not the kinematic relationships between the mechanical devices within the PSU. Yet, by engaging the other clutch S, we change our reference shafts for the calculation of the overall speed ratio. As a result, the slopes of the speed ratios of the CVU change accordingly to the newly linked shafts.

Nonetheless, the functioning of whichever PS-CVT is characterized by the mechanical points $\tau_{\#i}$ and $\tau_{\#o}$ and their relative CVU speed ratios $\tau_{o\,\#i}$ and $\tau_{i\,\#o}$, as they are the only parameters governing speed, torques and powers for given overall torque ratio Θ (see section 1). Accordingly, it is sufficient to assess the new functional parameters in order to evaluate the performances of the additional PS-CVT modes. The functional parameters can be calculated either analytically or graphically, but the last method is particularly intelligible and versatile if it is implemented with the aid of a parametric CAD. Despite all the planetary gears of the PSU may be active, the new modes will show functional parameters typical of a shunt transmission (crypto-shunt). Yet, in some circumstances, the new position of the additional mechanical points will benefit the functioning of the CVU.

Hereinafter we develop some examples of hybrid electric transmissions sharing an identical compound mode, analyzing the additional crypto-shunt modes if the switch is performed either before the mechanical points ($\tau_s < \tau_{\#i}$) or after them ($\tau_s > \tau_{\#o}$).

13.1.1. Direct link between "*i*" and "*out*"

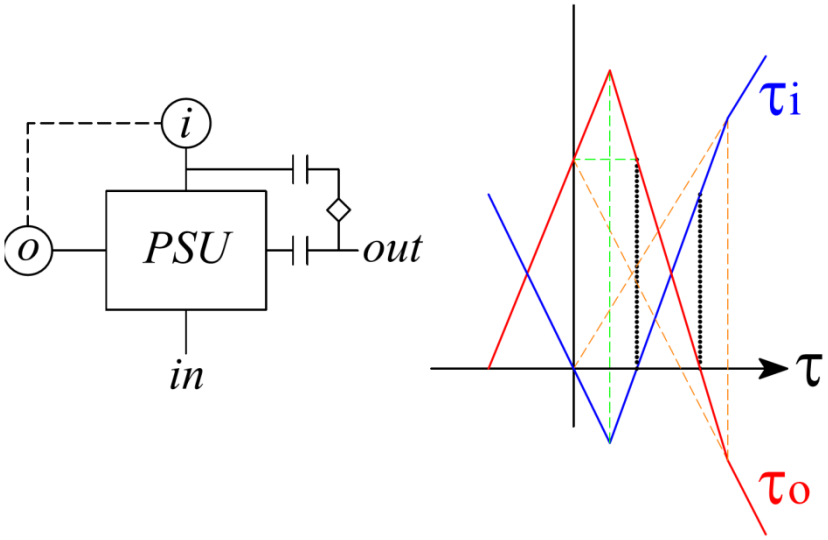

Fig. 28 Scheme i-out and graphic kinematic analysis

If the shaft "i" is now linked to "*out*", τ is proportional to τ_i, and then the new mechanical point $\tau_{\#i}$ is null, as $\tau_{i_{\#i}}$ is zero by definition. In other terms, the PSU is working as an input-split transmission. However, since the mechanical connections within the PSU have not changed, the new values of $\tau_{o\,\#i}$ and $\tau_{i_{\#o}}$, i.e. the speed ratio of the shaft "o" when the shaft "i" is motionless and vice versa, remain identical to the former ones. Accordingly, it is easy to find also the new mechanical point relative to the shaft "o", which is the only parameter depending on the switch speed ratio τ_s.

The dashed lines in Fig. 28 represent a trace of the graphic construction necessary to obtain the new slopes, and refer to a switch performed before both the mechanical points (green) or after them (orange). The two dotted lines identify the original mechanical points, but while the "green" solution ($\tau_s < \tau_{\#i}$) can provide an additional mechanical point for negative speed ratios, the orange one ($\tau_s > \tau_{\#o}$) is not beneficial, as it moves both the new mechanical point away from actual operation points of the new mode itself. Definitively, $\tau_s < \tau_{\#i}$ appears particularly suitable for transmissions intended to work across the stall condition.

13.1.2. Direct link between "*o*" and "*out*"

This concept is basically analogous to the previous one. The "green" solution ($\tau_s < \tau_{\#i}$) provides an additional mechanical point for small speed ratios, while the "orange" solution is again not beneficial, as it moves the mechanical points far away from operative speed ratios for that mode.

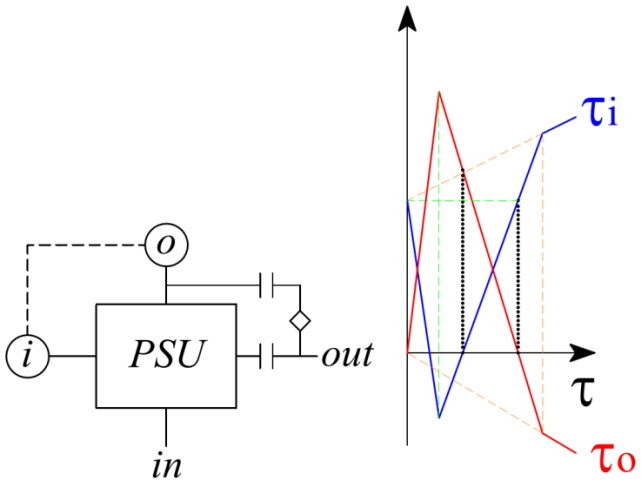

Fig. 29 Scheme o-out and graphic kinematic analysis

Eventually, the slope of both τ_i and τ_o is less steep, but their value is still increasing.

13.1.3. Direct link between "*o*" and "*in*"

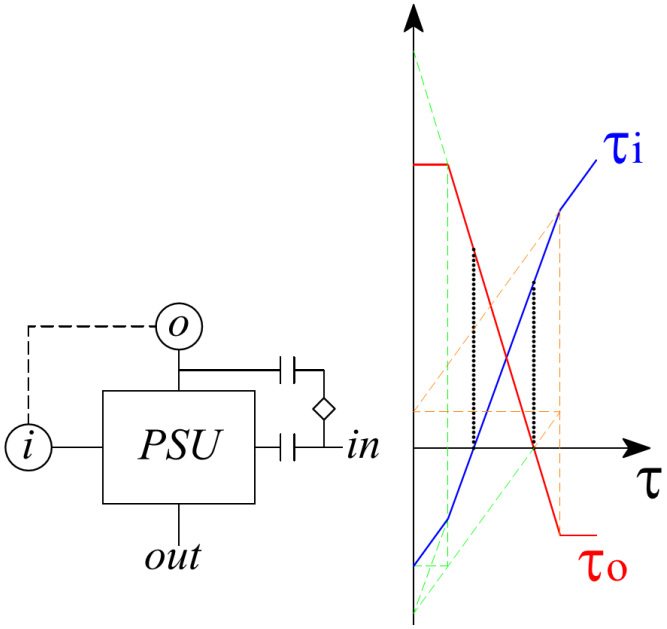

Fig. 30 Scheme o-in and graphic kinematic analysis

When we modify the input shaft of the PSU, the CVU speed ratio $\tau_v = \tau_o/\tau_i$ that makes null the speed of the output shaft does not change. Accordingly, we can use the ratio between projected intercepts of τ_o and τ_i for $\tau = 0$ in order to predict the new intercept of τ_i, since the new intercept of τ_o is known as the latter has become constant. Anyway, both the switching solutions do not provide significant benefits in their respective operation ranges, as the resulting mechanical points are farther from them now.

13.1.4. Direct link between "*i*" and "*in*"

This solution is conceptually analogous to the former one, but it is the only one beneficial for $(\tau_s > \tau_{\#o})$. Indeed, the additional mechanical point decreases the fraction of power flowing through the CVU, while the speed of "*i*" has stopped raising.

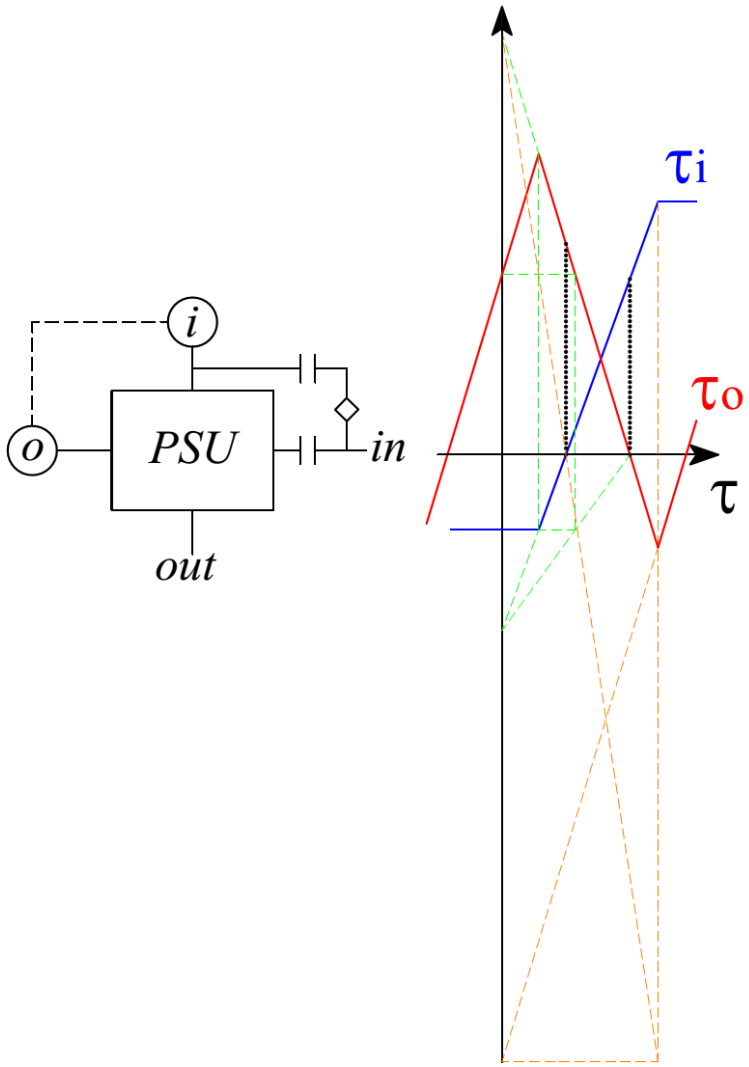

Fig. 31 Scheme i-in and graphic kinematic analysis

13.1.5. Generalization and analytical formulation

In general, configurations with switched positions of the EMs are equivalent, as in order to analyze them it is sufficient to assume:

$$i \leftrightarrow o \tag{129}$$

Vice versa, if we ideally switch the positions of the engine and of the output shaft, it should be:

$$\tau_j \leftrightarrow \frac{1}{\tau_j} \tag{130}$$

$$\tau_{j_{\#l}} \leftrightarrow \frac{\tau_{j_{\#l}}}{\tau_{\#l}} \tag{131}$$

Accordingly, the formulas of Table 16 can be obtained from one scheme to another by mean of simple indexes substitutions. Table 16 provides the kinematic relationships between base functional parameters and their "pseudo-shunt" counterparts. With k we represent the fixed speed ratio between the shaft of the PS-CVT and the shaft of the CVU, to be realized by mean of a gear set. Each scheme can perform one switch in correspondence of one mechanical point, while the other causes infeasible values for k.

Table 16 New functional parameters of Crypto-shunt modes calculated on the bases of their original compound counterparts

Crypto-Shunt	***out-i***	***out-o***	***in-o***	***in-i***
$\boldsymbol{\tau_{\#i}}$	0	$-\tau_s \frac{\tau_{\#o} - \tau_{\#i}}{\tau_s - \tau_{\#o}}$	$-\tau_{\#i} \frac{\tau_s - \tau_{\#o}}{\tau_{\#o} - \tau_{\#i}}$	∞
$\boldsymbol{\tau_{o\#i}}$	$\tau_{o_{\#i}}$	$\tau_{o_{\#i}}$	$-\tau_{o_{\#i}} \frac{\tau_s - \tau_{\#o}}{\tau_{\#o} - \tau_{\#i}}$	$\frac{\tau_{o_{\#i}}}{\tau_{\#i}} \infty$
$\boldsymbol{\tau_{\#o}}$	$\tau_s \frac{\tau_{\#o} - \tau_{\#i}}{\tau_s - \tau_{\#i}}$	0	∞	$\tau_{\#o} \frac{\tau_s - \tau_{\#i}}{\tau_{\#o} - \tau_{\#i}}$
$\boldsymbol{\tau_{i\#o}}$	$\tau_{i_{\#o}}$	$\tau_{i_{\#o}}$	$\frac{\tau_{i_{\#o}}}{\tau_{\#o}} \infty$	$\tau_{i_{\#o}} \frac{\tau_s - \tau_{\#i}}{\tau_{\#o} - \tau_{\#i}}$
$\boldsymbol{k}$	$\frac{\tau_s}{\tau_{i_{\#o}}} \frac{\tau_{\#o} - \tau_{\#i}}{\tau_s - \tau_{\#i}}$	$-\frac{\tau_s}{\tau_{o_{\#i}}} \frac{\tau_{\#o} - \tau_{\#i}}{\tau_s - \tau_{\#o}}$	$-\frac{1}{\tau_{o_{\#i}}} \frac{\tau_{\#o} - \tau_{\#i}}{\tau_s - \tau_{\#o}}$	$\frac{1}{\tau_{i_{\#o}}} \frac{\tau_{\#o} - \tau_{\#i}}{\tau_s - \tau_{\#i}}$

13.2. Crypto-Compounds

It is common in PS-CVTs to realize ordinary gear sets by mean of a PG with a framed shaft (crypto-compound). However, it is possible to exploit such devices in order to perform additional modes. In particular, by connecting the framed shaft to the CVU shaft in concurrence with the related mechanical ratio we obtain a synchronous switch. If the PSU has more than two PGs, in this case it is likely that the ordinary gear sets are present only on the external ports of the PSU, which implies that the PGs have a common synchronous ratio τ_*, so that the following relationships exist:

$$\tau_{i_{\#o}} = \tau_{i_*} \frac{\tau_{\#o} - \tau_{\#i}}{\tau_* - \tau_{\#i}} \tag{132}$$

$$\tau_{o_{\#i}} = \tau_{o_*} \frac{\tau_{\#i} - \tau_{\#o}}{\tau_* - \tau_{\#o}} \tag{133}$$

Accordingly, k_i, k_o, k_{out} and k_{in} are univocal, and the synchronous ratio and the related CVU ratios will be respectively:

$$\tau_* = \frac{k_{out}}{k_{in}} \tag{134}$$

$$\tau_{i_*} = \frac{k_i}{k_{in}} \tag{135}$$

$$\tau_{o_*} = \frac{k_o}{k_{in}} \tag{136}$$

However, if we operate a switch by mean of the PG that realizes the fixed ratio k_j, some of the previous quantities change, as it changes the speed ratio $k_j = \frac{\omega_j}{\omega_J}$ (which is not constant anymore) associated with the synchronous condition. In particular, it is possible to distinguish between two cases, i.e. when the shaft of the switching PG links directly to the other PGs and when it connects directly the CVU. In the first case, we will have that:

$$k_{j_*} = 1 \tag{137}$$

While in the last case it will be:

$$k_{j_*} = k_j + (1 - k_j)\, k_l \tag{138}$$

In which k_l is the fixed gear ratio associated with the shaft of the CVU motionless during the switch. Obviously, if k_l is not present, the aforementioned cases coincide.

In particular, we have to invert the eq. (132)-(133), as the switch will modify the other mechanical point.

$$\boldsymbol{\tau_{\#i}} = \frac{\tau_* \tau_{i_{\#o}} - \tau_{\#o} \tau_{i_*}}{\tau_{i_{\#o}} - \tau_{i_*}} \tag{139}$$

$$\boldsymbol{\tau_{\#o}} = \frac{\tau_* \tau_{o_{\#i}} - \tau_{\#i} \tau_{o_*}}{\tau_{o_{\#i}} - \tau_{o_*}} \tag{140}$$

Therefore, if for instance the switch occurs in correspondence of $\tau_{\#o}$, we know that also $\tau_{i_{\#o}}$ remains unaltered, and we have to calculate the new values of $\tau_{\#i}$ by mean of eq. (139) and of $\tau_{o_{\#i}}$ by mean of eq. (133), introducing the newly calculated synchronous ratios (eq. (134)-(136)), which will be different because of eq. (137) or (138). Similarly, if the switch occurs in correspondence of $\tau_{\#i}$, $\tau_{o_{\#i}}$ remains unaltered, and we have to calculate the new values of $\tau_{\#o}$ by mean of eq. (140) and of $\tau_{i_{\#o}}$ by mean of eq.(132).

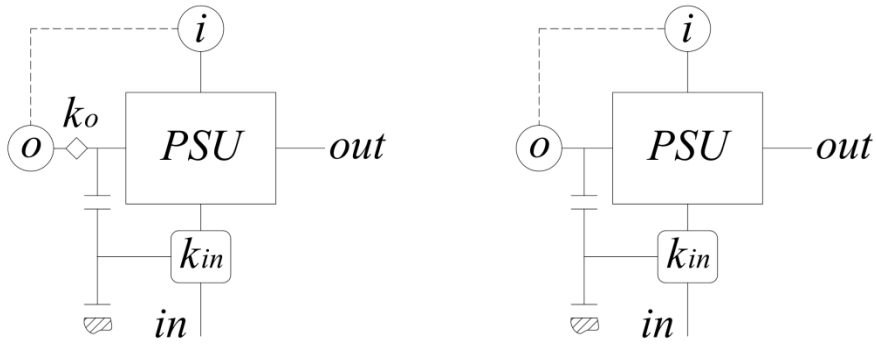

Fig. 32 Example of compound switch ($k_j = k_{in}$ and $k_l = k_o$). Direct link with the PGs (left figure) or direct link with the CVU (right)

Obviously, the synchronous switch can be performed for whichever couple of indexes j, l provided that $j \neq l$ and that the shaft l is motionless concurrently.

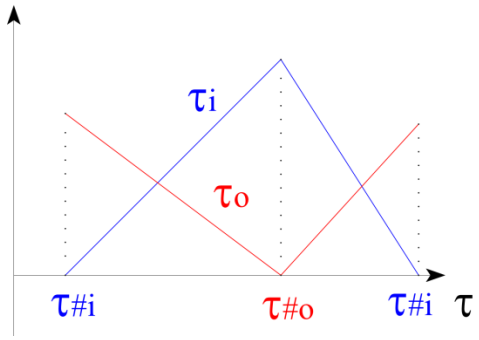

Fig. 33 Example of compound switch

The switch is effective only if the new mechanical points is outside the original range. This condition occurs for the switch in $\tau_{\#o}$ when the newly calculated synchronous ratios respect the following conditions:

$$\tau_* > \tau_{\#o} \qquad \text{If } \tau_{i_*} < \tau_{i_{\#o}} \tag{141}$$

$$\tau_* < \tau_{\#o} \qquad \text{If } \tau_{i_*} > \tau_{i_{\#o}} \tag{142}$$

Similarly, for the switch in $\tau_{\#i}$, the newly calculated synchronous ratios respect the following conditions:

$$\tau_* > \tau_{\#i} \qquad \text{If } \tau_{o_*} < \tau_{o_{\#i}} \tag{143}$$

$$\tau_* < \tau_{\#i} \qquad \text{If } \tau_{o_*} > \tau_{o_{\#i}} \tag{144}$$

Interestingly, if the PSU is a shunt, then the switch will determine a new compound mode. This kind of switch is studied in detail in the next section.

13.3. Shunt-compound switch

A common strategy to achieve a multimode transmission consist in disconnecting two shaft and blocking one of them, so that one PG becomes ordinary. This strategy is layout dependent, even though general rules can be extrapolated from the results of the previous section 13.2, as the switching PG is either connected to the motionless shaft of the PSU or it works as an OG, with the fundamental difference that the PSU is a shunt. In this section, we will study in detail the possible switches achievable with PSU including two TPMs, including the asynchronous ones.

13.3.1. Cross Bridge

If we consider the Cross-Bridge layout, we see that the switch can be performed on whichever internal branch of the PSU. The key concept is that this operation will affect just one PG, while the relationships introduced by the other one stay unaltered.

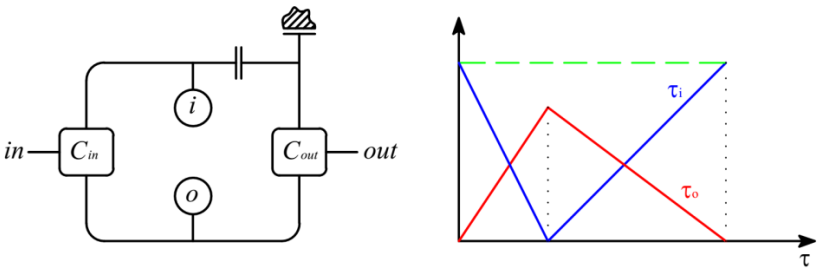

Fig. 34 Cross Bridge (shunt o-out)

In this case (shunt o-out) the clutch has not effect on the left PG. τ_o becomes proportional to the overall speed ratio τ, and the value of τ_i when τ_o is zero must be the same than that of the compound mode. The green line represent a trace of the graphic construction of the speed characteristic.

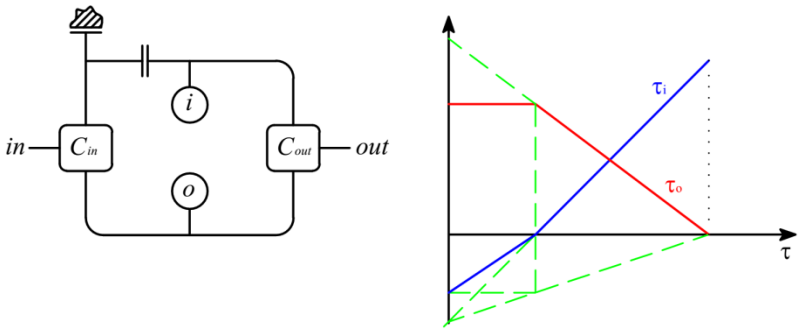

Fig. 35 Cross Bridge (shunt o-in)

In this case (shunt o-in), the clutch has not effect on the right PG, while τ_o becomes constant. The value of τ_o/τ_i must be the same as that of the compound mode when τ is zero. In order to achieve the new characteristic graphically we project the compound characteristics on the vertical axis, and thus we connect the intercepts with $\tau_{\#o}$. The coordinate for the common mechanical point is the new value of τ_i for $\tau = 0$.

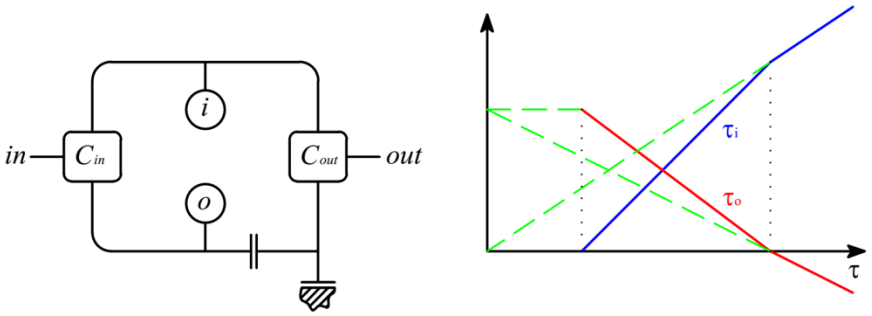

Fig. 36 Cross Bridge (shunt i-out)

This case (shunt i-out) is similar to the first one. The clutch has not effect on the left PG. The value of τ_o when τ_i is zero (function projection) must be the same as that of the compound mode. τ_i is simply proportional to τ.

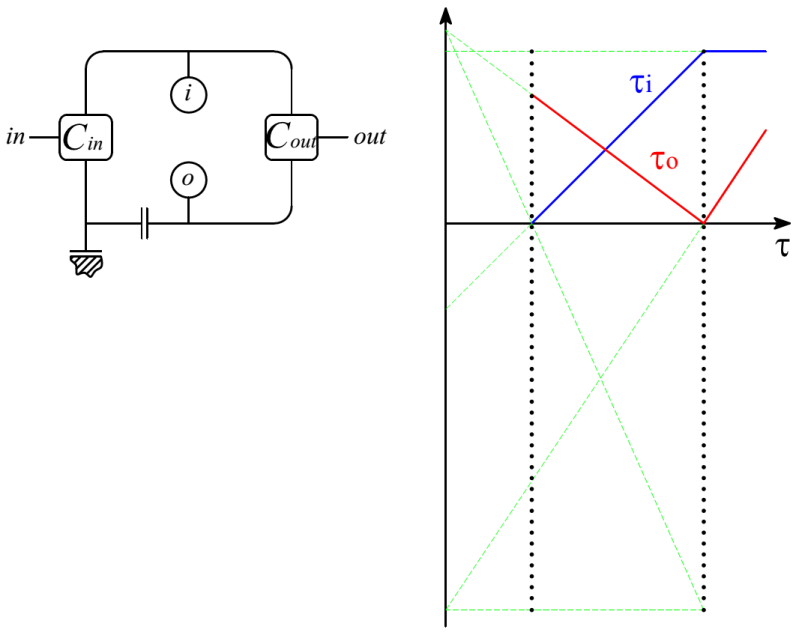

Fig. 37 Cross Bridge (shunt i-in)

The case (shunt i-in) is similar to the second one. The clutch has not effect on the right PG. The value of τ_o/τ_i must be the same when the τ is zero (functioning projection) for both the shunt and the compound mode. We exploit the similarity of the triangles with a vertex in $\tau_{\#i}$ the value that τ_o would assume for $\tau = 0$.

Obviously two shunt modes can coexist, if they refer to a different CVU shaft. In addition, an asynchronous switch can occur also if T_{in} or T_{out} are null (engine is idling or imminent braking) as the clutch can be disengaged and blocked as soon as its speed is adjusted.

Table 17 provides the analytical relationships between functional parameters.

Table 17 New functional parameters of the shunt modes of the Cross Bridge compound transmission

Shunt mode	$\tau_{\#i}$	$\tau_{i_{\#o}}$	$\tau_{\#o}$	$\tau_{o_{\#i}}$
o-out	=	=	0	=
o-in	=	$\frac{\tau_{i_{\#o}}}{\tau_{\#o}}\infty$	∞	=
i-out	0	=	=	=
i-in	∞	=	=	$\frac{\tau_{o_{\#i}}}{\tau_{\#i}}\infty$

13.3.2. Asymmetric Bridge – Synchronous switches

The Asymmetric bridge layout allow a synchronous switch only when the operation is performed on a particular branch of the driveline, as other solutions would determine either a parallel functioning or the need to be performed when the vehicle is still.

The key point is that the clutch has not effect on the left PG.

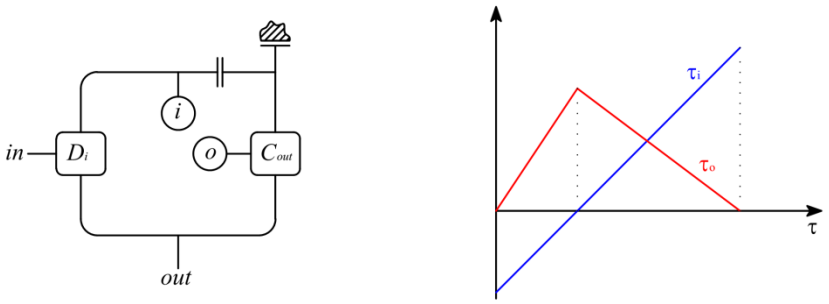

Fig. 38 Asymmetric Bridge (shunt o-out)

For the case (shunt o-out) the speed ratio τ_o becomes proportional to the overall speed ratio τ, while the function τ_i remains unaltered, as both the input and output speed are control variables.

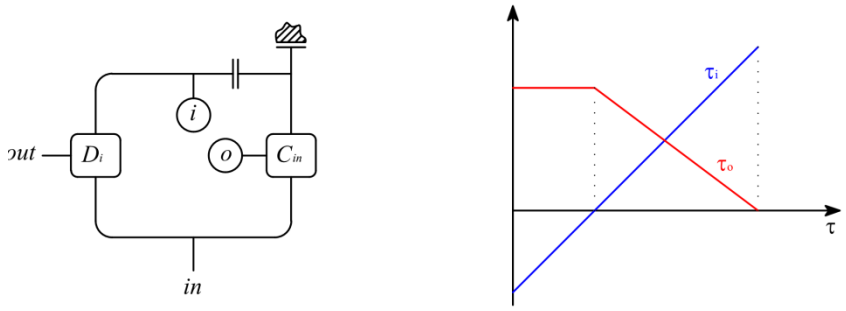

Fig. 39 Asymmetric Bridge (shunt o-in)

For the case (shunt o-in) the speed ratio τ_o becomes constant, while the function τ_i remains unaltered as well.

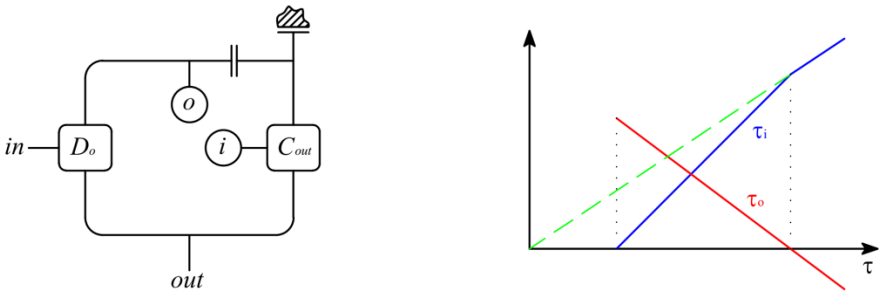

Fig. 40 Asymmetric Bridge (shunt i-out)

For the case (shunt i-out) the speed ratio τ_i becomes proportional to the overall speed ratio τ, while the function τ_o remains unaltered.

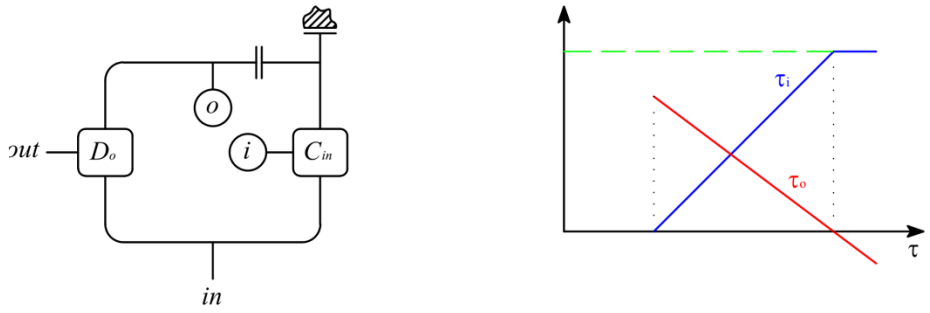

Fig. 41 Asymmetric Bridge (shunt i-in)

For the case (shunt i-in) the speed ratio τ_i becomes constant, while the function τ_o remains unaltered.

Table 18 New functional parameters of the shunt modes of the Asymmetric Bridge compound transmission when performed with a synchronous switch

Shunt mode	$\boldsymbol{\tau_{\#i}}$	$\boldsymbol{\tau_{i_{\#o}}}$	$\boldsymbol{\tau_{\#o}}$	$\boldsymbol{\tau_{o_{\#i}}}$
o-out	=	$\frac{-\tau_{i_{\#o}}\,\tau_{\#i}}{\tau_{\#o}-\tau_{\#i}}$	0	=
o-in	=	$\frac{\tau_{i_{\#o}}\,\infty}{\tau_{\#o}-\tau_{\#i}}$	∞	=
i-out	0	=	=	$\frac{\tau_{o_{\#i}}\,\tau_{\#o}}{\tau_{\#o}-\tau_{\#i}}$
i-in	∞	=	=	$\frac{-\tau_{o_{\#i}}\,\infty}{\tau_{\#o}-\tau_{\#i}}$

13.3.3. Asymmetric Bridge – Asynchronous switches

The key concept here is the following: if the engine is idling, the clutch linked to the same PG can be disengaged with no effects on the output torque. A synchronous coupling with the frame is still possible if $\tau = 0$ or by modifying the idling speed of the engine to match that the speed that makes the clutch itself motionless.

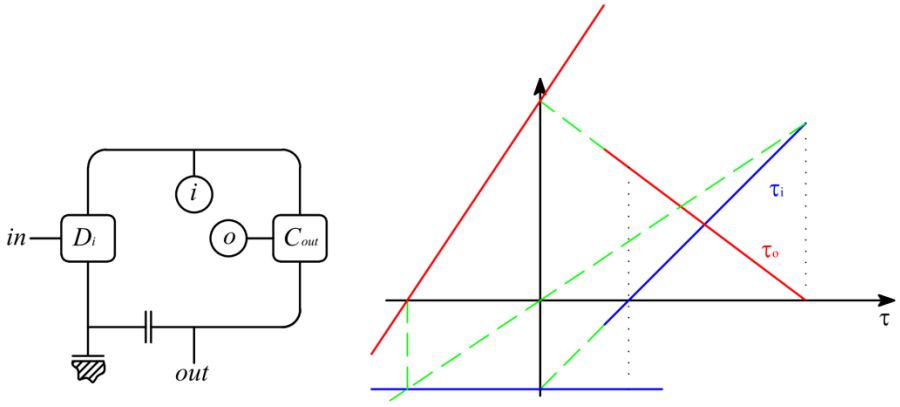

Fig. 42 Asymmetric Bridge (asynchronous shunt i-in)

In this case (shunt i-in) τ_o is zero for the same τ_i/τ ratio, while τ_i becomes constant.

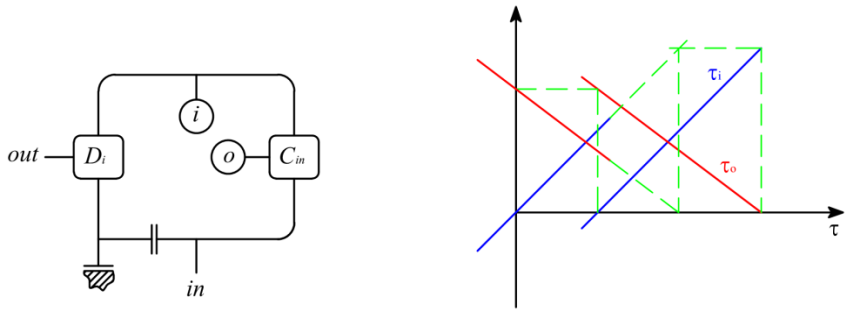

Fig. 43 Asymmetric Bridge (asynchronous shunt i-out)

In this case (shunt i-out) τ_i intercepts zero and is parallel to itself (the slope stays unaltered as it were $\tau \to \infty$). $\tau_{i\#o}$ and $\tau_{o\#i}$ remain the same as the right PG is not affected by the mode switch. The speed of the engine increases during the switch from compound to shunt.

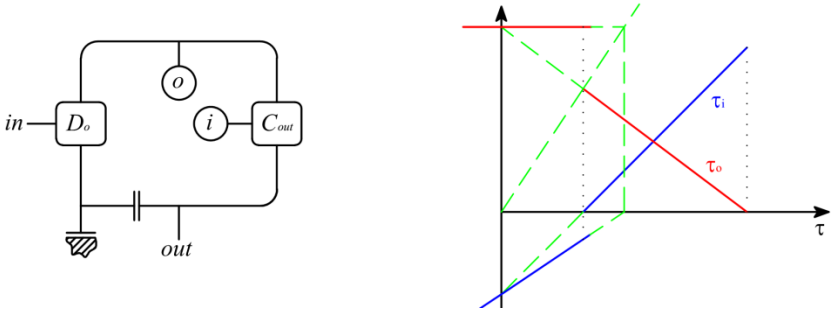

Fig. 44 Asymmetric Bridge (asynchronous shunt o-in)

In this case (shunt o-in) τ_i is zero for the same τ_o/τ ratio, and stay unaltered for $\tau = 0$.

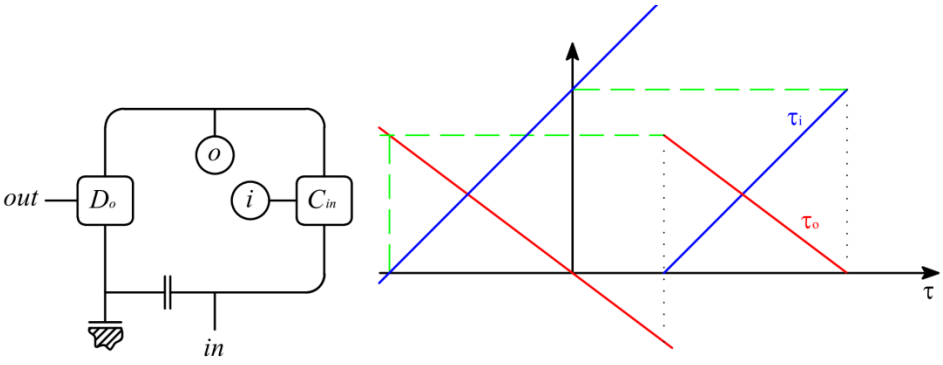

Fig. 45 Asymmetric Bridge (asynchronous shunt o-out)

In this case τ_o crosses the zero and is parallel to itself for either modes. $\tau_{\#i}$ and $\tau_{i\#o}$ remain the same as the right PG is not affected from the mode switch.

Table 19 New functional parameters of the shunt modes of the Asymmetric Bridge compound transmission when performed with an asynchronous switch

Shunt Mode	$\boldsymbol{\tau_{\#i}}$	$\boldsymbol{\tau_{i_{\#o}}}$	$\boldsymbol{\tau_{\#o}}$	$\boldsymbol{\tau_{o_{\#i}}}$
i-in	∞	$-\frac{\tau_{i_{\#o}}\,\tau_{\#i}}{\tau_{\#o}-\tau_{\#i}}$	$-\frac{\tau_{\#o}\,\tau_{\#i}}{\tau_{\#o}-\tau_{\#i}}$	$\frac{-\tau_{o_{\#i}}\,\infty}{\tau_{\#i}}$
i-out	0	=	$\tau_{\#o}-\tau_{\#i}$	=
o-in	$\frac{\tau_{\#i}\,\tau_{\#o}}{\tau_{\#o}-\tau_{\#i}}$	$\frac{\tau_{i_{\#o}}\infty}{\tau_{\#o}}$	∞	$\frac{\tau_{o_{\#i}}\,\tau_{\#o}}{\tau_{\#o}-\tau_{\#i}}$
o-out	$\tau_{\#i}-\tau_{\#o}$	=	0	=

13.3.4. Direct Bridge – Asynchronous switches

The direct bridge mode permits only asyncronous switches, as the internal branches are linked to either the input or output of the PS-CVT.

This switch is particularly simple to define since one speed characteristic will not be affected by it, while the other will be either parallel to itself (crossing the zero) or constant (crossing the original intercept with the vertical axis).

One characteristic is parallel to itself because its slope is also the limit for $\tau \to \infty$, the other one stay unaltered because input and output speed are our control parameters.

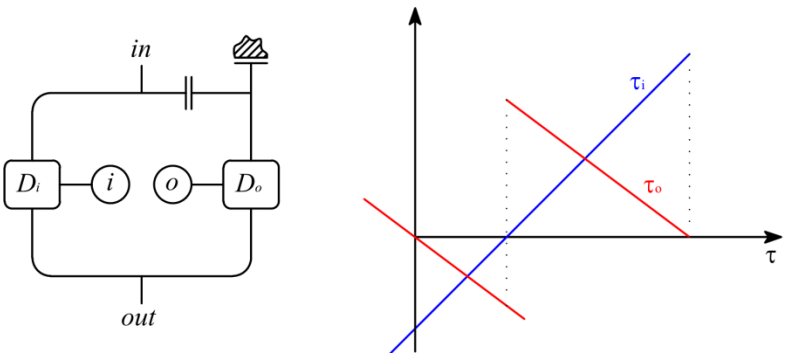

Fig. 46 Direct Bridge (asynchronous shunt i-in)

In this case (shunt i-in) τ_o is parallel to itself and it crosses the zero. τ_i is not modified.

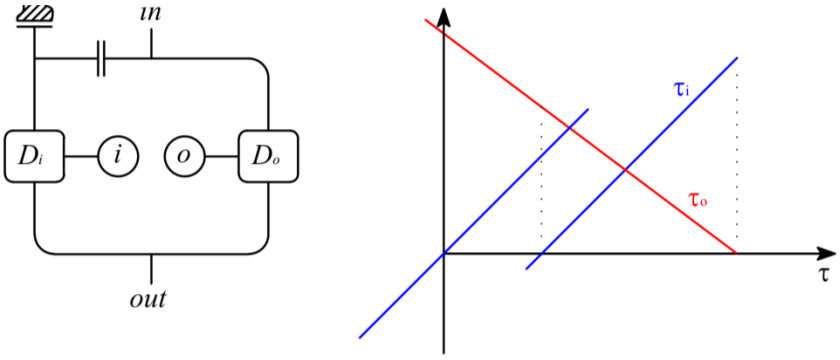

Fig. 47 Direct Bridge (asynchronous shunt o-in)

In this case (shunt o-in) τ_i is parallel to itself and it crosses the zero. τ_o is not modified.

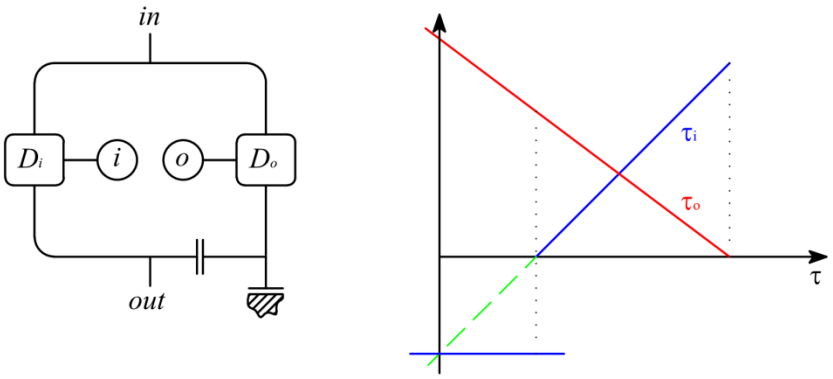

Fig. 48 Direct Bridge (asynchronous shunt i-out)

In this case (shunt i-out) τ_i takes the value that it had for the stall speed. τ_o is not modified.

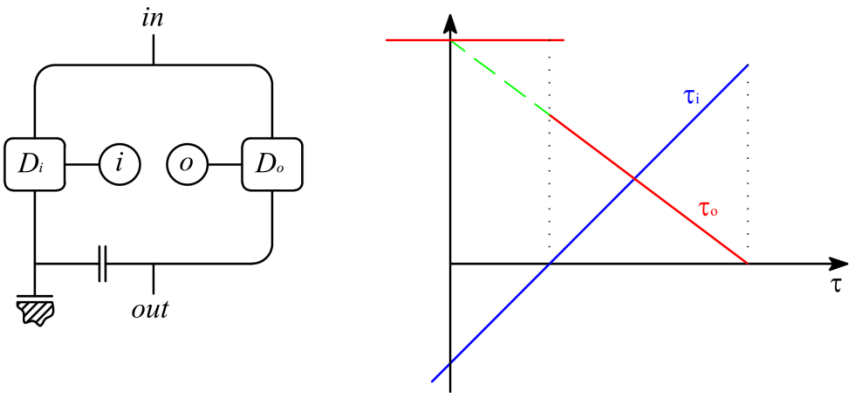

Fig. 49 Direct Bridge (asynchronous shunt o-out)

In this case (shunt o-out) τ_o takes the value that it had for the stall speed. τ_i is not modified

Table 20 New functional parameters of the shunt modes of the Direct Bridge compound transmission when performed with an asynchronous switch

Clutch	$\boldsymbol{\tau_{\#i}}$	$\boldsymbol{\tau_{i_{\#o}}}$	$\boldsymbol{\tau_{\#o}}$	$\boldsymbol{\tau_{o_{\#i}}}$
i-in	=	$\frac{-\tau_{i_{\#o}}\,\tau_{\#i}}{\tau_{\#o}-\tau_{\#i}}$	0	$\frac{-\tau_{o_{\#i}}\,\tau_{\#i}}{\tau_{\#o}-\tau_{\#i}}$
o-in	0	$\frac{\tau_{i_{\#o}}\,\tau_{\#o}}{\tau_{\#o}-\tau_{\#i}}$	=	$\frac{\tau_{o_{\#i}}\,\tau_{\#o}}{\tau_{\#o}-\tau_{\#i}}$
i-out	∞	$\frac{-\tau_{i_{\#o}}\,\tau_{\#i}}{\tau_{\#o}-\tau_{\#i}}$	=	$\frac{-\tau_{o_{\#i}}\,\infty}{\tau_{\#o}-\tau_{\#i}}$
o-out	=	$\frac{\tau_{i_{\#o}}\,\infty}{\tau_{\#o}-\tau_{\#i}}$	∞	$\frac{\tau_{o_{\#i}}\,\tau_{\#o}}{\tau_{\#o}-\tau_{\#i}}$

14. PSU design guidelines

14.1. Functional guidelines

The relationships between mechanical points and main power flows have been described in the previous sections 1.3. Obviously, since the CVU is often the most expensive (and less efficient) element of the PS-CVT, limiting the power flowing through it will benefit the overall performances.

The values of $\tau_{\#o}$ and $\tau_{\#i}$ should be the ones that guarantee the best fit between deliverable and delivered power, which implies a good sizing of the CVU. Since this choice can be strongly influenced by the CVU's apparent efficiency maps (which might model both the real efficiency and the presence of an energy storage system with its control strategy), it is clear that a rigorous choice of these parameters is possible only for a specific study case.

If the speed ratio of the CVU is restricted by constructive issues (e.g. when using a V-belt variator), it is no longer possible to work in correspondence of a mechanical point, as neither τ_i or τ_o can be null. Obviously, in this case it also exists a univocal relationship between η_v and Θ, which can be easily achieved considering the results of section 1.3.

$$\Theta = -\left(\frac{\eta_v\,(\tau_{\#o} - \tau_{\#i})}{\eta_v - \tau_v/\tau_{v_\#}} + \tau_{\#i}\right)^{-1} \tag{145}$$

The tuning variables here are $\tau_{\#o}$, $\tau_{\#i}$ and $\tau_{v_\#}$.Yet, the actual working range of the PS-CVT is restricted by the operative limits of the CVU, in terms of maximum and minimum speed ratio τ_{v_M} and τ_{v_m}, which means that establishing the related maximum and minimum overall speed ratio τ_M and τ_m introduce two new constraints. The optimization the previous expression will close the problem.

Interestingly, in this case the condition that minimize the absolute value of $|p_i|$ (and thus maximizes the overall efficiency) in always ideally reached for a CVU speed ratio:

$$\tau_{v_{opt}} = \sqrt{\eta_v \, \tau_{v_M} \, \tau_{v_m}} \tag{146}$$

So assigning this particular condition to a specific overall speed ratio will reduce the problem to a simple system of three eq. (10). The CVU efficiency η_v is mostly a function of the CVU speed ratio itself, but also of the absolute working conditions (torque and speed), so it is necessary to follow an iterative approach starting with a constant guess value.

If the CVU is electrical, then the overall torque ratio Θ is a controllable parameter. In this case, the functional optimization requires to select the best pair of mechanical points and a proper control strategy in order to minimize the size of the electric machines, in terms of overall speed ratio τ and torque ratio Θ. In particular, the conditions that make equal and opposite P_i and P_o are:

$$P_i = -P_o = \frac{(\tau - \tau_{\#i})\,(\tau - \tau_{\#o})}{\tau_{\#i} - \tau_{\#o}} P_{out} \tag{147}$$

$$\Theta = -1/\tau \tag{148}$$

While P_i and P_o are identical if:

$$P_i = P_o = \frac{(\tau - \tau_{\#i})\,(\tau - \tau_{\#o})}{\tau_{\#i} + \tau_{\#o} - 2\tau} P_{out}; \tag{149}$$

$$\Theta = \frac{(\tau_{\#i} + \tau_{\#o}) - 2\,\tau}{\tau\,(\tau_{\#i} + \tau_{\#o}) - 2\,\tau_{\#i}\,\tau_{\#o}} \tag{150}$$

Eq. (147) and (148) imply that the engine is delivering the required output power, while eq. (149) and (150) imply either a deficit or a surplus. In particular, the electrical power calculated by eq. (147) is smaller than that calculated by eq. (149) within mechanical points. According to the previous criteria, the optimal value of the overall torque ratio Θ is always within the range $-1/\max(\tau_{\#i}, \tau_{\#o}) > \Theta > -1/\min(\tau_{\#i}, \tau_{\#o})$, and in such conditions the engine will deliver more power ($\tau < \min(\tau_{\#i}, \tau_{\#o})$) or less power ($\tau > \max(\tau_{\#i}, \tau_{\#o})$) than necessary when working outside the mechanical points.

Eventually, if $\Theta > -1/\max(\tau_{\#i}, \tau_{\#o})$, it is always possible (and beneficial) to choke the engine in order to meet eq. (148) or eq. (150) . Vice versa, if it is $\Theta < -1/\min(\tau_{\#i}, \tau_{\#o})$ and the engine is at WOT (because of the high power demand), choking the engine will always worsen the MGs' operating conditions, because raising Θ implies both higher P_i and P_o.

14.2. Constructive guidelines

For given mechanical points, the CVU power flows are mostly independent from the actual constructive arrangement of the gear sets, as small variations are entirely due to the mechanical losses. Obviously, the mechanical losses depend on the internal power flow circulation, which changes depending on the functional layout, and, for a given layout, on the arrangement of the gear within each TPM. Accordingly, it exist an ideal solution in terms of both mechanical and electrical losses, but such solution may not be always viable.

14.2.1. Planetary gear sets

Generally speaking, a TPM is a gear set used to combine multiple sources of mechanical power with one or more loads. The core of the TPM is the planetary gear set (PG), yet wrapping pairs and/or ordinary gear sets (OGs) are often included as well. Most automatic transmission use two or more PGs and a hydraulic torque converter to deliver a discrete number of gear ratios without torque shocks. Power-split units (PSUs) used in hybrid electric vehicles (HEVs) are conceptually similar, but the transmission can work seamlessly between mechanical points thanks to two electric motors. As a result, in HEVs the torque converter is omitted.

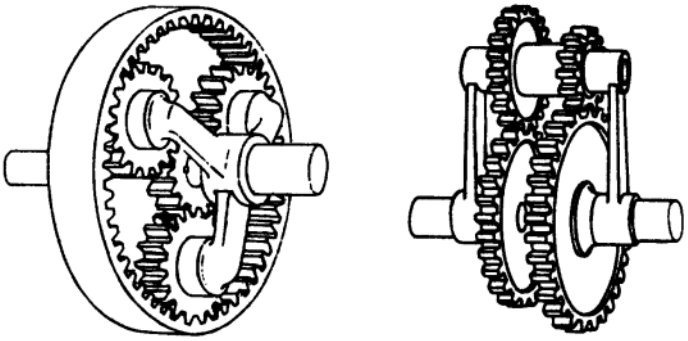

Fig. 50 Simple planetary gear sets

A detailed design of PGs and OGs is not the main aim of this work, but some practical guidelines are indeed necessary in order to restrain the dominion of feasible solutions. As regards the gear ratios, AGMA [110] prescribes a maximum teeth ratio of five for external meshing gears:

$$1/5 < z_1/z_2 < 5 \tag{151}$$

And the following interval for internal meshing gears (z_1 is the ring):

$$11/5 < z_1/z_2 < 7 \tag{152}$$

The constructive parameter (aka Willis' ratio) of simple PGs is determined by the ratio between teeth of their sun and ring gears:

$$\psi = -z_S/z_R \tag{153}$$

And usually it is comprised between -1/3 and 2/3. In theory, the number of teeth of each planet is equal to:

$$z_P = (z_R - z_S)/2 \tag{154}$$

Nonetheless, a few teeth less still guarantee a proper functioning thanks to the resilience of the involute profile in respect of inter-axis distance. The PG is also subject to manufacturing tolerances, strains and thermic deformation, so at least one element of the PG should be able

to adapt its position in order to allow a uniform load distribution among planets. In addition, the planets must be equally spaced, which is possible only if the total number of teeth of the central gears is a multiple of the planets engaging with them.

Stepped-planet and double pinion PGs offer a wider range of feasible constructive ratios than simple PGs, thanks to the additional planets. The planets of the stepped PG are coaxial, so an additional geometric constraint has to be taken into account. The planets of double pinions PGs must fit into the space between ring and sun gear. Other limitations occur for PGs with multiple planets, as their diameters' ratio should not exceed a value of three. However, this is not a direct constraint on the number of teeth of stepped planet PGs, as their module can be different ($D = m\ z$):

$$1/3 < D_1/D_2 < 3 \tag{155}$$

Extreme speed ratios might be easily obtained by mean of compound PGs, but with additional weight and costs. A compound PG can be made of two simple PGs with two isokinetic joints, but some gears can also be shared, as in the Ravignaux gear set. A compound PG can have at least 4 potential output shafts, but if a

In terms of longitudinal encumbrances, the face width of a gear should be comprised between three times and five times the pitch length $p = \pi\ m$:

$$3p < W < 5p \tag{156}$$

In addition, a minimum number of teeth is required in order to avoid interference and undercut. For instance, for a pressure angle of 20 degrees, it is:

$$z \geq 18 \tag{157}$$

In conclusion, the choice of the module, and thus the gear's size, is subordinate to the resistance of the tooth.

14.2.2. PG efficiency

For a given layout, functionally equivalent TPMs could be obtained with three different Willis' ratios, according to the position of the planet carrier. In this section, we are going to show which of the three possible choices can achieve better results, i.e. lower mechanical losses, keeping unaltered the functional parameters.

In particular, in the previous sections we have shown that the mechanical losses of a PG, for given functional parameters (i.e. kinematics and ideal power flows), depend mostly on the parameter $\eta_{Y/X}^{Z}$, which is just function of the position of the planet carrier (and related constructive Willis' ratio, see Table 5). Accordingly, in order to compare the efficiency of the three possible constructive solutions, we have to:

- take one of them (and its constructive Willis' ratio Ψ) as a reference
- calculate in function of Ψ the constructive Willis' ratios ψ of the other two solutions according to the position of their planet carriers (first column of Table 21)
- calculate their respective parameters $\eta_{Y/X}^{Z}$ from Table 5 (second column of Table 21)
- express the same parameters as functions of Ψ using Table 4 to ease the comparison (third column of Table 21)
- approximate the loss factor (last column of Table 21)

If we choose $\Psi = \psi_{Y/X}^{Z}$ as a reference for the Willis' ratio and, consequently, Z for the position of the planet carrier, then the relationships of Table 4 and Table 5 lead to the results listed in Table 21 for the carrier linked to either Y (second row) or X (last row) instead of Z (first row). The farther would be the value of $\eta_{Y/X}^{Z}(\Psi)$ (second-last column of Table 21) from unity, calculated both for $\eta_o < 1$ and for its reciprocal, the worst would be the losses related to that constructive solution. Moreover, it is worth noting that η_o can change from one constructive solution to another because of the different number of meshing pairs necessary to realize certain values of the constructive Willis' ratio $\psi(\Psi)$ (and a proper ring gear may not be present as well). However, considering that the basic efficiency η_0 is generally high, i.e. $\eta_o \to 1$, it is possible to simplify the results as shown in the last column of Table 21, following the same procedure exemplified by eq.(67).

Table 21 Apparent efficiency of the PG for different positions of the planet carrier.

$\boldsymbol{Z}$	$\boldsymbol{Y}$	$\boldsymbol{X}$	$\boldsymbol{\psi}(\Psi) = \boldsymbol{\psi}^{\boldsymbol{C}}_{\boldsymbol{R/S}}$	$\boldsymbol{\eta}^{\boldsymbol{Z}}_{\boldsymbol{Y/X}}(\psi)$	$\boldsymbol{\eta}^{\boldsymbol{Z}}_{\boldsymbol{Y/X}}(\Psi)$	$\lvert\mathbf{1} - \boldsymbol{\eta}^{\boldsymbol{Z}}_{\boldsymbol{Y/X}}\rvert$ for $\eta_0 \to 1$
C	R	S	Ψ	$\eta^{C}_{R/S} = \eta_o$	η_o	$\lvert 1 - \eta_o \rvert$
S	C	R	$1 - \frac{1}{\Psi}$	$\eta^{S}_{C/R} = \frac{\eta_o - \psi}{\eta_o(1-\psi)}$	$\frac{1-\Psi}{\eta_o} + \Psi$	$\lvert 1 - \eta_o \rvert$ $\lvert 1 - \Psi \rvert$
R	S	C	$\frac{1}{1-\Psi}$	$\eta^{R}_{S/C} = \frac{1-\psi}{\eta_0 - \psi}$	$\left(\frac{1-\Psi^{-1}}{\eta_o^{-1}} + \Psi^{-1}\right)^{-1}$	$\lvert 1 - \eta_o \rvert$ $\left\lvert\frac{1-\Psi}{\Psi}\right\rvert$

From the analysis of the functions in Table 21, we get that whichever is the value of the reference Willis' ratio Ψ, two out of the three possible solutions have their constructive Willis' ratio $\psi(\Psi) > 0$ and both are worse than that with $\psi(\Psi) < 0$, whichever are the working conditions. Indeed, $|1 - \eta^{Z}_{Y/X}|$ is the only factor modifying eq. (68), since the kinematics and the ideal power flows stay unaltered. In addition, it results that the worst of the two solutions with $\psi > 0$ is the one requiring $0.5 < \psi < 2$, which is obtained if the carrier of the PG is linked to the shaft that should be connected to the sun of the PG with $\psi < 0$. For the above reasons, we suggest to try to limit the design chart to the negative values of the Willis' ratio, as in [20]. If a negative Willis' ratio is not feasible, the designer can try, at worst, to connect the carrier to the ring position of the ideally optimal (but not feasible) solution. In other terms, it is strongly recommended to exclude the possibility of using constructive Willis' ratios in the range $0.5 < \psi < 2$ as early as in the preliminary design process.

14.2.3. Feasibility

Practical designs require the physical feasibility of the necessary connections. While it is easy to design shunt transmissions, it can be difficult to obtain the desired compound PSU, especially when internal shafts must be accessible for clutch operations. In particular, the frame should offer anchorage points close to the axis of the driveline, especially in order to support the electric machines directly, as it is better to limit the size of the bearings. At the same time, it is necessary to avoid intricate coaxial designs, as it makes the driveline difficult to construct and mount, thus affecting negatively both volumes and costs.

Fixed gear sets should be avoided when possible. Often some ordinary joint is necessary anyway because of unavoidable space constraints, as it is not always possible to mount the driveline on the same axis of the engine and/or the traction wheels. Similarly, the CVU might be intrinsically not coaxial (for instance a V-belt variator), thus requiring some intermediate reduction stages. On the other hand, internal gearing are likely to require a countershaft, which is conceptually equivalent to an additional fixed-carrier PG. In this case, it may be more convenient to design directly a higher order of PSU, fully exploiting the PG with a multimode transmission.

Eventually, although not particularly binding, torque and speed limitations for the gear sets exist, so it is necessary to maintain these values within their specifics. In theory, gears working at higher speeds generate more noise and vibrations, as well as higher viscous losses and a faster damaging of the bearings. However, if the constructive layout is unaltered, the resulting lower torques will lead to an overall lighter design, which is beneficial in terms of volumes and weights, but also vibrations and reliability.

15. Modeling of the power sources

Despite noteworthy improvements, chemical energy carriers still show overwhelming energy density in comparison to their electrical counterparts [1-13]. Yet, the medium-term storage capacity of batteries and super capacitators offers significant opportunities for the improvement of the overall transmission efficiency. For these reasons, several car manufacturers are trying to comply with the legislators by developing hybrid electric vehicles. In particular, the ability to store energy can be a solution to recuperate the kinetic energy of the vehicle, but also to assist the prime engine, enhancing both its peak performances and part-load operation. Nonetheless

In this section, we will describe some simple parametrization techniques for the main components of Hybrid electric PS-CVTs.

15.1. Internal combustion engines

The quasi-static behavior of internal combustion engines (ICE) is defined by mean of torque-speed maps. Such maps can represent either their specific fuel consumptions directly, or the engine's efficiency, calculated as the ratio between output power and required fuel enthalpy flow. Such efficiency is low on average because of frequent part load operations, but also because the definition of the parameter itself is not very fair, as the engine operates the transformation of low quality energy (heat) into high quality power (mechanical).

The power yield of ICEs is the result of complex thermodynamic phenomena and cannot be predicted easily. Experimental results are reliable, but also expensive and hardly scalable. Similarly, numerical simulation tools offer verisimilar results, but at the cost of high computational efforts.

Nonetheless, the Willans description offers a rather good approximation of an ICE:

$$\wp_e = \eta_{fe}\,\wp_f - \wp_l \tag{158}$$

In other terms, the mean effective pressure $\wp_e$ is a fraction η_{fe} of the ideal fuel pressure $\wp_f$, net of the mechanical and pumping pressure losses $\wp_l$. The two parameters η_{fe} and $\wp_l$ can be considered functions of the engine's speed only, while $\wp_f$ is function of the fuel charge into the cylinder:

$$\wp_f = \frac{4}{\pi}\,\frac{m_f\,H_f}{S\,B^2} \tag{159}$$

For a 4-stroke engine, it is well known that the mean effective pressure is related to the torque by the following relationship:

$$T = \wp_e\,\frac{S\,B^2}{16} \tag{160}$$

In which S is the stroke, B is the bore of the cylinder, m_f is the mass of fuel and H_f is its lower specific heat. Interestingly, for given type of engine, the mean effective pressure is barely influenced by its size, making the obtained results easily scalable. The specific consumption is then:

$$c_f = \frac{m_f}{2\,\pi\,T} = \frac{2}{\eta_{fe}\,H_f}\left(1+\frac{\wp_l}{\wp_e}\right) = \frac{2}{\eta_{fe}\,H_f}\left(1+\wp_l\,\frac{S\,B^2}{16\,T}\right) \tag{161}$$

The pressure loss $\wp_l$ raises with the speed, while the thermodynamic parameter η_{fe} shows a maximum for speeds slightly higher than the maximum torque regime. As a result, the speed related to the least specific consumption decreases along with the loads, as the effect of $\wp_l$ becomes more relevant than the thermodynamic efficiency η_{fe}. Eq. (159) does not take into account mixture enrichment at high loads, which may be necessary in order to avoid detonation phenomena due to high temperatures, but assumes a strictly stoichiometric air/fuel ratio; in other terms, m_f is considered to be completely burnt. Accordingly, if enrichment occurs, c_f must be multiplied by a corrective factor (equal to the ratio between

supplied and burnt fuel) in order to express the real specific consumptions. For these reasons, in such conditions the best operating conditions will not occur at WOT.

Eventually, inertial effects should be taken into account. The torque delivered by the engine will be altered by the quantity:

$$T_J = -J_e \dot{\omega}_e \tag{162}$$

In which J_e is the inertia of the engine, which can be considered roughly proportional to its displacement, and $\dot{\omega}_e$ is its angular acceleration.

From eq. (161), it is obvious that an engine tends to be more efficient at high loads. Yet, the former is often oversized in order to guarantee minimum acceleration performances, thus being forced to work at part loads in most of the driving cycle.

Turbocharging is a solution widely recognized as simple, effective and economic, as it permits to satisfy the peak requirements with a downsized engine. Similarly, different levels of hybridization can help sustaining performances while sensibly reducing fuel consumptions.

In particular, start&stop devices remove the idling losses of the engine during standstill, while proper hybrid electric vehicles can also operate the engine more efficiently, thanks to their alternate functioning. Yet, beyond the additional costs, weights and complexity, the control of such systems is not trivial, as the definition of the cost function tends to be elusive. Indeed, the cost of the energy stored into the batteries depends primarily on its sources (fuel, regenerative braking, electric grid), but also on the charging conditions themselves (engine operating point, currents, state of charge).

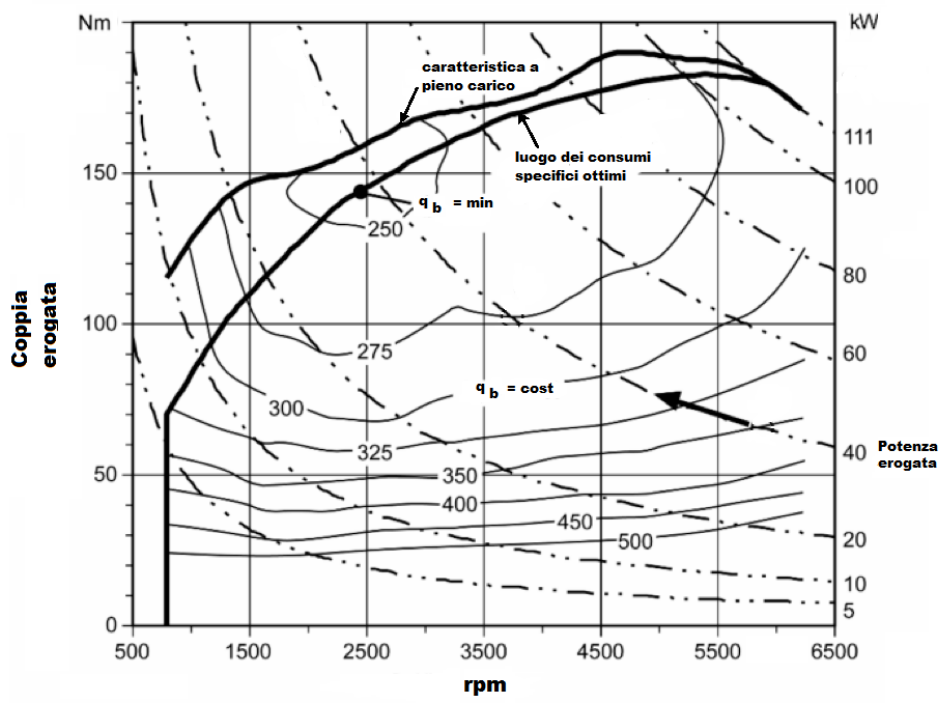

Fig. 51 ICE map

15.2. Electric motors

Currently, permanent magnets synchronous motors are widespread in HEVs. Their main advantage over asynchronous induction machines is the overall better controllability, efficiency and power density. On the other hand, they are more expensive because of the rare-earth materials, and their speed range tends to be sensibly tighter, especially when the magnets are mounted on the rotor's surface. Eventually, switched reluctance motors show low costs and good performances, but control and functioning issues have prevented their success.

Electric motors can be modeled by mean of the Willans approach as well. The neat mechanical torque T is the difference between the indicated torque, solely due energy conversion, and mechanical losses P_l.

$$T = \frac{\eta_m P_{el} - P_l}{\omega} \tag{163}$$

Obviously the electrical efficiency η_m switches accordingly to the sign of P_{el}, and, along with P_l, it is mostly function of the speed, but can be averaged with good approximation. In order to make the model easily scalable, it is possible to refer the torque to an equivalent quantity, namely the mean effective tension t_m, i.e. a uniform tangential stress distributed on the surface of the rotor:

$$T = t_m \left(\frac{\pi D^2 L}{2} \right) \tag{164}$$

The value of t_m tends to be an order of magnitude lower than the main effective pressure of the engines, and similarly to the eq. (158) and (163), it can be calculated as:

$$t_m = \eta_m t_{el} - t_l \tag{165}$$

Obviously, eq. (165) is simply equivalent to eq. (163) if both terms are multiplied for $\pi D^2 L/2$. The specific electric consumption will be:

$$c_{el} = \frac{P_{el}}{\omega T} = \frac{1}{\eta_m}\left(1 + \frac{t_l}{t_m}\right) = \frac{1}{\eta_m}\left(1 + \frac{P_l}{P}\right) \tag{166}$$

15.3. Batteries and Super Capacitors

Batteries are electro-chemical converters used to store energy. They are characterized by their maximum power (kW) and nominal capacity (Ah), which depends on the reference discharge current and cut voltage. The nominal capacity can be used to assess the instantaneous capacity by mean of the Peukert equation:

$$\frac{Q}{Q_0} = \left(\frac{I}{I_0}\right)^{\beta} \tag{167}$$

In which Q_0 and I_0 are the reference capacity and current, and β is a constant depending on the battery. If I_0 is the current that discharge the battery in one hour, then the ratio I/I_0 is the C-rate.

To preserve their lifespan, batteries are not depleted or charged completely; accordingly, their state of charge (SOC) is maintained within a certain range, and the available energy (Wh) remains just a fraction (up to 70% for lithium-ion batteries) of the stored energy.

The SOC is defined as the ratio between charge and nominal battery capacity. Since the SOC affects the internal resistance R and the open circuit voltage V_0, the nominal voltage usually refers to a 50% SOC. Both the resistance and the open circuit voltage can be considered linear functions of the SOC, but the former depends also on the sign of the current. In particular, the battery will show more resistance when the current forces the SOC to its extreme values. The voltage applied to the battery will be:

$$V = \frac{V_0}{2}\left(1 + \sqrt{1 - 4\,R\,P/V_0^2}\right) \tag{168}$$

In which P is the delivered power. In theory, the maximum available power is equal to $V_0^2/4R$, the current I is equal to $V_0/2R$ and the voltage V is equal to $V_0/2$ (in this circumstance, the power loss equals P, and applying a lower voltage would not have benefits, as the power losses would exceed the yield). In practice, the maximum power is subject to a tighter constraint, as the battery has current limits.

For given delivered power and SOC, it is possible to predict the current, and therefore the discharge rate of the battery. Vice versa, parasitic reactions occur when charging the battery and a corrective factor η_C (Coulombic efficiency) for the charging current has to be taken into account:

$$\dot{Q} = -\eta_C \, I \tag{169}$$

More complex models, addressing fatigue, self-discharge, aging, temperature etc., are profusely available in literature.

Super capacitors fulfill the same duties of batteries, but differ in terms of specific power and energy, which makes them suitable for intense brief operations. Eq. (168) may still apply, but the open circuit voltage depends on the charge Q and capacity C of the super capacitor.

$$V_0 = \frac{Q}{C} \tag{170}$$

16. Design applications

16.1. Shunt electric PS-CVT

Our goal is to design a PS-CVT able to mimic the behavior of a full electric vehicle in terms of output torque.

In our example [123] , the available internal combustion engine delivers its maximum torque of 170 N m at 2500 rpm and its maximum power of 80 kW at 5500 rpm. In order to facilitate the reproducibility of the results, the previous data is used to interpolate its WOT torque function by mean of a third grade polynomial (see Fig. 52); nonetheless, experimental data can be used as well. The engine operative speed range is between 800 rpm and 5800 rpm.

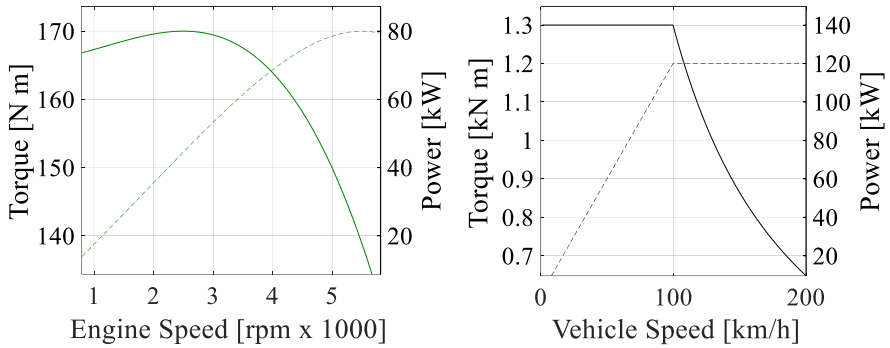

Fig. 52 Left figure: WOT torque and power (dashed green line) for the available I.C.E. Right figure: desired torque and power (dashed black line) at wheels.

The vehicle must be able to deliver its maximum torque until it reaches the speed of about 100 km/h (1300 N m in the speed range between 0 and 100 km/h), and then it must provide at least the same amount of output power until it reaches the maximum speed of 200 km/h (120 kW between 100 and 200 km/h, See Fig. 52).

These performances require the assistance of the electric motors, so the charge condition of the batteries is assumed to be adequate. In particular, the engine alone can deliver up to 80 kW, so it is not able to provide enough power starting from 67 km/h (see Fig. 52). The

electric motors can deliver their (maximum) constant torque up to their base speed of 3500 rpm, and then their (maximum) constant power up to 10000 rpm. As usual for PS-CVTs, they will be used also to perform full electric operations, regenerative breaking, cranking of the engine and general speed control.

The main optimization objective is to minimize the size of the electric motors and, consequently, of the related power electronics. Since the vehicle will be equipped with a couple of electric motors/generators (MGs), it is appropriate to provide at least for a full electric vehicle (FEV) functioning within urban areas. Accordingly, alternative functioning modes for low speeds will be addressed in this paper.

16.1.1. Optimization of the functional parameters

The optimization, which changes the mechanical points and the local torque ratio Θ until the least maximum electrical power is obtained, converged to an output-split solution, as for a wheel radius $R = 0.3\ m$, the optimal mechanical points are $\tau_{\#i} \to \infty$ and $\tau_{\#o} = 0.218$. For most of the vehicle's speed range, the overall torque ratio Θ follows the condition (150) that makes equal the power supplied by the MGs.

The engine is always operated at WOT, and each MG must deliver about 34.3 kW. Interestingly, the speed ratio and the torque ratio are almost constant ($\tau = 0.305,\ \Theta = -7.72$) for speeds up to $100\ km/h$, then τ changes very slowly until the engine reaches its top speed (at about $172\ km/h$), beyond which Eq. (150) cannot be fulfilled anymore. As a result, P_i and P_o diverge, and the latter takes again its peak value at the top speed of the vehicle, for $\tau = \frac{25}{3\pi}\ \frac{V_{max}}{n_{max}\ R} = 0.305$ and $\Theta = \frac{P_{out}\ (V_{max})}{\tau\ P_{in}\ (n_{max})} = -4.96$ (see Fig. 53).

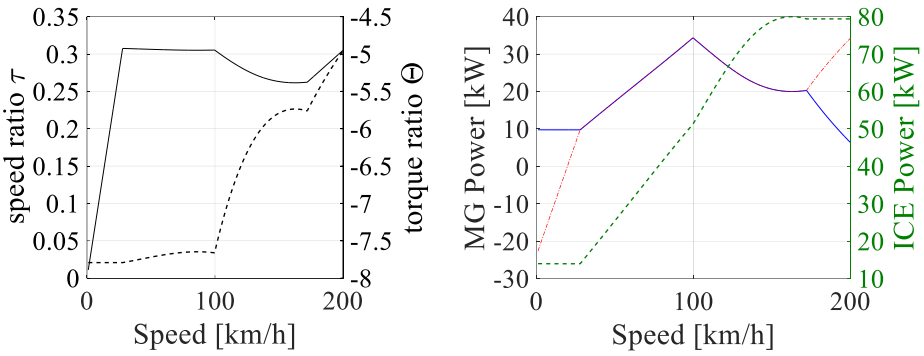

Fig. 53 Left figure: Optimal overall speed and torque (dashed line) ratios for the PS-CVT. Right figure: powers supplied by motors (blue for P_i, dash-dot red for P_o) and engine (dashed green).

Basically, the optimization makes equal and minimize the peak electrical power for the critical conditions, which are the base speed of $100\ km/h$ (the vehicle must provide both the maximum torque and power) and the top speed (P_o reaches its peak again). Unfortunately, the downsizing of the engine forces the control strategy to resort to Eq. (150) instead of Eq. (148) between mechanical points, while the engine's speed limits cause the divergence between electrical powers for speed lower than $27\ km/h$ and higher than $172\ km/h$. Accordingly, P_i and P_o overlap only between 27 km/h and 172 km/h.

It is worth noting that between 100 and $200\ km/h$ the electric motors could deliver more power than necessary, so in this speed range the real performances can exceed the design requirements.

16.1.2. Synchronous ratio

Both the MGs have to be faster than their base speed at 100 km/h (first power peak), and slower than their maximum speed in the whole operation range. At 100 km/h, the engine is rotating at about $2900\ rpm$ (see Fig. 54). In particular, assuming that the base speed of both the MGs is higher ($3500\ rpm$) and choosing $\tau_* = 0.305$ (see Fig. 53) as the synchronous ratio, an additional gear stage $k_{in} = 0.82$ linking the engine to the input shaft is required in order to make the MGs reach their base speed at $100\ km/h$; accordingly, the final drive ratio

is $k_{out} = \tau_* \, k_{in} = 0.25$, and since the additional multiplication gear stages are on main shafts, the relative CVU speed ratios are ($\tau_{\#i} \to \infty$ and $\tau_{\#o} = 0.218$):

$$\tau_{i_{\#o}} = \frac{1}{k_{in}} \frac{\tau_{\#o} - \tau_{\#i}}{\tau_* - \tau_{\#i}} = 1.22 \tag{171}$$

$$\tau_{o_{\#i}} = \frac{1}{k_{in}} \frac{\tau_{\#i} - \tau_{\#o}}{\tau_* - \tau_{\#o}} = 14.0 \cdot \infty \tag{172}$$

The functioning of the PS-CVT is now totally defined and absolute torques and speeds (see Fig. 54) can be calculated thanks to the relationships of section 1.1.

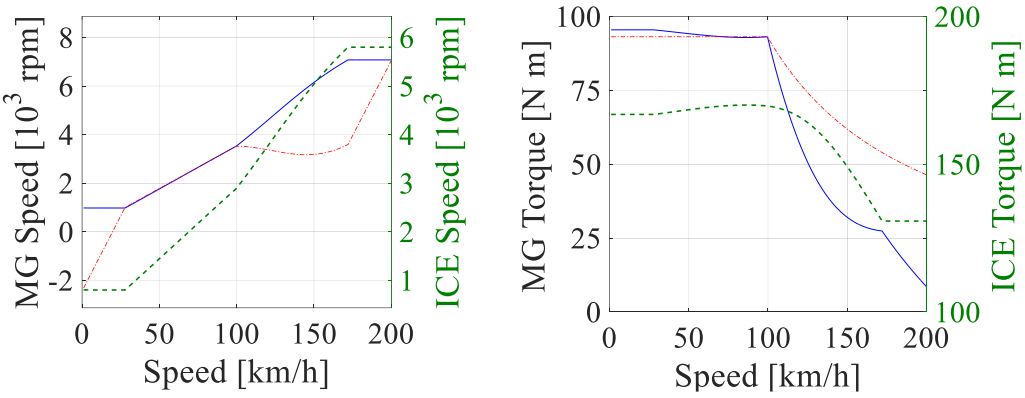

Fig. 54 Overall speeds (left figure) and torques (right figure) for the PS-CVT operating with the overall torque and speed ratios of Fig. 53 (blue for MG_i, dash-dot red for MG_o, dashed green for the ICE)

The speed of $2900\ rpm$ would be the upper limit for the base speed of the MGs in order to avoid the additional multiplication gear stage k_{in}. In theory, eliminating k_{in} would be beneficial for overall efficiency, encumbrances and costs. Yet, since the base speed of the available MGs is higher ($3500\ rpm$), in this circumstance significantly bigger machines would be necessary, because the electric motors would be supposed to deliver more torque than about 95 N m between zero and 100 km/h. In particular, they should be able to deliver about 43 kW each, thus being oversized in respect of the required maximum power, which is inferior to 35 kW.

16.1.3. Functional Layout

The PS-CVT layout can be identified thanks to the design chart [20]. The characteristic curve that offers constructive ratios within -1/3 and -2/3 for synchronous ratios around 0.3 is $\phi_{in/o}^{out}$ (see Fig. 55), and its value, calculated for $\tau_* = 0.305$ ($\tau_{\#out} = 0$ and $\tau_{\#in} = \infty$ by definition) is:

$$\psi_{R/S}^{C} = -\frac{z_S}{z_R} = \phi_{in/o}^{out}(\tau_*) = \frac{\tau_* - \tau_{\#o}}{\tau_* - \tau_{\#in}} \frac{\tau_{\#out} - \tau_{\#in}}{\tau_{\#out} - \tau_{\#o}} = -0.4 \tag{173}$$

$\psi_{R/S}^{C}$ is known as the Willis' ratio of the planetary gear train. According to the position of the indexes, the engine is linked to the ring gear (and MG_i) by mean of the fixed-ratio k_{in}, while MG_o is linked to the sun gear; the output shaft links the wheels to the planet-carrier by mean of the final drive k_{out} (see Fig. 55).

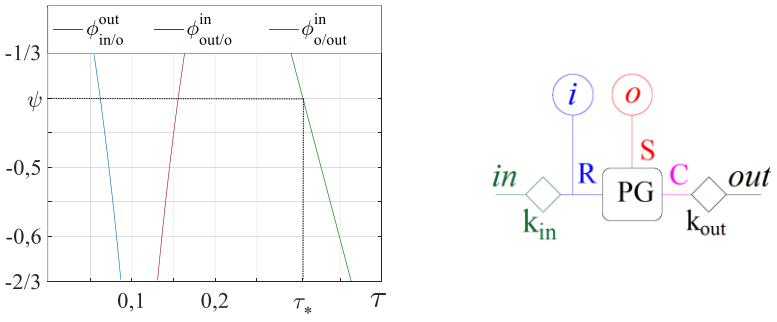

Fig. 55 Design chart for $\tau_{\#i} = -\infty$ and $\tau_{\#o} = 0.218$ and functional PS-CVT layout for $\tau_* = 0.305$ and $\psi = -z_S/z_R = -0.4$, $k_{in} = \omega_{in}/\omega_R = 0.82$, $k_{out} = \omega_{out}/\omega_C = 0.25$.

In the functional layout depicted in Fig. 55, the square represent a PG, while R,C,S denote the shafts linking respectively its ring, carrier and sun gear. Rhombi represent fixed gear ratios, and circles electric machines.

16.1.4. FEV modes

The electric machines have a maximum torque of $95.5\ N\ m$ each and a combined power of $70\ kW$, which should be enough to guarantee the required torque of $1300\ N\ m$ (see Fig. 52) up to $58\ km/h$, i.e. within urban areas.

A full electric mode E1 can be achieved by disengaging the engine from the input shaft by mean of a clutch 1 (see Fig 5 and Fig. 57), albeit such mode is not able to comply with the maximum torque requirements, as MG_o cannot deliver its maximum torque. The reason is that the latter is proportional to the torque applied to the input shaft, which is now operated by MG_i alone, without the contribution of the engine. As a result, the E1 mode is able to deliver just $535\ N\ m$ until the overall output power reaches $70\ kW$ at about $140\ km/h$. This condition takes place when MG_i is running at its base speed of $3500\ rpm$ and MG_o spins at $8750\ rpm$. On the bright side, E1 permits to regulate the speed of the electric machines, letting them work towards the best average efficiency. It is possible to start the engine at any moment provided that the speed of MG_i is higher than the idling speed of the former. A synchronous cranking of the engine can be accomplished if MG_i has been kept still, which limits the concurrent maximum vehicle's speed to about $80\ km/h$.

In conclusion, mode E1 cannot accomplish the high performances specified in Fig. 52. Such performances might be achieved without sophisticating the design concept by changing the final drive ratio to a steep $k_{out} = 0.103$ (and thus it would be also $k_{in} = 0.338$), but this would require MGs able to spin at over $17000\ rpm$ in PS-CVT mode (at $200\ km/h$) and possibly one additional reduction stage in order to realize k_{out} itself. Accordingly, the constructive parameters will stay unaltered and the full electric mode E1 will be restricted to general part-load operations, which constitute the most part of common driving cycles. It is worth noting that the proposed sign of k_{in} and k_{out} is not binding, as what matters for the motors are their absolute speeds, so either can be changed for constructive reasons.

A different solution E2 requires to block the input shaft altogether by mean of a brake 2 (see Fig. 57), so that MG_o could deliver its maximum torque. In this condition the speed of MG_o is 14 times the speed of the wheels, and thus the output torque can be even slightly higher

than required ($1340\ N\ m$). Obviously, this result is limited to a narrow speed range across the neutral gear (within $29\ km/h$), and MG_o is going to over-speed at about $80\ km/h$. Yet, starting from $70\ km/h$ the mode E1 offers better performances, so a switch is supposed to take place concurrently. Such switch is necessary also in order to crank the engine, which means that, before performing it, adapting the output torque to the E1 levels is necessary. Such operation may be perceived as particularly uncomfortable, as the torque jump can be consistent especially at low speeds.

Definitively, E2 can provide the necessary torque for uphill driving, but cannot guarantee acceleration performances comparable to the output-split mode. On the other hand, the output-split is capable of delivering slightly more than the prevented $1300\ N\ m$ in the $0-100\ km/h$ range, and up to $150\ kW$ at about $175\ km/h$.

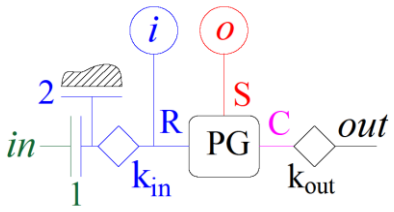

Fig. 56 Modified functional scheme for the PS-CVT with $\tau_{\#i} = -\infty$ and $\tau_{\#o} = 0.218$, $\tau_* = 0.305$, $\tau_{i_{\#o}} = 1.22$ and $\tau_{o_{\#i}} = 14.0\ \infty$ with switching clutches.

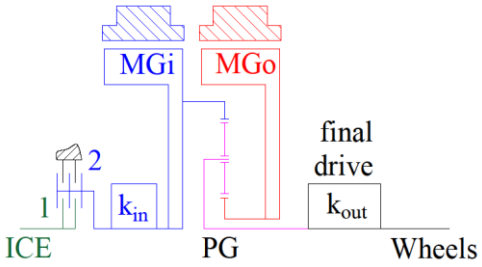

Fig. 57 Proposed constructive scheme for the PS-CVT with $k_{in} = 0.82$, $k_{out} = 0.25$, $\psi = -0.4$.

In Fig. 57 the engine ($in = ICE$) is linked to the electric motor MG_i ($i = MG_i$) by mean of the clutch 1 (green-blue) and the gearbox k_{in}. The planet carrier (purple) of the PG is linked to the wheels ($out = wheels$) by mean of the final drive k_{out}. MG_i spins with the

ring gear (blue) of PG, while MG_o spins with the sun gear (red). If the clutch 2 (blue-black) is engaged, the FEV mode E2 occurs.

CONCLUSIONS

In this manuscript, an innovative approach to the analysis and design of Power-Split Continuously variable transmissions has been proposed. The main ambition of this work is to offer general knowledge to the transmission engineer, mostly in terms of performances and functional requirements of multimode PS-CVTs, and by mean of a simple parametric description of the driveline.

Indeed, previous attempts to address the problem often indulge in a particularistic approach, which does not allow the reader to grasp the real influence of the design choices on the behavior of the driveline, frequently as a result of the mutual interference of the constructive parameters and of the layout of the transmission on the final performances of the PS-CVT itself. Furthermore, significant research efforts have been spent on the formulation of systematic approaches to the generation of the constructive designs, which have the main drawback to require tiresome and time-consuming screenings within the domain of the obtained solutions.

On the other hand, the method described in this manuscript invert the traditional design process, allowing the designer to pursue optimal performances even before that a concept of the driveline itself has been conceived. Furthermore, the method is intended to be as modular as possible, which means that the study of the transmission can be performed gradually and on several levels of detail; as a result, the design choices are progressive and can be adapted to address different aspects of the driveline, limiting their mutual interference.

The first chapter offer a general insight on the parametric description of PS-CVTs. Indeed, whichever it is the layout of the driveline, four kinematic parameters, i.e. the mechanical points and the related speed ratios of the shafts linked to the variator drive, govern the functioning of the prime mover and of the variator drive in relation to the load. Since these devices represent the most expensive parts of the PS-CVT, their optimization is a priority in respect of the planetary transmission itself, and can be performed independently in the preliminary stages of the design process.

The following three chapters focus on the description of the planetary transmission. In particular, the planetary driveline is conceived as a combination of fundamental structures,

called three-port mechanisms. The generic three-port mechanism is characterized by a particular set of relationships, called characteristic functions, which can be described in terms of the aforementioned functional parameters as well. Such functions represent both a design and an analysis tool, as they primarily represent a power ratio, but also link the planetary gear train with its synchronous conditions, which represent an important design parameter; indeed, working across the synchronism is a fundamental circumstance for the functioning of a planetary gear train, as it as a major impact on its efficiency. The most common planetary driveline solutions adopted in PS-CVTs are described in detail, and a systematic method for the generation of drivelines with a higher order of complexity is provided. The main advantage is that the method is conceived starting from the general kinematic properties of PS-CVTs, which means that the former provides only physically consistent solutions, thus avoiding degenerate structures. A general method in order to calculate the functional parameters of known driveline is provided as well. Such method is useful because it allows the engineer to analyze the system by mean of general relationships, which means that the comparison between different solutions is easier and the implementation of the model is much more straightforward. Furthermore, such method will be necessary in order to verify newly designed drivelines, as it is often not possible to obtain exactly the desired functional parameters because of the inherently discrete nature gear ratios.

The next three chapters focus on the power flow analysis within the planetary transmission. Indeed, for given functional parameters, the power flowing through the main ports of the driveline are independent from the layout. However, the internal power flows are not, and significant power recirculation phenomena can occur, thus hindering the performances of the PS-CVT as a whole in terms of both efficiency and dimensioning. Firstly, a simple method for the calculation of the power flows in absence of mechanical losses is described. This is important because it allows the designer to have awareness about the magnitude of the power flows and their directions, and it is a particularly intuitive task tanks to the use of the aforementioned characteristic functions. Later, a model for the calculation of the mechanical losses is proposed, it being formulated to be perfectly analogous to the method used to assess the ideal power flow distribution. However, since the planetary driveline is subject to many power flow inversions, the rigorous mathematical description of the driveline is subject to numerous discontinuities, which makes the application of the exact

method cumbersome. For this reason, a brief approximated method is proposed as well. Independently from the method used to assess the mechanical losses, a general relationship between losses and real power flowing through the variator drive is proposed. Assessing with precision these quantities is important not only in terms of optimization, but also for control purposes, because in electric PS-CVTs the variator drive is supposed to compensate the mechanical losses in order to provide the required output torque.

In the following chapter, a different approach to the problem is proposed. The key concept is to alter the kinematic relationships between the main ports by mean of fictitious constructive parameters, which are modified by their loss factors. This approach has the disadvantage of being mostly implicit, which means that a clear understanding of the influence of the each functional parameters and of the impact of each device on the global yield of the PS-CVT is lost. Furthermore, it is an iterative approach, although this computational effort can be greatly reduced by mean of the identification of the transition zones of the efficiency parameters of the driveline. On the other hand, it partly maintains the generality of the parametric approach and its implementation is particularly straightforward, which means that it is particularly suitable for numerical applications.

The inertial effects of the PS-CVT are addressed by mean of equivalent input and output torques, which will modify the torque applied to the variator drive accordingly to the relationships already used above. In particular, this approach can be successfully pursued thanks to the implicit iterative approach, as it makes superfluous to study the altered internal power flow distribution. Indeed, possible effects on the loss factors (due to power flow inversions) are automatically addressed by the automatic approach, because each loss factor is established on the basis on the simple rule that it must determine an increase of the global power loss.

A general design procedure is described. The design model makes use of the characteristic functions as the constraints for the constructive ratios of the planetary gear sets. All the solutions obtained with this procedure satisfy the functional requirement, which means that the operative conditions of the engine and variator drive will be close to optimal whichever it is the adopted layout. The procedure is detailed for the most common designs and generalize, thus being applicable to potentially any PS-CVT. Furthermore, it is worth noting that the same procedure can be easily adapted to address discrete planetary transmissions, as

in most cases the nodal ratios coincide, in fact, with the fixed ratios achieved by such transmissions. The design of multimode PS-CVTs is later address by investigating the effects that the most common switch strategies determine on the functional parameters. In particular, both a graphic and an analytical approach is proposed. Some switch strategies permit a more general formulation of the problem, while other require a more specific insight within the layout of the transmission, but still maintain a certain degree of generality.

Simple functional and constructive guidelines for the design of planetary transmissions are proposed. In particular, noteworthy results about the control of the torque ratio and the choice of the constructive ratio range within to select the planetary gear trains have been obtained. These simple rules permit to enhance the performances of the driveline with no impact on its functionality.

Eventually, simple models for the descriptions of the power sources of the PS-CVT are described. These models are supposed to permit to assess the operative conditions of the engine and of the electric motors so that the optimization of the functional parameters could take also them into account.

SYMBOLS

All Chapters

Symbol	***Description***	***Unit***
PS-CVT	Power-Split Continuously Variable Transmission	
PSU	Power-Split Unit	
CVU	Continuously Variable Unit	
TPM	Three-port Mechanism	
PG	Planetary Gear Set	
OG	Ordinary Gear Set	
IJ	Isokinetic Joint (node)	
i	Conventional input of the CVU	
o	Conventional output of the CVU	
in	input of the PS-CVT	
out	input of the PS-CVT	

Chapter 1

Symbol	***Description***	***Unit***
ω_i	Angular speed of the shaft i	rad/s
ω_o	Angular speed of the shaft o	rad/s
ω_{in}	Angular speed of the shaft in	rad/s
ω_{out}	Angular speed of the shaft out	rad/s
τ_i	Transmission ratio of the shaft i	
τ_o	Transmission ratio of the shaft o	
τ	Overall transmission ratio	
τ_v	Transmission ratio of the CVU	

$\tau_{\#i}$	τ when $\omega_i = 0$	
$\tau_{\#o}$	τ when $\omega_o = 0$	
$\tau_{o_{\#i}}$	τ_o when $\omega_i = 0$	
$\tau_{i_{\#o}}$	τ_i when $\omega_o = 0$	
$\tau_{v\#}$	Asymptotic transmission ratio of the CVU	
T_i	Torque applied to the shaft i (ideal)	N m
T_o	Torque applied to the shaft o (ideal)	N m
T_{in}	Torque applied to the shaft in (ideal)	N m
T_{out}	Torque applied to the shaft out (ideal)	N m
θ_i	Torque ratio at the shaft i (ideal)	
θ_o	Torque ratio at the shaft o (ideal)	
Θ	Overall torque ratio (ideal)	
P_i	Power flowing through the shaft i (ideal)	kW
P_o	Power flowing through the shaft o (ideal)	kW
P_{in}	Power flowing through the shaft in (ideal)	kW
P_{out}	Power flowing through the shaft out (ideal)	kW
p_i	Relative power flowing through the shaft i (ideal)	
p_o	Relative power flowing through the shaft o (ideal)	
η_v	Apparent efficiency of the CVU	
η	Apparent efficiency of the PS-CVT	
τ_b	Base overall speed ratio	
p_{i_b}	p_i calculated in τ_b	
p_{o_b}	p_o calculated in τ_b	
p_i'	Ratio between p_i and p_{i_b}	
p_o'	Ratio between τ_o and τ_{o_b}	
τ_{i_b}	τ_i calculated in τ_b	
τ_{o_b}	τ_o calculated in τ_b	
τ_i'	Ratio between τ_i and τ_{i_b}	
τ_o'	Ratio between τ_o and τ_{o_b}	
τ'	Ratio between τ and τ_b	

Symbol	***Description***	***Unit***
ψ	Constructive ratio of the PG of the TPM	
k_j	Constructive ratio of the OG on the *j-th* shaft of the TPM	
x	*Generic x-th* shaft of the TPM	
y	*Generic y-th* shaft of the TPM	
z	*Generic z-th* shaft of the TPM	
X	*Generic X-th* shaft of the PG	
Y	*Generic Y-th* shaft of the PG	
Z	*Generic Z-th* shaft of the PG	
$\phi_{x/y}^{z}$	Generic characteristic function of the TPM	
τ_x	Transmission ratio of the shaft x	
τ_y	Transmission ratio of the shaft y	
τ_z	Transmission ratio of the shaft z	
$\tau_{\#x}$	τ when $\omega_x = 0$	
$\tau_{\#y}$	τ when $\omega_y = 0$	
$\tau_{\#z}$	τ when $\omega_z = 0$	
$\tau_{\#in}$	τ when $\omega_{in} = 0$, always equal to ∞	
$\tau_{\#out}$	τ when $\omega_{out} = 0$, always equal to 0	
C_{in}	TPM linked to i, o, in	
C_{out}	TPM linked to i, o, out	
D_i	TPM linked to i, out, in	
D_o	TPM linked to o, out, in	
φ	Generic symbol for the basic characteristic function	
P_x	Power flowing through the shaft x of the TPM (ideal)	kW
P_y	Power flowing through the shaft y of the TPM (ideal)	kW
P_z	Power flowing through the shaft z of the TPM (ideal)	kW
T_x	Torque applied to the shaft x of the TPM (ideal)	N m
T_y	Torque applied to the shaft y of the TPM (ideal)	N m
T_z	Torque applied to the shaft z of the TPM (ideal)	N m

τ_*	τ when the PG is synchronous	
C	Planet carrier of the PG	
R	Ring gear of the PG	
S	Sun gear of the PG	
$\phi^C_{R/S}$	Characteristic function of the constructive ratio of the PG	

Chapter 3 - 4 - 5

Symbol	***Description***	***Unit***
k_{out}	OG on the output shaft of the Input Split shunt	
k_{in}	OG on the input shaft of the Output Split shunt	
n	Dummy index for the generic node	
j	Dummy index for the generic *j-th* shaft of the TPM	
J	Dummy index for the generic *j-th* shaft of the PG	
τ_n	Transmission ratio of the node n	
$\tau_{\#n}$	τ when $\omega_n = 0$	
$\tau_{j_{\#n}}$	τ_j when $\omega_n = 0$	
$\psi^Z_{Y/X}$	Transmission ratio of the shaft o	
$[Y_{\#i}]$	Matrix of coefficients for $\omega_i = 0$	
$[Y_{\#o}]$	Matrix of coefficients for $\omega_o = 0$	
$\{b\}$	Vector of coefficients	
$P_n\|_j$	Power flowing through the shaft of the *j-th* TPM linked to n	

Chapter 6 - 7

Symbol	***Description***	***Unit***
$\bar{P}_X$	Power flowing through the shaft X of the PG (real)	kW
$\bar{P}_Y$	Power flowing through the shaft Y of the PG (real)	kW

$\bar{P}_Z$	Power flowing through the shaft Z of the PG (real)	kW
$\bar{P}_L$	Overall mechanical loss in the PSU	kW
$\bar{T}_X$	Torque applied to the shaft X of the PG (real)	N m
$\bar{T}_Y$	Torque applied to the shaft Y of the PG (real)	N m
$\bar{T}_Z$	Torque applied to the shaft Z of the PG (real)	N m
$\eta_{Y/X}^{Z}$	efficiency between Y and X of the PG when Z is blocked	
$\eta_{Z/X}^{Y}$	efficiency between Z and X of the PG when Y is blocked	
$\eta_{Y/Z}^{X}$	efficiency between Y and Z of the PG when X is blocked	
η_0	Basic efficiency of the PG	
$\bar{P}_L\|_{PG}$	mechanical loss in the PG	kW
$\bar{P}_L\|_{OG}$	mechanical loss in the OG	kW
$\eta_{X/x}$	efficiency of the OG linking X and x	
$\eta_{Y/y}$	efficiency of the OG linking Y and y	
$\eta_{y/x}^{z}$	efficiency between Y and X of the TPM when Z is blocked	
$\bar{P}_n\|_j$	Real power flowing through the shaft of the *j-th* TPM linked to *n*	kW
$\bar{P}_i$	Power flowing through the shaft i (real)	kW
$\bar{P}_o$	Power flowing through the shaft o (real)	kW
$\bar{P}_{in}$	Power flowing through the shaft in (real)	kW
$\bar{P}_{out}$	Power flowing through the shaft out (real)	kW
$\bar{p}_L$	Relative overall mechanical loss in the PSU	
$\bar{p}_L\|_{PG}$	Relative mechanical loss in the PG	
$\bar{p}_L\|_{OG}$	Relative mechanical loss in the OG	
$\bar{p}_i$	Relative power flowing through the shaft i (real)	
$\bar{p}_o$	Relative power flowing through the shaft o (real)	
$\bar{\theta}_i$	Relative torque applied to the shaft i (real)	
$\bar{\theta}_o$	Relative torque applied to the shaft o (real)	
$\hat{\tau}$	Unit vector in the direction of τ	
$\hat{\eta}$	Unit vector in the direction of η	
$\nabla\bar{p}_L$	Gradient of $\bar{p}_L$	

Symbol	Description	Unit
$[\Omega]$	Kinematic matrix	
$[T]$	Torque matrix	
$[\widetilde{\mathrm{T}}]$	Real torque matrix	
η_j^{cj}	Efficiency parameter of the *j-th* device	
$\tilde{k}_j$	Fictitious constructive parameter of the *j-th* device	
$\bar{T}_{out}$	Torque applied to the shaft out (real)	N m
$\bar{T}_{in}$	Torque applied to the shaft in (real)	N m
$\bar{T}_i$	Torque applied to the shaft i (real)	N m
$\bar{T}_o$	Torque applied to the shaft o (real)	N m
$\widetilde{\Omega}$	Fictitious kinematic matrix	
$\tilde{\tau}_{i_{\#o}}$	Fictitious τ_i when $\omega_o = 0$ (altered by efficiencies)	
$\tilde{\tau}_{\#o}$	Fictitious τ when $\omega_o = 0$ (altered by efficiencies)	
$\tilde{\tau}_{\#i}$	Fictitious τ when $\omega_i = 0$ (altered by efficiencies)	
$\tilde{\tau}_{o_{\#i}}$	Fictitious τ_o when $\omega_i = 0$ (altered by efficiencies)	
$\{\}'$ or $[]'$	Transpose	
$[]^{-1}$	Inverse	
$[I]$	Identity matrix	
c_j	Efficiency coefficient (± 1)	
$\tilde{\Omega}_j$	Fictitious kinematic matrix at the *j-th* iteration	
$\bar{P}_{L_j}$	Overall mechanical loss at the *j-th* iteration	
N	Number of iterations	
$\widetilde{\Omega}_{\not j}$	Fictitious kinematic matrix for $c_j = 0$	
$[\Lambda_j]$	Boundary matrix for the *j-th* device	
$\Theta_{\not j}$	Torque ratio boundary for the *j-th* device	
$\tau_{\not j}$	Speed ratio boundary for the *j-th* device	
$\lambda_{j(\mathrm{m,n})}$	Element of Λ_j in the row m column n	
$\bar{\theta}_x\big\vert_{TPM}$	Real relative torque applied to the shaft x of the TPM	
$\bar{p}_x\vert_{TPM}$	Real relative power applied to the shaft x of the TPM	

Symbol	***Description***	***Unit***
$\dot{\omega}_i$	Angular acceleration of the shaft i	rad/ s^2
$\dot{\omega}_o$	Angular acceleration of the shaft o	rad/s^2
$\dot{\omega}_{in}$	Angular acceleration of the shaft in	rad/ s^2
$\dot{\omega}_{out}$	Angular acceleration of the shaft out	rad/ s^2
$\dot{\tau}$	Speed ratio time derivative	1/ s
ΔT_i	Toque variation on the shaft i	N m
ΔT_o	Toque variation on the shaft o	N m
ΔT_{in}	Toque variation on the shaft in	N m
ΔT_{out}	Toque variation on the shaft out	N m
I_i	Inertia on the shaft i	Kg m^2
I_o	Inertia on the shaft o	Kg m^2
I_{in}	Inertia on the shaft in	Kg m^2
I_{out}	Inertia on the shaft out	Kg m^2
I_j^{eq}	Equivalent inertia on the generic shaft j	Kg m^2
$I_j\|_{TPM}$	inertia of the shaft of the PG linked to j	Kg m^2
$k_j\|_{TPM}$	Fixed ratio on the shaft j of the TPM	
ΔT_n	Toque variation on the generic neutral node n	N m
$\hat{T}_{in}$	Equivalent input torque due to inertias	N m
$\hat{T}_{out}$	Equivalent output torque due to inertias	N m
$\tau_{j_{\#l}}$	τ_j when $\omega_l = 0$, with $l \neq j$	
$\tau_{\#l}$	τ when $\omega_l = 0$, with $l \neq j$	
P_I	Kinetic power of the PS-CVT	kW
$\tilde{\tau}_{j_{\#l}}$	Fictitious τ_j when $\omega_l = 0$ (altered by efficiencies)	
$\tilde{\tau}_{\#l}$	Fictitious τ when $\omega_l = 0$ (altered by efficiencies)	
$\tilde{\tau}_{\#j}$	Fictitious τ when $\omega_j = 0$ (altered by efficiencies)	

Chapter 11

Symbol	***Description***	***Unit***
m	vehicle mass	kg
m_{eq}	equivalent vehicle mass	kg
V	vehicle speed	m/s
V_W	wind speed	m/s
V_r	Relative speed $V - V_W$	m/s
V_α	uphill speed	m/s
V_{max}	top speed	m/s
V_0	acceleration's reference speed	m/s
$\dot{V}$	vehicle acceleration	m/s^2
A	vehicle frontal area	m^2
c_x	aerodynamic factor	
f_R	rolling resistance factor	
ρ	air density	kg/m^3
g	earth acceleration	m/s^2
α	slope angle	rad
f_0	acceleration factor	
t_0	acceleration's reference time	s
SOC	State of charge	
WOT	wide open throttle	
ECMS	Equivalent Consumption Minimization Strategy	

Chapter 12-13

Symbol	Description	Unit
ω_R	Angular speed of the ring gear	rad/s
ω_S	Angular speed of the sun gear	rad/s
ω_C	Angular speed of the planet carrier	rad/s

$\psi_{R/S}^{C}$	Constructive ratio	
$\omega_x\|_{\tau_*}$	Speed of x of the TPM when the PG is synchronous	rad/s
$\omega_y\|_{\tau_*}$	Speed of y of the TPM when the PG is syncronous	rad/s
$\omega_z\|_{\tau_*}$	Speed of z of the when the PG is syncronous	rad/s
$\tau_{x_{\#y}}$	τ_x when y is motionless	
$\tau_{y_{\#x}}$	τ_y when x is motionless	
$\tau_{x_{\#z}}$	τ_x when z is motionless	
$\tau_{z_{\#x}}$	τ_z when x is motionless	
τ_s	τ concurrent with the switch to the shunt mode	
k	OG necessary for the switch	
τ_{i_*}	τ_i when the PG is synchronous	
τ_{o_*}	τ_o when the PG is synchronous	
k_{j_*}	Speed ratio between j and J during synchronism	
k_l	fixed gear ratio on the motionless shaft of the CVU	

Chapter 14

Symbol	Description	Unit
τ_{v_M}	Maximum CVU speed ratio	
τ_{v_m}	Minimum CVU speed ratio	
$\tau_{v_{opt}}$	Optimal CVU speed ratio	
z_1	Number of teeth of generic gear 1	
z_2	Number of teeth of generic gear 2	
z_S	Number of teeth of sun gear	
z_R	Number of teeth of ring gear	
z_P	Number of teeth of planet gear	
m	Teeth module	m
D_1	Gear 1 diameter	m
D_2	Gear 2 diameter	m

p	Pitch length	m
W	Gear width	m

Chapter 15

Symbol	***Description***	***Unit***
ICE	Internal Combustion Engine	
$\mathscr{p}_e$	mean effective pressure	bar
η_{fe}	thermodynamic efficiency	
$\mathscr{p}_f$	ideal fuel pressure	bar
$\mathscr{p}_l$	mechanical and pumping pressure losses	bar
m_f	mass of fuel	g
H_f	Lower specific heat	kJ/g
S	Stroke of the cylinder	m
B	Bore of the cylinder	m
c_f	Specific consumption	g/kJ
T	Engine torque	N m
WOT	Wide open throttle	
T_I	Inertial torque of the engine	N m
I_e	Inertia of the engine	Kg m^2
$\dot{\omega}_e$	Angular acceleration of the engine	rad/s^2
η_m	electrical efficiency of the motor	
P_{el}	Electric power	kW
D	Diameter of the rotor	m
L	Length of the rotor	m
t_m	mean effective tangential tension	N/m^2
t_{el}	mean electric tangential tension	N/m^2
t_l	loss tangential tension	N/m^2
c_{el}	Specific electric consumption	

ω	Angular speed of the motor	rad/s
Q	Charge of the battery	Ah
Q_0	Reference charge of the battery	Ah
I_0	Reference current of the battery	A
I	current of the battery	A
β	Characteristic constant of the battery	
R	Internal resistance	Ohm
V_0	Open circuit voltage	Volts
P	Delivered power	kW
V	voltage	Volts
η_C	Coulombic efficiency	
$\dot{Q}$	Discharge rate	A
C	Capacity of the battery	F

Chapter 16

MG	Motor / Generator	
FEV	Full Electric Vehicle	
V_{max}	Max speed of the vehicle	Km/h
n_{max}	Max speed of the engine	rpm
R	Rolling radius of the wheels	m
P_{out}	Required power	kW
MG_i	MG linked to the port i	
MG_o	MG linked to the port o	
E1	Full electric mode 1	
E2	Full electric mode 2	

TABLES

FIGURES

REFERENCES

[1] H. Naunheimer, B. Bertsche, J. Ryborz, W. Novak, Automotive Transmissions: Fundamentals, Selection, Design and Application, Springer-Verlag, Berlin, 2011.

[2] R. Fischer, F. Küçükay, G. Jürgens, R. Najork, B. Pollak, The Automotive Transmission Book, Springer International Publishing Switzerland, 2015.

[3] Giancarlo Ferrari, Motori a combustion interna, Edizioni il Capitello Torino

[4] Alberto Beccari, Carmelo Caputo, Motori termici volumetrici, Torino: UTET (1987).

[5] A. Stotsky, Automotive Engines: Control, Estimation, Statistical Detection, Springer (2009). doi: 10.1007/978-3-642-00164-2.

[6] L. Guzzella, A. Sciarretta, Vehicle Propulsion Systems. Introduction to Modelling and Optimization, Springer-Verlag, Berlin, 2013.

[7] I. Husain, Electric and Hybrid Vehicles Design Fundamentals, Taylor & Francis (2005). ISBN 0-203-00939-8.

[8] Bogdan Ovidiu Varga, Florin Mariasiu, Dan Moldovanu, Calin Iclodean, Electric and Plug-In Hybrid Vehicles: Advanced Simulation Methodologies, Springer. doi 10.1007/978-3-319-18639-9.

[9] Chris Mi, M. Abul Masrur, David Wenzhong Gao, Hybrid Electric Vehicles - Principles and Applications with practical perspectives. ISBN 978-0-470-74773-5

[10] W. Liu, Introduction to hybrid vehicle system modeling & control, Wiley (2013). ISBN 978-1-118-30840-0

[11] W. Liu, Hybrid Electric Vehicle System Modeling And Control, Wiley (2017). ISBN 9781119279334

[12] Mehrdad Ehsani, Yimin Gao, Ali Emadi, Modern Electric, Hybrid Electric, and Fuel Cell Vehicles, Taylor & Francis (2010).

[13] K. Reif, Fundamentals of Automotive and Engine Technology: Standard Drives, Hybrid Drives, Brakes, Safety Systems, Springer (2014). doi:10.1007/978-3-658-03972-1.

[14] Reif, Automotive Mechatronics: Automotive Networking, Driving Stability Systems, Electronics, Springer (2015). doi:10.1007/978-3-658-03975-2

[15] K. Reif, Brakes, Brake Control and Driver Assistance Systems Function, Regulation and Components, Springer (2014). doi:10.1007/978-3-658-03978-3.

[16] Tsai, Lung-Wen, Mechanism design: enumeration of kinematic structures according to function, ISBN 0-8493-0901-8

[17] D. Rotella, M. Cammalleri, Direct analysis of power-split CVTs: A unified method, Mech. Mach. Theory 121 (2018) 116–127.

[18] M. Cammalleri, Efficiency of Split-Way CVT's. A Simplified Model, SAE Technical Paper 2007-24-0133 (2007), doi: 10.4271/2007-24-0133.

[19] D. Rotella, M. Cammalleri, Power losses in power-split CVTs: A fast black-box approximate method, Mech. Mach. Theory 128 (2018) 528–543.

[20] M. Cammalleri, D. Rotella, Functional design of power-split CVTs: An uncoupled hierarchical optimized model, Mech. Mach. Theory 116 (2017) 294–309.

[21] P. Mattsson. Continuously Variable Split-Power Transmission with Several Modes. Chalmers University of Technology, Göteborg, Sweden, 1996, ISBN 91-7197-356-7.

[22] D.J. Sanger, The determination of power flow in multiple-path transmission systems, Mech. Mach. Theory. 7 (1972) 103–109.

[23] A. Villeneuve, Dual Mode Electric Infinitely Variable Transmission, SAE Technical Paper 2004-40-0019 (2004).

[24] Beccari, M. Cammalleri, F. Sorge, Experimental Results for a Two-Mode Split-Way CVT, VDI Berichte, vol. 1709 (2002) 237-250.

[25] Conlon, Comparative Analysis of Single and Combined Hybrid Electrically Variable Transmission Operating Modes, SAE World Congr. 2005 (2005).

[26] J.M. Miller, Hybrid electric vehicle propulsion system architectures of the e-CVT type, IEEE Trans. Power Electron. 21 (2006) 756–767.

[27] F. Bottiglione, G. Mantriota, MG-IVT: an infinitely variable transmission with optimal power flows, ASME J. Mech. Des. 130 (11) (2008).

[28] K. Pettersson, K. E. Rydberg, P. Krus, Comparative Study of Multiple Mode Power Split Transmissions for Wheel Loaders, 12th Scand. Int. Conf. Fluid Power (SICFP2011), May 18-20 (2011).

[29] M. Cammalleri, A new approach to the design of a speed-torque-controlled rubber V-belt variator, Proc. Inst. Mech. Eng. Part D: J. Automob. Eng. 219 (2005) 1413–1427.

[30] J.R. Gomà Ayats, U. Diego-Ayala, J. Minguella Canela, F. Fenollosa, J. Vivancos, Hypergraphs for the analysis of complex mechanisms comprising planetary gear trains and other variable or fixed transmissions, Mech. Mach. Theory. 51 (2012) 217–229.

[31] M. Cammalleri, F. Sorge, Approximate Closed-Form Solutions for the Shift Mechanics of Rubber Belt Variators, Proceeding of ASME (IDETC 2009), August 30 - September 2, 2009, San Diego, California, USA, doi: 10.1115/DETC2009-86638

[32] F. Yang, J. Feng, H. Zhang, Power flow and efficiency analysis of multi-flow planetary gear trains, Mech. Mach. Theory 92 (2015) 86–99.

[33] Conlon et al., The Next Generation "Voltec" Extended Range EV Propulsion System, SAE Int. J. Alt. Power 4 (2015), doi:10.4271/2015-01-1152.

[34] A.G. Holmes, M.R. Schmidt, Hybrid electric powertrain including a two-mode electrically variable transmission. US Patent 6 478 705 B1, 2002.

[35] M. Conlon, R. Hills, K. M. Rahman, T. J. Blohm, S. Jurkovic, Multimode electrically variable transmission having a ferrite magnet motor and method of operating the same. US Patent US 8 602 938 B1, 2013.

[36] X. Zhang, S. E. Li, H. Peng, and J. Sun, Design of Multimode Power-Split Hybrid Vehicles - A Case Study on the Voltec Powertrain System, *IEEE Transactions on Vehicular Technology*, *65 (2016) 4790-4801*.

[37] A M. Kluger, D. Long, An Overview of Current Automatic, Manual and Continuously Variable Transmission Efficiencies and Their Projected Future Improvements, SAE Technical Paper 1999-01-1259 (1999). doi:10.4271/*1999-01-1259*.

[38] J.M. Miller, S.E. Schulz, B. Conlon, M. Duvall, M.D. Kankam, N. Nagel, Adjustable speed drives transportation industry needs part I: automotive, Veh. Technol. Conf. 2003, VTC 2003-Fall. 2003 IEEE 58th, Vol.5 (2003) 3220–3225.

[39] M. Pasquier, Continuously Variable Transmission Modifications and Control for a Diesel Hybrid Electric Powertrain, SAE Technical Paper 2004-08-23 (2004).

[40] G. Carbone, L. Mangialardi, G. Mantriota, A comparison of the performances of full and half toroidal traction drives, Mech. Mach. Theory 39 (2004) 921–942.

[41] N. Srivastava, I. Haque, A review on belt and chain continuously variable transmissions (CVT): Dynamics and control, Mech. Mach. Theory 44 (2009) 19–41.

[42] F. Sorge, M. Cammalleri, Helical Shift Mechanics of Rubber V-Belt Variators, Journal of Mechanical Design, Volume 133, Issue 4, (2011) doi: 10.1115/1.4003803

[43] J.D. Wishart, Y. Zhou, Z. Dong, Review, Modelling and Simulation of Two-Mode Hybrid Vehicle Architecture, 19th Int. Conf. Des. Theory Methodol.; 1st Int. Conf. Micro- Nanosyst.; 9th Int. Conf. Adv. Veh. Tire Technol., Vol. 3 Parts A B (2007) 1091–1112.

[44] E.I. Radzimovsky, A simplified approach for determining power losses and efficiencies of planetary gear drives, Machine design (1956) 101–110.

[45] E.I. Radzimovsky, How to find efficiency, speed and power losses in planetary gear drives, Machine design (1959) 144–153.

[46] J.W. Polder, A Universal Mathematical Model for Epicyclic Gear Trains, In, Gearing and transmissions: mechanisms conference and international symposium, 1972, San

Francisco. - New York: American Society of Mechanical Engineers (ASME) (1972) 1-11.

[47] D.Yu, N. Beachley, Mechanical Efficiency of Differential Gearing, Gear technology, July/August 1986 (1986) 9-16.

[48] Pennestrì, F. Freudenstein, The mechanical effieciency of epicyclic gear trains, Journal of Mechanical design 115, (1993) 645-651.

[49] Pennestrì, L. Mariti, P.P. Valentini, V.H. Mucino, Efficiency evaluation of gearboxes for parallel hybrid vehicles: Theory and applications, Mech. Mach. Theory. 49 (2012) 157–176. doi:10.1016/j.mechmachtheory.2011.10.012.

[50] A.K. Gupta, C.P. Ramanarayanan, Analysis of circulating power within hybrid electric vehicle transmissions, Mech. Mach. Theory. 64 (2013) 131–143. doi:10.1016/j.mechmachtheory.2013.01.011.

[51] White, Derivation of high efficiency two-stage epicyclic gears, Mech. Mach. Theory. 38 (2003) 149–159. doi:10.1016/S0094-114X(02)00093-9.

[52] M.J. French, A Carnot Theorem For Split torque Variable Speed Gears, Proc. Inst. Mech. Eng. Part C J. Mech. Eng. Sci. 10 (1968) 198–201.

[53] Freudenstein, a. T. Yang, Kinematics and statics of a coupled epicyclic spur-gear train, Mech. Mach. Theory. 7 (1972) 263–275. doi:10.1016/0094-114X(72)90008-0.

[54] W. Wang, R. Song, M. Guo, S. Liu, Analysis on compound-split configuration of power-split hybrid electric vehicle, Mech. Mach. Theory 78 (2014) 272–288. doi:10.1016/j.mechmachtheory.2014.03.019.

[55] L. Mangialardi, G. Mantriota, Power flows and efficiency in infinitely variable transmissions, Mech. Mach. Theory 34 (1999) 973–994. doi:10.1016/S0094-114X(98)00089-5.

[56] Mantriota, Performances of a series infinitely variable transmission with type I power flow, Mech. Mach. Theory. 37 (2002) 555–578. doi:10.1016/S0094-114X(02)00018-6.

[57] G. Mantriota, Performances of a parallel infinitely variable transmissions with a type II power flow, Mech. Mach. Theory. 37 (2002) 555–578. doi:10.1016/S0094-114X(02)00018-6.

[58] F. Bottiglione, S. De Pinto, G. Mantriota, Infinitely Variable Transmissions in neutral gear: Torque ratio and power re-circulation, Mech. Mach. Theory. 74 (2014) 285–298. doi:10.1016/j.mechmachtheory.2013.12.017

[59] C. Chen, J. Chen, Efficiency analysis of two degrees of freedom epicyclic gear transmission and experimental validation, Mech. Mach. Theory. 87 (2015) 115–130. doi:10.1016/j.mechmachtheory.2014.12.017.

[60] J.M. Del Castillo, The analytical expression of the efficiency of planetary gear trains, Mech. Mach. Theory. 37 (2002) 197–214. doi:10.1016/S0094-114X(01)00077-5.

[61] D.R. Salgado, J.M. Del Castillo, Analysis of the transmission ratio and efficiency ranges of the four-, five-, and six-link planetary gear trains, Mech. Mach. Theory. 73 (2014) 218–243. doi:10.1016/j.mechmachtheory.2013.11.001.

[62] P. Valentini, E. Pennestrì, A Review of Formulas for the Mechanical Efficiency Analysis of Two Degrees-of-Freedom Epicyclic Gear Trains, Journal of Mechanical Design 125 (2003). 602-608. doi:10.1115/1.1587157.

[63] P.M.T. Marques, R.C. Martins, J.H.O. Seabra, Power loss and load distribution models including frictional effects for spur and helical gears, Mech. Mach. Theory. 96 (2016) 1–25. doi:10.1016/j.mechmachtheory.2015.09.005.

[64] Mantriota, G., and Pennestrì, Theoretical and Experimental Efficiency Analysis of Multi Degrees-of-Freedom Epicyclic Gear Trains, Multi- body Syst. Dyn. 7 (2003), 389–406.

[65] L.P. Laus, H. Simas, D. Martins, Efficiency of gear trains determined using graph and screw theories, Mech. Mach. Theory 52 (2012) 296–325, doi:10.1016/j.mechmachtheory.2012.01.011.

[66] A. Kahraman, D.R. Hilty, A. Singh, An experimental investigation of spin power losses of a planetary gear set, Mech. Mach. Theory. 86 (2015) 48–61. doi:10.1016/j.mechmachtheory.2014.12.003.

[67] Sciarretta, L. Serrao, P.C. Dewangan et al., A control benchmark on the energy management of a plug-in hybrid electric vehicle, Control Eng. Pract. 29 (2014) 287–298.

[68] D.R. Salgado, J.M. Del Castillo, Selection and Design of Planetary Gear Trains Based on Power Flow Maps, J. Mech. Des. 127 (2005) 120.

[69] J.R. Gomà Ayats, J. Vivancos Calvet, J. Minguella Canela, U. Diego-Ayala, F. Fenollosa Artes, Power transmitted through a particular branch in mechanisms comprising planetary gear trains and other fixed or variable transmissions, Mech. Mach. Theory. 46 (2011) 1744–1754.

[70] G. Mantriota, Comments on "Power transmitted through a particular branch in mechanisms comprising planetary gear trains and other fixed or variable transmissions" Mech. Mach. Theory 73 (2013).

[71] S. De Pinto, G. Mantriota, A simple model for compound split transmissions, Proc. Inst. Mech. Eng. Part D J. Automob. Eng. 228 (2013) 549–564.

[72] F. Bottiglione, S. De Pinto, G. Mantriota, A Simple Approach for Hybrid Transmissions Efficiency, Recent Res. Environ. Geol. Sci. (2014) 386–391.

[73] F. Bottiglione, G. Mantriota, Power flows and efficiency of Output Compound e-CVT, International Journal of Vehicular Technology, Volume 2015 (2015) 1–19.

[74] R. H. Macmillan, Power flow and loss in differential mechanisms. Proceedings of the Institution of Mechanical Engineers, Part C: Journal of Mechanical Engineering Science 3 (1961), 37-41.

[75] R. H. Macmillan, P. B. Davies, Analytical Study of Systems for bifurcated power transmission, Proceedings of the Institution of Mechanical Engineers, Part C: Journal of Mechanical Engineering Science 7 (1965), 40-47. (1965).

[76] J.W. Polder, Lumped Parameter Model of Planetary Gear Systems, Proceedings of the Institution of Mechanical Engineers, June 1978 192, 251-258.

[77] A. Beccari, F. Sorge, Experimental Results for a Variable Speed Differential Drive, II British - Italian Workshop on Heat Engines, Bath, March 1991.

[78] M. Andolina, A. Beccari, Continuous Variation Transmission in Automotive Application: Extension of the Working Range of Automotive Transmission to Start and Reverse Motion with Minimization of Variator Dimension, The JSAE Intern. Conf. CVT '96, Yokohama, Japan.

[79] F. Sorge, A. Beccari, M. Cammalleri, Operative Variator Characterization for CVT Improvement, Proceedings of the JSME International Conference on Motion and Power Transmissions, Fukuoka, Japan, 15–17 November 2001, 751–756.

[80] A. Beccari., M. Cammalleri., Implicit regulation for automotive variators, Proceedings of Institution of Mechanical Engineering part D, Vol. 215 D6 2001, pag. 697-708, doi: 10.1243/0954407011528275.

[81] G. Carbone, L. Mangialardi, G. Mantriota, Fuel Consumption of a Mid Class Vehicle with Infinitely Variable Transmission, SAE Technical Paper 2001-01-3692 (2001).

[82] G. Mantriota, Fuel consumption of a vehicle with power split CVT system, Int. J. Veh. Des. 37 (2005) 227-242.

[83] A. Rossetti, A. Macor, Multi-objective optimization of hydro-mechanical power split transmissions, Mech. Mach. Theory 62 (2013) 112–128.

[84] R. Mathis, Y. Rèmond, Une théorie unifiée des trains épicycloidaux, C. R. Acad. Sci. Paris, t. 327 (1999) 1115–1121.

[85] R. Mathis, Y. Remond, Kinematic and dynamic simulation of epicyclic gear trains, Mech. Mach. Theory. 44 (2009) 412–424.

[86] C.H. Hsu, J.J. Hsu, An Efficient Methodology for The Structural Synthesis of Geared Kinematic Chains, Mech. Mach. Theory 32 (1997) 957–973.

[87] T.S. Mruthyunjaya, Kinematic structure of mechanisms revisited, Mech. Mach. Theory 38 (2003) 279–320.

[88] D.R. Salgado, J.M. Del Castillo, A method for detecting degenerate structures in planetary gear trains, Mech. Mach. Theory 40 (2005) 948–962.

[89] H.T. Ngo, H. Sen Yan, Configuration synthesis of series-parallel hybrid transmissions, Proc. Inst. Mech. Eng. Part D J. Automob. Eng. 230 (2015).

[90] K. Ahn, S. Cho, W. Lim, Y. Park, J.M. Lee, Performance analysis and parametric design of the dual-mode planetary gear hybrid powertrain, Proc. Inst. Mech. Eng. Part D J. Automob. Eng. 220 (2006) 1601–1614.

[91] Kim, J. Kang, Y. Kim, T. Kim, B. Min and H. Kim, Design Of Power Split Transmission: Design Of Dual Mode Power Split Transmission, International Journal of Automotive Technology, Vol. 11 (2010) 565−571.

[92] Liu, H. Peng, A systematic design approach for two planetary gear split hybrid vehicles, Veh. Syst. Dyn. 48 (2010) 1395–1412.

[93] X. Zhang, H. Peng, J. Sun, S. Li, Automated modeling and mode screening for exhaustive search of Double-Planetary-Gear power split hybrid powertrains, ASME 2014 Dyn. Syst. Control Conf. DSCC 2014. 1 (2014).

[94] Y. Yang, X. Hu, H. Pei, Z. Peng, Comparison of power-split and parallel hybrid powertrain architectures with a single electric machine: Dynamic programming approach, Appl. Energy 168 (2016) 683–690. doi:10.1016/j.apenergy.2016.02.023.

[95] H. Pei, X. Hu, Y. Yang, X. Tang, C. Hou, D. Cao, Configuration optimization for improving fuel efficiency of power split hybrid powertrains with a single planetary gear, Appl. Energy 214 (2018) 103–116. doi:10.1016/j.apenergy.2018.01.070.

[96] A. Veenhuizen, B. Bonsen, T. Klaassen, K. Van De Meerakker, F. Veldpaus, Variator loading and control in a V-belt type geared neutral transmission in and around the geared neutral point. Information and Computation/information and Control – IANDC (2002).

[97] Diego-Ayala, P Martinez-Gonzalez, N McGlashan, and K R Pullen, The Mechanical Hybrid Vehicle, an investigation of a vehicular regenerative energy capture system, Proceedings of the IMechE, Part D Journal of Automobile Engineering 222 (2008) 2087-2101.

[98] Z. Qin, Y. Luo, W. Zhuang, Z. Pan, K. Li, H. Peng, Simultaneous optimization of topology , control and size for multi-mode hybrid tracked vehicles, Appl. Energy 212 (2018) 1627–1641. doi:10.1016/j.apenergy.2017.12.081.

[99] Y. Baidak, V. Smyk, Determination of the needed power of an electric motor on the basis of acceleration time of the electric car, IOP Conf. Series: Materials Science and Engineering 252 (2017). doi:10.1088/1757-899X/252/1/012063.

[100] Kim, N., Kwon, J., and Rousseau, A., Comparison of Powertrain Configuration Options for Plug-in HEVs from a Fuel Economy Perspective, SAE Technical Paper 2012-01-1027 (2012). https://doi.org/10.4271/2012-01-1027.

[101] O. Sundström, D. Ambühl, L. Guzzella, On Implementation of Dynamic Programming for Optimal Control Problems with Final State Constraints, Oil &Gas Science and Technology – Rev. IFP 65 (2010) 91–102.

[102] X. Zhou, D. Qin, J. Hu, Multi-objective optimization design and performance evaluation for plug-in hybrid electric vehicle powertrains, Appl. Energy (2017). doi:10.1016/j.apenergy.2017.08.201.

[103] Propfe, M. Redelbach, D.J. Santini, H. Friedrich, Cost analysis of Plug-in Hybrid Electric Vehicles including Maintenance & Repair Costs and Resale Values, EVS26 International Battery, Hybrid and Fuel Cell Electric Vehicle Symposium (2012) 1–10.

[104] Schlegel, A. Hösl, S. Diel, Detailed Loss Modelling of Vehicle Gearboxes, Proceedings 7th Modelica Conference, Como, Italy (2009) 20–22. doi:10.3384/ecp09430059.

[105] V. Nezhadali, L. Eriksson, A framework for modeling and optimal control of automatic transmission systems, IFAC-PapersOnLine 48 (2015) 285-291. https://doi.org/10.1016/j.ifacol.2015.10.041.

[106] Y. Su, M. Hu, L. Su, D. Qin, T. Zhang, C. Fu, Dynamic coordinated control during mode transition process for a compound power-split hybrid electric vehicle, Mech. Syst. Signal Process 107 (2018) 221–240. doi:10.1016/j.ymssp.2018.01.023.

[107] P. Linares, V. Méndez, H. Catalán, Design parameters for continuously variable power-split transmissions using planetaries with 3 active shafts, Journal of Terramechanics 47 (2010) 323-335, https://doi.org/10.1016/j.jterra.2010.04.004.

[108] Zhuang, Weichao & Zhang, Xiaowu & Zhao, Ding & Peng, Huei & Wang, Liangmo, Optimal design of three-planetary-gear power-split hybrid powertrains. International

Journal of Automotive Technology 17 (2016) 299-309. doi: 10.1007/s12239-016-0030-0.

[109] G. Mantriota, Reversibility of Power-Split Transmissions, Journal of Mechanical Design (2014). doi:10.1115/1.4004586.

[110] İ. Hüseyin Filiza, S. Olgunera, E. Evyapan, A Study on Optimization of Planetary Gear Trains, Acta Physica Polonica A 132 (2017). doi: 10.12693/APhysPolA.132.728

[111] A. AïtTaleb, A. Chaâba and M. Sallaou, Efficiency Evaluation of Continuously Variable Transmissions Including a Planetary Gear Train, Energy and Power Engineering 5 (2013) 153-160. doi: 10.4236/epe.2013.52015.

[112] Ahn, P.Y. Papalambros, Engine optimal operation lines for power-split hybrid electric vehicles, Proc. IMechE Part D: J. Automobile Engineering 223 (2009) 1149–1162. doi:10.1243/09544070JAUTO1124.

[113] Holmes, J. Liu, D. Ames, V. Neelakantan, K. Rahman, General Motors Electric Variable Transmission for Cadillac CT6 Sedan, SAE Technical Paper 2016-01-1150 (2018). doi:10.4271/2016-01-1150.

[114] T. M. Grewe, B. M. Conlon and A. G. Holmes, Defining the General Motors 2-Mode Hybrid Transmission, SAE Technical Paper 2007-01-0273 (2007).

[115] S. Golbuff, Design Optimization of a Plug-In Hybrid Electric Vehicle, SAE Technical Paper 2007-01-1545 (2007).

[116] S. Senthilvelan, R. Gnanamoorthy, Influence of reinforcement on composite gear metrology, Mechancism and Machine Theory 43 (2008) 1198–1209. doi:10.1016/j.mechmachtheory.2007.09.002.

[117] Z. Yuan, Influence of rotor ' s radial rub-impact on imbalance responses, Mechanism and Machine Theory 42 (2007) 1663–1667. doi:10.1016/j.mechmachtheory.2006.09.002.

[118] H. Kim, J. Jeong, M. Yoon, J. Moon, Simple Size Determination of Permanent-Magnet Synchronous Machines, Ieee Transactions On Industrial Electronics 64 (2017) 7972–7983.

[119] S. Seisenberger, M. Ried, P. Reupold , K. Voigt, Electric vehicles — A cost model of electric propulsion systems, 2012 2nd International Electric Drives Production Conference (EDPC), Nuremberg, 2012, 1-6. doi: 10.1109/EDPC.2012.6425138

[120] Chen, Power flow and efficiency analysis of epicyclic gear transmission with split power, Mechanism and Machine Theory 59 (2013) 96–106. http://dx.doi.org/10.1016/j.mechmachtheory.2012.09.004

[121] Khan, A., Grewe, T., Liu, J., Anwar, M. et al. The GM RWD PHEV Propulsion System for the Cadillac CT6 Luxury Sedan, SAE technical papers series. doi: 10.4271/2016-01-1159

[122] Jurkovic, S.,Rahman, K., Savagian, P., and Dawsey, R , Electric Traction Motors for Cadillac CT6 Plugin Hybrid-Electric Vehicle SAE technical papers series. doi: 10.4271/2016-01-1220.

[123] D.Rotella et Al., A simple method for the design of hybrid electric Power-Split CVTs: A case study, IFToMM ITALY 2018 MMS 68 (2018) 70-79

[124] X. Zhou et Al., Hybrid electric vehicle powertrain design: construction of topologies and initial design schemes, IFToMM ITALY 2018 MMS 68 (2018) 49-60

[125] E.L. Esmail, E. Pennestrì, A. Hussein Juber, Power losses in two-degrees-of-freedom planetary gear trains: A critical analysis of Radzimovsky's formulas, Mechanism and Machine Theory, 128, October 2018, pp.191-204

APPENDIX – Full Papers

- **D. Rotella, M. Cammalleri, Direct analysis of power-split CVTs: A unified method, Mech. Mach. Theory 121 (2018) 116–127. https://doi.org/10.1016/j.mechmachtheory.2017.10.006**
- **D. Rotella, M. Cammalleri, Power losses in power-split CVTs: A fast black-box approximate method, Mech. Mach. Theory 128 (2018) 528–543. https://doi.org/10.1016/j.mechmachtheory.2018.06.011**
- **M. Cammalleri, D. Rotella, Functional design of power-split CVTs: An uncoupled hierarchical optimized model, Mech. Mach. Theory 116 (2017) 294–309. https://doi.org/10.1016/j.mechmachtheory.2017.06.003**
- **D. Rotella et Al., A simple method for the design of hybrid electric Power-Split CVTs: A case study, IFToMM ITALY 2018 MMS 68 (2018) 70-79. DOI: 10.1007/978-3-030-03320-0_8**
- **X. Zhou et Al., Hybrid electric vehicle powertrain design: construction of topologies and initial design schemes, IFToMM ITALY 2018 MMS 68 (2018) 49-60. DOI: 10.1007/978-3-030-03320-0_6**